CRANFIELD UNIVERSITY

CHAO ZENG

DEVELOP A ROBUST NONLINEAR CONTROLLER for LARGE AIRCRAFT by APPLYING NDI, SMC and ADAPTIVE CONTROL

SCHOOL OF ENGINEERING

MSc THESIS

CRANFIELD UNIVERSITY

SCHOOL OF ENGINEERING

MSc THESIS

Academic Year 2011-12

CHAO ZENG

Develop A Robust Nonlinear Controller For Large Aircraft By Applying Nonlinear Dynamic Inversion, Sliding Mode Control and Adaptive Control.

Supervisor: Dr Antonios Tsourdos

December 2012

Abstract

A nonlinear dynamic inversion (NDI) controller and a sliding mode controller are developed for large civil transport Boeing 747 in this thesis. Furthermore adaptive control theory is applied on both NDI controller and SMC controller to improve the performance. Nonlinear dynamic inversion is an advanced control method which is able to directly handle nonlinear system with less gain schedule and provides inherent decoupled property. The system is linearized as a pure integrator by inner loop feedback, whilst the desired control law is fulfilled by the outer loop linear controller. However, the NDI controller is considerably sensitive to uncertainty due to the incomplete cancellation. SMC, a well known nonlinear robust control method, is utilized to endow the controller with more robustness. The results show that SMC controllers perform better than NDI controllers, but are still not perfect. Finally, a parameter on-line estimation adaptive scheme is applied to improve NDI controller meanwhile a disturbance observer is designed in addition to SMC controller. It is drawn from assessments that the disturbance observer based SMC controller achieves the best performance for all flight points: fast rising-up speed, little overshoot, short settle time and very small steady state error.

In addition, the classical and modern linear control theories as well as nonlinear control methods are reviewed. Moreover, some flying and handling quality criteria are also given as literature review.

Acknowledgements

I would like to express my sincere gratitude to my supervisor Professor Antonios Tsourdos for his continual advice and support throughout the whole project. His clear guidance and encouragement help me to continue the project at the hardest time. I am also very grateful to Dr. Hyo-Sang Shin and Dr. Mudassir Lone. Dr. Sang attended every meeting and always explicitly explained theory and gave me useful suggestions. Dr. Mudassir Lone who is my supervisor before 5 months review really helped me a lot at the beginning, and provided me some very good books for fundamental knowledge. I am also indebted to Dr. James Whid- borne, Dr. Alastair Cooke and Mr. Mike Cook for the brilliant lectures given by them. My thanks also go to my colleagues in COMAC and the officemates for their help in this research. Their advice, cooperation and comments have facilitated this research greatly. Furthermore, I would like to give my deeply gratitude to my family and my girlfriend for their unconditional support, understanding and encouragement all the time.

I would like to acknowledge China Scholarship Council (CSC), Commercial Aircraft Corporation of China (COMAC), and COMAC's subsidiary: Shanghai Aircraft Design and Research Institute (SADRI). My research and study would not have been possible without financial support from CSC and COMAC, and the nurturing environment of SADRI.

Contents

List of Figures

List of Tables

Abbreviations

NDI	Nonlinear Dynamic Inversion
SMC	Sliding Mode Control
MIMO	Multi-Inputs and Multi-Outputs
SISO	Single Input and Single Output
LQR	Linear Quadratic Regulator
LTI	Linear Time Invariant
LPV	Linear Parameter Varying
QLTI	Quasi-Linear Time Invariant
QLPV	Quasi-Linear Parameter Invariant
QFC	Quantitative Feedback Control
TVC	Trust Vectoring Control
P SMC	Sliding Mode Control law with Proportional term
PI SMC	Sliding Mode Control law with Proportional and Integral terms
RCAH	Rate Command-Attitude Hold
FBW	Fly-By-Wire
SAS	Stability Augmentation System

Chapter 1

Introduction

1.1 Background

The flight control system is defined as a system which enables the pilot to control the aircraft by altering the control surface deflections and throttle to modify flight dynamics in order to perform desired manoeuvre [8]. It plays a vital role in airplane operation which determines how the aircraft responds for certain command. It is also commonplace that the stability properties and control characteristics of civil aircraft are artificially augmented by employing flight control system in case the aerodynamic design cannot meet requirements or the airplane is required to operate in extended flight envelop. These also help to enhance the flight dynamics to satisfy flying and handling quality requirements.

Flight control system have been developed for several decades from a traditional flight control system which is mechanical control system, to a fly-by-wire (FBW) system where the mechanical flying controls are dispensed with altogether and replaced by an electrical or electronic link [9]. A typical flight control system comprises of two parts: the inner loop feedback, also called stability augmentation system (SAS) which functions to augment the stability characteristic of the aircraft; the outer loop feedback, which implements the autopilot functions. The classical control theory have been implemented very well for traditional aircraft. However, it has problems. The classical control theory is a linear-based design method and can only handle the single input and single output system. But aircraft is not a linear system especially for those combat aircrafts which have very large flight envelop and high maneuverability. The nonlinearities are introduced by not only the nonlinearities of aerodynamic characteristic but also, rather common, the nonlinear characteristics of common flight control system components, such as actuator rate limiting or saturation. Therefore, gain scheduling technique is commonly applied for a classical flight controller to cope with the nonlinearity of aircraft. More explicitly, a set of local flight controllers are designed based on local linearized aircraft model and then the controller gain is blended and scheduled between the operation region according to a function of external variable. The major disadvantages of this method are: firstly,

the aircraft has to possess smooth nonlinearity; secondly, it is usually cumbersome and time consuming to design the set of local flight controllers.

Intuitively, the aerospace industry tried to find a way to design control law directly for nonlinear system. After decades of development of control theory, there are several control techniques to handle nonlinear system currently among which nonlinear dynamic inversion and sliding mode control are quite successful. Nonlinear dynamic inversion can directly deal with multi-variables control laws for nonlinear dynamic system without gain schedule or with less gain schedule. Moreover, it has inherent property of decoupling the control axes. For these reasons, this method has attracted extensive researches during recent years, and some aircraft flight controllers have been designed through this new technology such as Lock-heed F-35 Lightning II [10] and X-38 space reentry vehicle. However, NDI controller is very sensitive to uncertainties, which might degrade the controller as a whole. Thus, robustness performance of NDI controller should be guaranteed.

Sliding mode control is well known as a robust nonlinear control theory originated in Russia at around the 1960s. Until now, this theory has been widely applied in the electromechanical industry. The principal benefit is that SMC controller is totally insensitive to matched uncertainty, such as parametric uncertainty or external disturbance. In addition, the SMC could reduce the system order to $n - m$, the discrepancy between number of states and number of inputs. The concept is that the controller always tries to drive system trajectory on to the desired sliding surface even in the presence of matched uncertainty.

In this thesis, adaptive control is considered to improve the performance of both NDI controller and SMC controller. With respect to NDI controller, the NDI controller parameters are recursively updated to make the response approaching the desired dynamics when the parametric uncertainties are present. For SMC controller, a disturbance observer is utilized to estimate the disturbance and to compensate the real disturbance, therefore the boundary of disturbance is dramatically reduced in turn the performance of SMC controller is significantly improved.

1.2 Outline

This thesis illustrates the developments of nonlinear controllers for large civil aircraft Boeing 747. Both a NDI controller and a SMC controller are developed and both are further improved by applying adaptive control technique. This thesis is started by formulating aims and objectives, then some classical and modern linear control theories and nonlinear control methods are briefly introduced respectively in chapter 3 and chapter 4. After that, some flying and handling quality requirements are given as assessment criteria in chapter 5. Then a NDI controller is developed for Boeing 747 in chapter 7 after the introduction of nonlinear dynamic inversion theory in chapter 6. A SMC controller is designed for Boeing 747 in chapter 8 before the adaptive control theory is implemented to improve the performances of both NDI

controller and SMC controller in chapter 9. The final chapter 10 highlights the conclusions and future work.

1.3 Motivation and contribution

As stated previously, the typical way to design a controller for large civil aircraft is gain scheduling, through which a set of linear controllers are designed corresponding to the set of linear aircraft models. This method is cumbersome and time consuming since all the gains need to be updated as the flight conditions changing. More importantly, the stability of the controllers in the regions between the local linear aircraft models can not be guaranteed by designer. Consequently, tremendous flight tests which are expensive and dangerous are needed to verify the stabilities in those regions. Other linear control methods also have these similar shortcomings. In this thesis, I am looking for nonlinear control design methods which could proofs the stabilities theocratically throughout the overall flight profile meanwhile possesses good control performances.

The primary contributions of this thesis are:

- Nonlinear dynamic inversion theory is applied to a nonlinear Boeing 747 aircraft model and NDI controllers are developed for both longitudinal and lateral mode;
- Sliding mode control method is applied to the parameter varying Boeing 747 aircraft model and a SMC controller that can cope with the whole flight envelop is developed for the longitudinal mode;
- A disturbance observer is combined with sliding mode control for the Boeing 747 aircraft, which considerably improves the robustness performance of sliding mode controller.

Chapter 2

Aim and objectives

Aim: develop a robust nonlinear controller for large aircraft by using nonlinear dynamic inversion (NDI), sliding mode control (SMC) and adaptive control to satisfy handling quality criteria.

Objectives:

1. Learn classical and modern control theories for linear system, and implement applications on linear Boeing 747 model;

   Classical and some modern control theories have been successfully applied on linear system. It is necessary to understand how do these theories work. Some classical theories applications on Boeing 747 model are carried out for better understanding of classical control methods.

2. Learn nonlinear control theories;

   There are several control techniques particularly for nonlinear control system design such as NDI and backsteping. These nonlinear control methods are briefly introduced and contrasted.

3. Develop a NDI controller for the nonlinear Boeing 747 aircraft model;

   First of all, the NDI control theory is introduced and some key issues of NDI theory are discussed such as internal dynamics and desired dynamics. Then NDI controllers with different desired dynamics are designed for nonlinear Boeing 747 model. Finally, the most suitable design point is selected according to robustness performance of the overall flight envelop.

4. Develop a SMC controller for the nonlinear Boeing 747 aircraft model;

   Since the NDI controller is very sensitive to uncertainties such as parametric uncertainty and external disturbance, a robust nonlinear control design theory so called sliding mode control is employed to handle matched uncertainties. In order to improve the performance, 3 types of SMC control laws are worked out and assessed.

5. Develop both adaptive-NDI controller and adaptive-SMC controller.

   Adaptive control technique could adjust controller gain recursively, eventually make the response to behave as expected at the presence of unknown parameters or slow varying parameters. Thus, NDI controller could be improved by combining it with adaptive control to degrade the incomplete cancellation of the feedback linearization. A disturbance observer is developed to reduce the magnitude of uncertainty boundary in SMC controller, which in turn improve the performance of the SMC controller significantly.

Chapter 3

Classical and modern linear control theory

3.1 Classical control theory

3.1.1 An overview of Classical control theory

Classical methods are approaches which use feedbacks to augment the stability of system, based on proportional, integral and differential control components. Through adjusting the gains of the proportional, integral and differential terms, the desired stability features are achieved.[11, p.11] The popular feedback variables of longitudinal control are pitch rate, normal acceleration and C*. The pitch rate feedback is practical in longitudinal stability augmentation since it can effectively increase the short period mode damping ratio which is commonly lower than the flying and handling quality requirements. In other words, the pitch rate feedback can raise the damping of airplane if you treat the airplane as a classical mass-spring-damper system. The normal acceleration is the most visible motion cue for pilots. C* is the combination of pitch rate and normal acceleration which has the advantage of these two feedbacks. Classical control was applied broadly in flight control system and has been very successful [3].

However, it might be argued that the classical control techniques have some limitations. The classical control design approaches assess one loop at a time, aided by such tools as root locus, Bode and Nyquist plots which visualizes that how the dynamics of system change due to the varying of the feedback gain. Thus, the design procedure becomes considerably difficult when multiple loops are added to the control system and does not guarantee success when dealing with multi-variable control system, namely multiple inputs, multiple outputs or multiple feedback loops. Moreover, it is time consuming and requires many trails and errors.[12, p.383]

3.1.2 Root locus

The feedback gains of a classical controller can be determined in two ways: root locus and pole placement. Root locus plot is relatively simple and easy to implement. The plot illustrates the roots of closed loop system characteristic equation varying due to the change of single feedback loop gain variable [9, p.287]. It clearly shows the effects of stability characteristic for different values of the feedback gain. The root locus plots are totally different if choose different feedback variable. Following equation illustrate the process of root locus method.

For example using pith attitude feedback to elevator deflection input[9, p.284]. The control law is given by

$$\eta(t) = \delta_\eta(t) - K_\theta \theta(t) \tag{3.1}$$

The corresponding transfer function is

$$\frac{\theta(s)}{\eta(s)} = G(s) = \frac{N_\eta^\theta(s)}{\Delta(s)} \tag{3.2}$$

Then, the closed loop transfer function of the augmented aircraft is

$$\frac{\theta(s)}{\delta_\eta(s)} = \frac{N_\eta^\theta(s)}{\Delta(s) + K_\theta N_\eta^\theta(s)} \tag{3.3}$$

The augmented characteristic equation is

$$\Delta(s)_{aug} = \Delta(s) + K_\theta N_\eta^\theta(s) = 0 \tag{3.4}$$

From above equation, it is easily seen that the roots of augmented characteristic equation are varied according to the value of feedback gain K_θ. By choosing the appropriate value of K_θ, the poles could be shifted at the expected point along the loci, and then stability objectives can be achieved.

An example of pitch angle rate feedback is presented here. Consider following longitudinal aircraft model of B747 from reference [13].

$$\begin{bmatrix} 1 & 0 & 0 & 0 \\ 0 & 0.99296 & 0 & 0 \\ 0 & 0.905e-4 & 1 & 0 \\ 0 & 0 & 0 & 1 \end{bmatrix} \cdot \begin{bmatrix} \dot{u} \\ \dot{w} \\ \dot{q} \\ \dot{\theta} \end{bmatrix} = \begin{bmatrix} 0.00187 & 0.0263 & -86.15 & -31.939 \\ -0.0696 & -0.292 & 668.184 & -4.09148 \\ 0.000259 & -0.00101 & -0.284 & 0 \\ 0 & 0 & 1 & 0 \end{bmatrix} \cdot \begin{bmatrix} u \\ w \\ q \\ \theta \end{bmatrix} + \begin{bmatrix} 1.93 \\ -15.1 \\ -0.97 \\ 0 \end{bmatrix} \cdot \eta \tag{3.5}$$

The following table 3.1 shows the flight condition of the aircraft. First of all, rewrite

Table 3.1: Flight condition of aircraft model

Flight condition data	
Altitude	40000ft
Mach	0.7
Velocity	678ft/s
Trimmed body incidence	7.3deg
Trimmed pitch attitude	7.3deg
Flight path angle	0
Control anticipation parameter	0.131
Gravitation constant	32.2ft/s2
Pilot axial coordinate about cg	86ft
Pilot normal coordinate about cg	-10ft

the state space equation into standard form (3.6).

$$\begin{bmatrix} \dot{u} \\ \dot{w} \\ \dot{q} \\ \dot{\theta} \end{bmatrix} = \begin{bmatrix} 0.00187 & 0.0263 & -86.15 & -31.939 \\ -0.07 & -0.2941 & 672.9 & -4.12 \\ 0.0002653 & -0.0009834 & -0.3449 & 0.0003729 \\ 0 & 0 & 1 & 0 \end{bmatrix} \cdot \begin{bmatrix} u \\ w \\ q \\ \theta \end{bmatrix} + \begin{bmatrix} 1.93 \\ -15.21 \\ -0.9686 \\ 0 \end{bmatrix} \cdot \eta \tag{3.6}$$

The open loop stability characteristics are

$$\varsigma_p = 0.0633, \omega_p = 0.0782 rad/s$$

$$\varsigma_s = 0.356, \omega_s = 0.88 rad/s$$

where the ς_p and ς_s respectively denote the damping ratios of phugoid mode and short period mode; the ω_p and ω_s respectively denote the frequencies of phugoid mode and short period mode. And the normal load factor per unit angle of attack also could be calculated.

$$n_\alpha = -\frac{z_w \cdot U_e}{g} = -\frac{-0.2941 \cdot 672.5}{32.2} = 6.14 g/rad$$

From the MIL-STD-1797A [2], for class III aircraft B flight phase, following requirements should be satisfied.

$$\begin{aligned} &0.3 \leq \varsigma_s \leq 2 \\ &0.7 rad/s \leq \omega_{ns} \leq 4.2 rad/s \end{aligned} \tag{3.7}$$

As it can be seen, the short period damping is acceptable but a little low, and the natural frequency has the same condition. Therefore a stability augmentation system is needed.

When use pitch rate as proportional feedback, the control law is

$$u = \delta_\eta - K \cdot q \tag{3.8}$$

The figure 3.1 is the control system structure for pitch rate proportional feedback control law.

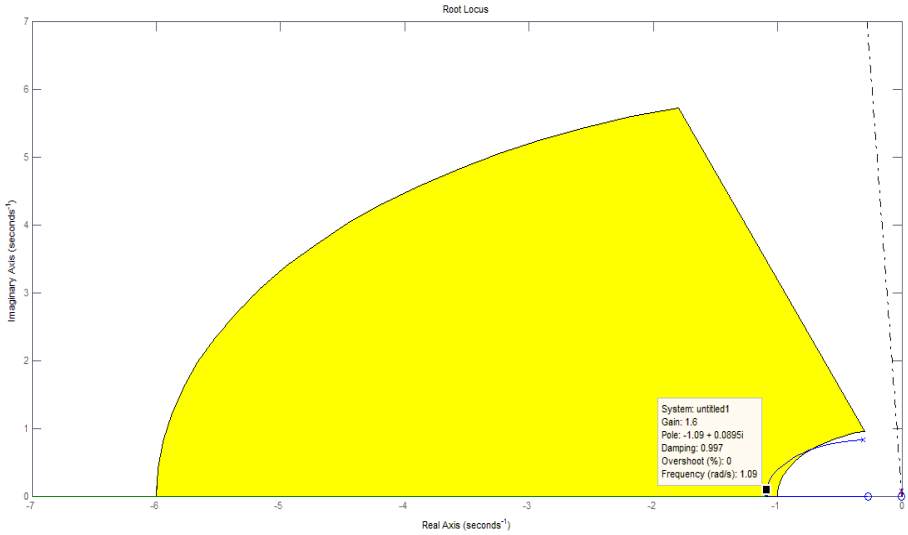

Figure 3.2: Short period mode

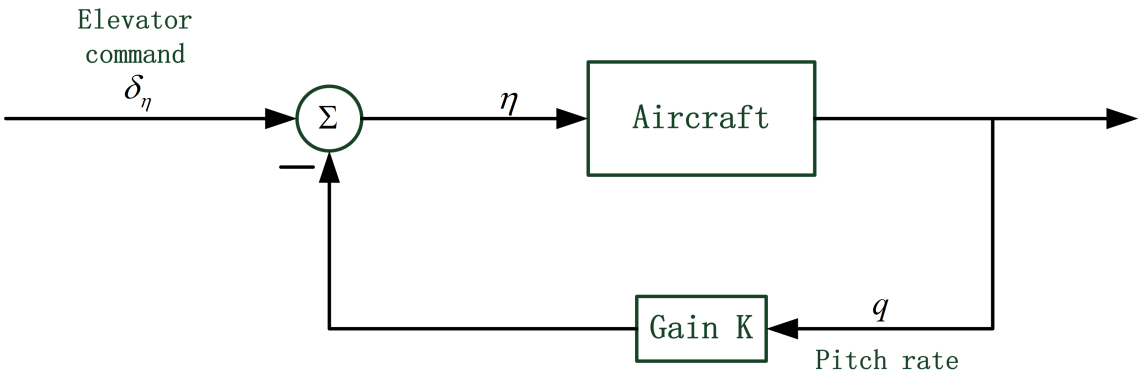

Figure 3.1: pitch rate proportional feedback control system

The stability characteristic is determined as shown below by deciding a point on root locus corresponding to a feedback gain value. From figure 3.2 and figure 3.3 it could be seen that short period mode stability is satisfactory meanwhile the phugoid mode stability is just a little lower than the requirement.

$$K = -1.6$$
$$\varsigma_s = 1, \omega_{ns} = 1.1 rad/s$$
$$\varsigma_p = 0.03$$

The u terms could be omitted since in short period mode u almost remains constant, whereas θ cannot be eliminate as this is not the wind axes coordinate. Then the closed transfer function of reduced order model is yielded for q feedback with $K = 1.6$.

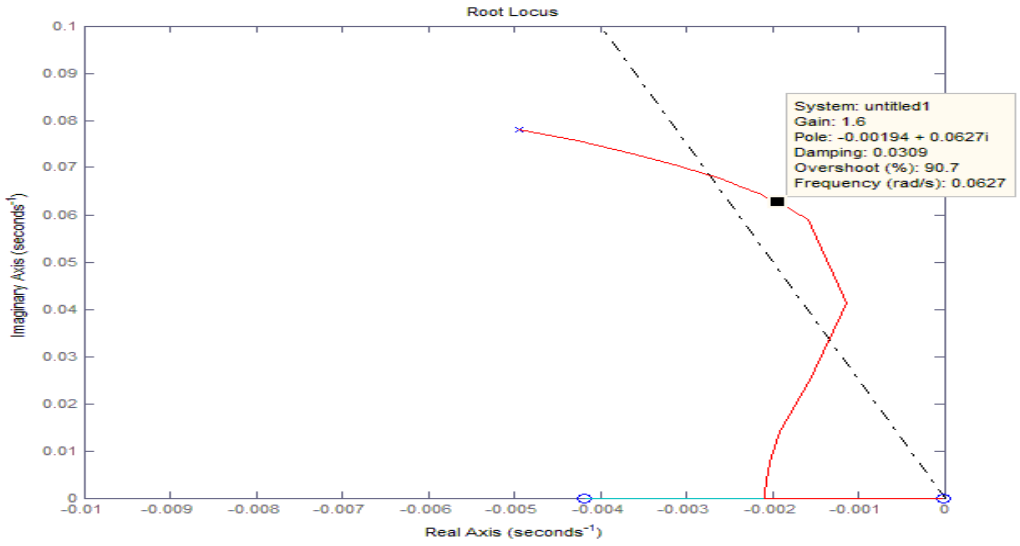

Figure 3.3: Phugoid mode

The reduced order state space equation:

$$\begin{bmatrix} \dot{w} \\ \dot{q} \\ \dot{\theta} \end{bmatrix} = \begin{bmatrix} -0.2941 & 672.9 & -4.12 \\ -0.0009834 & -0.3449 & 0.0003729 \\ 0 & 1 & 0 \end{bmatrix} \begin{bmatrix} w \\ q \\ \theta \end{bmatrix} + \begin{bmatrix} -15.21 \\ -0.9686 \\ 0 \end{bmatrix} \eta \quad (3.9)$$

The reduced order close loop transfer function for q:

$$\frac{q}{q_c} = \frac{0.96862s\,(s + 0.2786)}{(s - 0.003462)(s^2 + 2.192s + 1.202)}$$

If we allocate the feedback gain to the forward path, the steady state gain is computed, eliminating the first item in the denominator.

$$\left(\frac{q}{q_c}\right)_{steady} = \frac{0.96862 \cdot 0.2786}{1.202} \cdot 1.6 = 0.3592$$

And the time lag is

$$T_\theta = \frac{1}{0.2786} = 3.5894s$$

The responses of w, q and θ for 1 deg/s q commands are shown in figures 3.4, 3.5 and 3.6. It can be seen that the augmented system has a better transient time responses for step input. Although the damping ratio of short period mode is 1, the q response still has a big overshoot as a result of the big time lag T_θ.

A second order linear actuator model is added in the system, which has following the dynamic characteristic:

$$\varsigma_a = 0.7, \omega_a = 21 rad/s$$

The steady state gain remains unchanged. The q response changed a little in contrast to the model without actuator, as shown in figure 3.7. Thus, the controller redesign is not necessary.

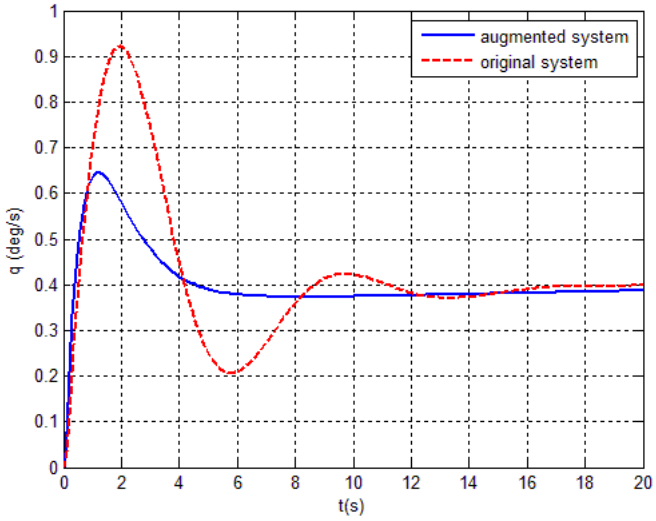

Figure 3.4: q response for the pitch rate command

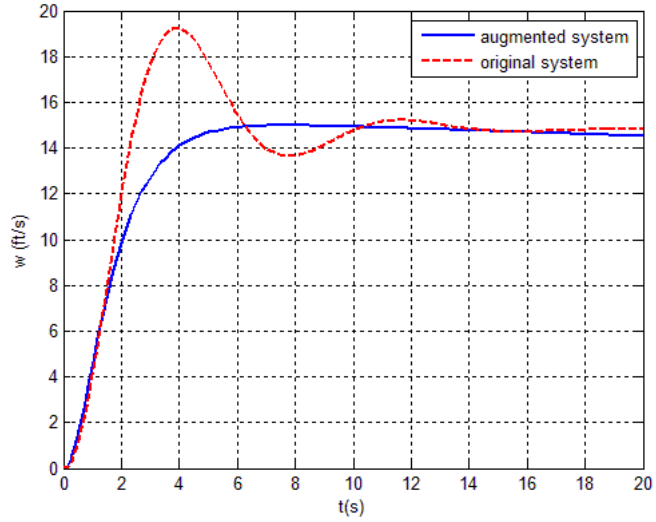

Figure 3.5: w response for the pitch rate command

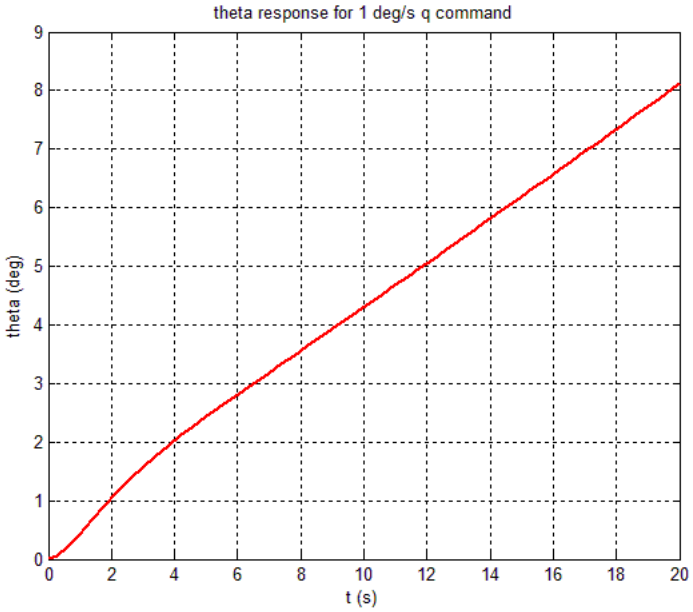

Figure 3.6: θ response for the pitch rate command

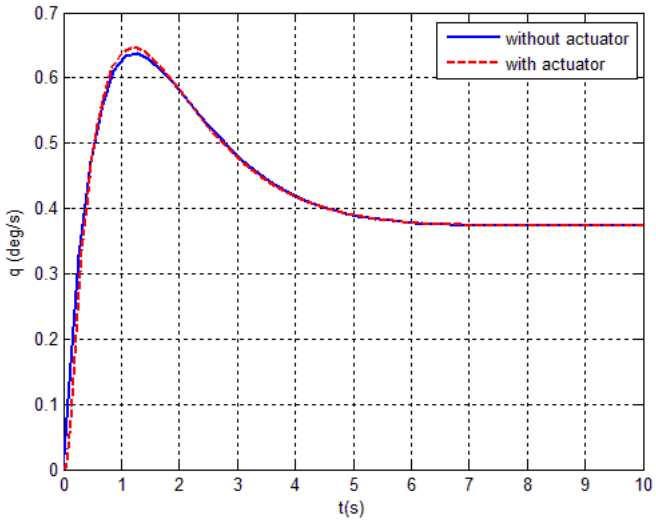

Figure 3.7: q responses comparison between cases with actuator and without actuator

3.1.3 PID controller

The PI controller is the combination of proportional states feedback and error integral feedback. The state feedback augments the stability of the system, meanwhile the error integral feedback can reduce the steady state error. In other words, it has good tracking performance [3].

The utilization of differential items is aiming to diminish the influence of steady output on the control system when the input is zero. For example, in a steady turn, the yaw rate will be non-zero and the negative feedback will drive the error to zero. The pilot will centre the rudder and merely use aileron to maintain the bank angle as soon as the turn is established, therefore the rudder command input will be zero. As a result, the yaw negative feedback will give rise to roll out of turn. The washout filter, an approximate controller of differential controller, is used to pass the transient response and jam the steady output feedback [3].

An example of application of a PI controller is given below. Consider the longitudinal reduced order aircraft model of B747.

$$\begin{bmatrix} \dot{w} \\ \dot{q} \end{bmatrix} = \begin{bmatrix} -0.2941 & 672.9 \\ -0.0009834 & -0.3449 \end{bmatrix} \begin{bmatrix} w \\ q \end{bmatrix} + \begin{bmatrix} -15.21 \\ -0.9686 \end{bmatrix} \eta \tag{3.10}$$

The integral error feedback gain and other state variables proportional feedback gain are determined by pole placement technique. First of all, organise the block diagram like below, and then obtain the open loop state space equation for the system below, where the integral error will become a new state variable in the equation.

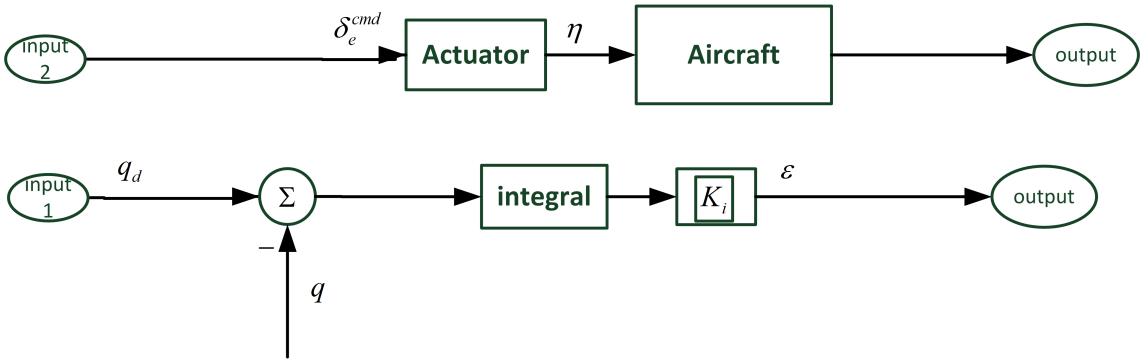

Figure 3.8: Adding integral error as a state variable

The open loop state space equation for above system is given

$$\begin{bmatrix} \dot{w} \\ \dot{q} \\ \dot{\varepsilon} \end{bmatrix} = \begin{bmatrix} -0.2941 & -0.2941 & 0 \\ -0.0009834 & -0.3449 & 0 \\ 0 & -1 & 0 \end{bmatrix} \begin{bmatrix} w \\ q \\ \varepsilon \end{bmatrix} + \begin{bmatrix} -15.21 \\ -0.9686 \\ 0 \end{bmatrix} \eta + \begin{bmatrix} 0 \\ 0 \\ 1 \end{bmatrix} q_c \tag{3.11}$$

Secondly, let us place all the poles to the desired values by implementing place command in MATLAB. The desired short period stability characteristics are selected as follows:

- Desired short period damping ratio: 0.9
- Desired short period frequency: 3 rad/s
- Integral lag time constant: 1/6s for giving fast integral action and avoiding introducing large phase lag.

Thus, desired poles are: P=-2.7+1.3i, -2.7-1.3i and -6. The result values of K_i and K_p are respectively

$$Ki = 199.6376, Kq = -14.8554, Kw = 0.2386$$

The augmented stability characteristics are

$$\zeta_s = 0.9, \omega_n = 3rad/s$$

Overall flight control system structure is shown below.

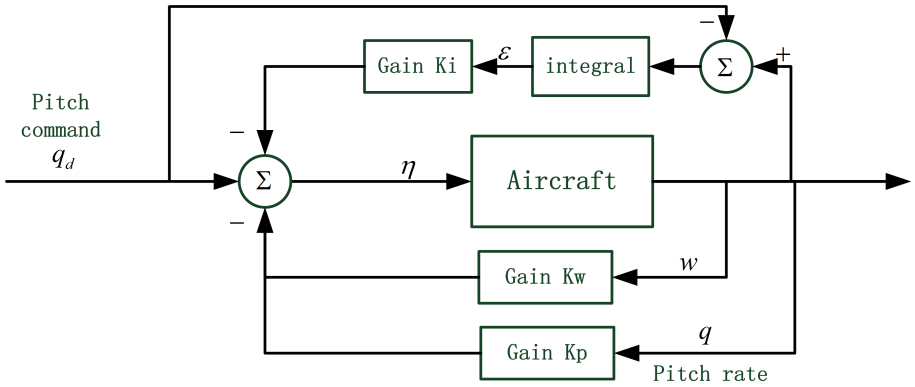

Figure 3.9: PI controller for Boeing 747 reduced order model

For 1 degree per second pitch rate step command, we have figure 3.10.

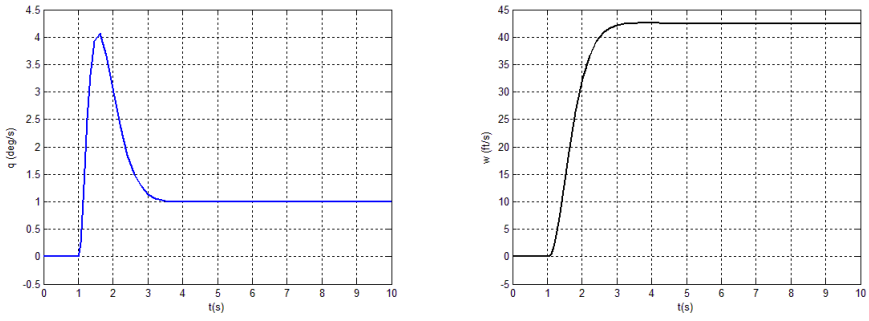

(a) q response (b) w response

Figure 3.10: q and w responses of the PI controller for 1 deg/sec step command

It can be seen that the steady state value of pitch rate response is $1 degree/s$. Comparing to the result in pitch rate feedback controller, the steady state error is zero

for the PI controller, which means that the PI controller have good tracking performance. Nevertheless, the overshoot is unacceptably big and the dropback is too big. So the shaping filter at command path is needed.

Consider the same second order actuator with above example included in the system. Below, figure 3.11 shows the comparison between the response with actuator and without actuator.

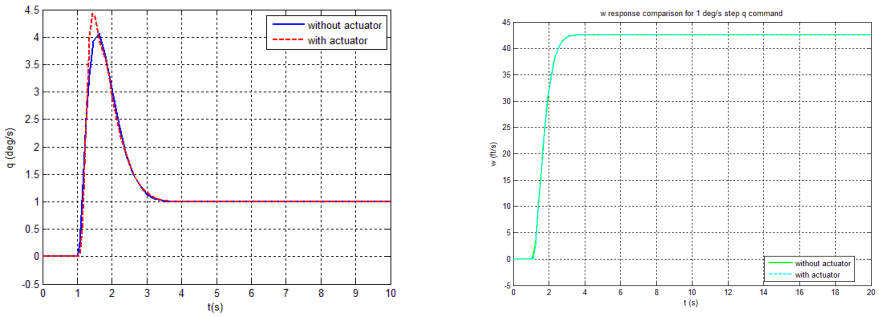

(a) q comparison (b) w comparison

Figure 3.11: q and w responses comparison between with actuator and without actuator for 1 deg/sec step command

The new control system performance deteriorates

- Short period mode: $\varsigma_s = 0.9, \omega_s = 3rad/s$ to $\varsigma_s = 0.9, \omega_s = 2.7rad/s$.
- Actuator mode: $\varsigma_a = 0.7, \omega_a = 21rad/s$ to $\varsigma_a = 0.296, \omega_a = 13.8rad/s$.
- Integral lag time constant: $1/6s$ to $1/7s$.

The figure 3.12 below shows the PI controller for a reduced order model of B747 including the actuator.

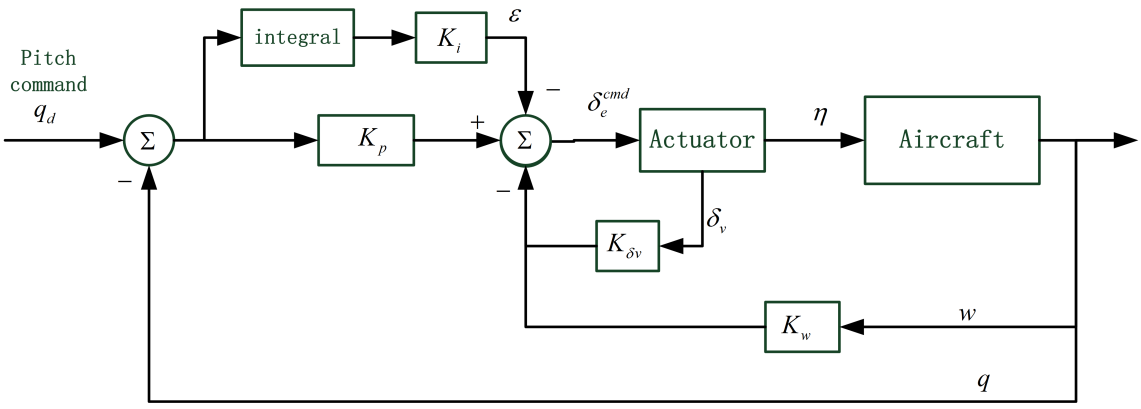

Figure 3.12: PI controller block diagram with actuator

3.1.4 C* control law

The normal acceleration was considered as the main sense cue of a pilot and the response of a normal acceleration is only determined by damping ratio and natural frequency. Hence, the rule of thumb criterion is based on damping ratio and undamped natural frequency. It was also stated that pilots were able to sense the pitch rate cue afterward. However, pitch rate transfer function has a numerator $\left(s+\frac{1}{T_\theta}\right)$, and incidence lag T_θ has a profound effect on pitch rate response. Big time lag introduces huge overshoot for pitch rate response. Hence, the satisfaction of the rule of thumb criterion can not guarantee good handling quality feature.

At low flight speed, the pitch rate is the major motion cue for a pilot, meanwhile normal acceleration cues are weak. At high flight speed, slight pitching give rise to large normal accelerations, therefore normal acceleration cues dominate. Thus, it is suggested that a new variable, a blend of pitch rate and normal acceleration called C*, could be introduced. C* variable is defined as

$$C^* = n_{zp} + \frac{V_{co}}{g} q \tag{3.12}$$

V_{co} is cross velocity at which normal acceleration cues and pitch rate cue are equal. V_{co} is chosen as $400 ft/s$. C* control law use C* as control variable to augment the stability characteristic. It could be cooperated with the proportional control law or PI control law.

A $C*$ controller example for longitudinal B747 model is given as following.

First of all, the C* control variable is calculated in terms of state variables. The cross over velocity V_{co} is selected as 400ft/s.

$$a_{zp} = \dot{w} - U_e q + (g \sin\theta_e)\,\theta - x_p \dot{q} = -0.0929u - 0.2095w + 30.0787q - 0.0611\theta \tag{3.13}$$

$$n_{zp} = -\frac{a_z}{g} = 0.0029u + 0.0065w - 0.9341q + 0.0019\theta \tag{3.14}$$

$$C^* = n_z + \frac{V_{co}}{g} q = 0.0029u + 0.0065w + 11.4882q + 0.0019\theta \tag{3.15}$$

Then compute the open loop transfer function of C* variable with the same actuator as former example, which is

$$\frac{C^*}{C^*_{cmd}} = \frac{-4950.9839(s+0.6606)(s-0.003438)}{(s-0.005431)(s^2+0.6444s+0.7663)(s^2+29.4s+441)} \tag{3.16}$$

where C^*_{cmd} stands for the command of $C*$. The $C*$ feedback gain is selected as 0.19 by root locus method, such that the damping ratio and frequency are both acceptable, shown in figure 3.13. The stability characteristics are contrasted as indicated in table 3.2.

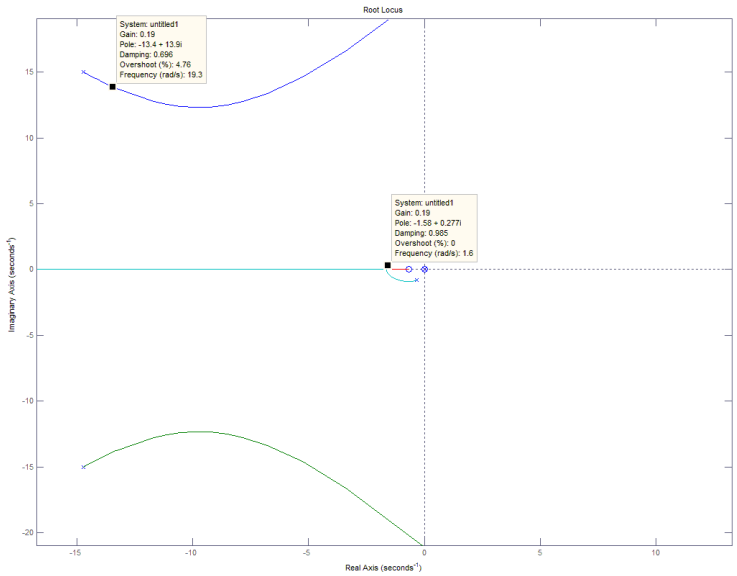

Figure 3.13: C* feedback root locus

Table 3.2: The stability characteristic comparison

	Short period mode	Actuator
Unaugmented	$\varsigma_s = 0.356, \omega_s = 0.88 rad/s$	$\varsigma_s = 0.7, \omega_s = 21 rad/s$
Augmented	$\varsigma_s = 0.985, \omega_s = 1.6 rad/s$	$\varsigma_a = 0.696, \omega_{na} = 19.3 rad/s$

The close loop transfer function of C* is given as follows.

$$\frac{C^*}{C^*_{cmd}} = \frac{940.6869(s + 0.6606)(s - 0.003438)}{(s - 0.004139)(s^2 + 3.155s + 2.571)(s^2 + 26.89s + 373.3)} \tag{3.17}$$

The steady state gain of C* is

$$\left(\frac{C^*}{C^*_{cmd}}\right)_{s=0} = 0.6475$$

The normalized C* response is obtained and indicated as follows.

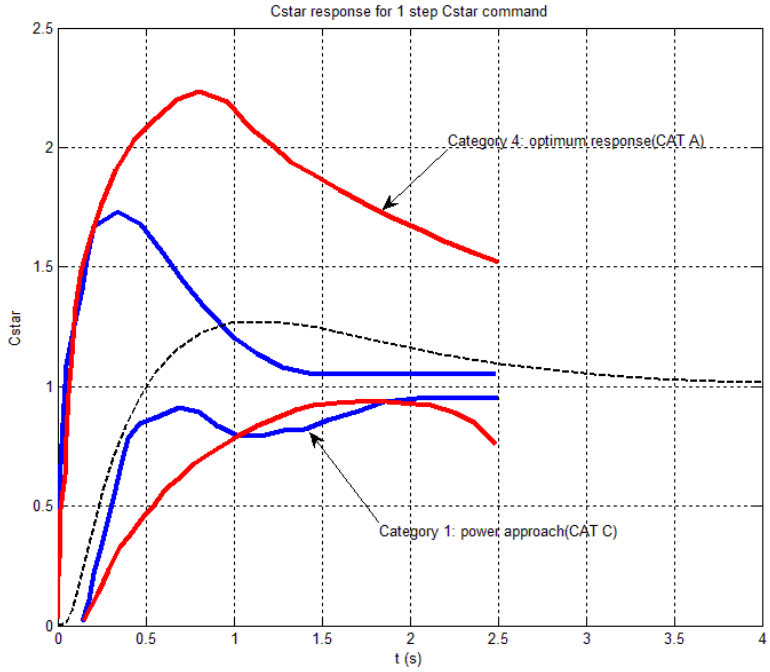

Figure 3.14: C* response for 1 step C* command

It can be seen that C* response could meet the category 4 requirement of C* criterion which is equal to flight phase C in military requirement. Meanwhile, pitch rate response still has huge overshoot which is undesired. Normal acceleration has good transient time response, playing a dominating role at this speed.

3.2 Modern linear control techniques

In recent years, modern control techniques have had significant effect on the flight control system design. Modern control theories are base on state-variable model, which describes not only the relationship between outputs and inputs, but also the relationship between inputs and states of the system. In contrast to the limitations of the classical control theory, modern control theory have several principal advantages: the capability of dealing with MIMO systems, designing nonlinear controller and robustness. Eigenstructure assignment technique can handle multiple feedback loops simultaneously through placing the eigenvalues and eigenvectors. Linear quadratic optimal control theory provides the methods to tune the controller through minimizing the cost function with specified weighing matrix which represents the design objectives. Moreover, H_∞ is a robust control method which tries to minimize the influence of the uncertainties on the control system. Those three modern linear control methods are introduced in following sections.

3.2.1 Eigenstructure assignment

Eigenstructure assignment is defined as a control design technique which obtains the controller by assigning both the eigenvalue and eigenvector of the system to meet the desired close loop performance. The responses of any vibration systems could be represented as a set of mode shapes and frequencies shown below.

$$\begin{aligned} x(t) &= \sum_{i=1}^{n} \alpha_i z_i e^{\lambda_i t} \\ &= Z\Lambda\alpha \end{aligned} \tag{3.18}$$

where

$$\begin{aligned} Z &= (z_1 z_2 \cdots z_n) \\ \Lambda &= \begin{pmatrix} \lambda_1 & 0 & \cdots & 0 \\ 0 & \lambda_2 & \cdots & \vdots \\ \vdots & & & \vdots \\ 0 & \cdots & 0 & \lambda_n \end{pmatrix} \\ \alpha &= \begin{pmatrix} \alpha_1 \\ \vdots \\ \alpha_n \end{pmatrix} \end{aligned} \tag{3.19}$$

As stated in [14], eigenvalues determine the speed and stability whereas the eigenvectors stand for the distribution of the eigenvalues within the states. More explicitly, below conclusions are drawn by A.N. Andry, JR.E.Y. Shapir, and OJ.C. Chung [15]:

- eigenvalues, which determine the decay or growth rate of the response;
- eigenvectors, which determine the shape of the response;
- initial condition, which determine the degree to which each mode will participate in the free response.

Considering following LTI (linear time invariant) system, the equation (3.21) is given in case of unity feedback with a fixed forward path gain.

$$\begin{aligned} \dot{x} &= Ax + Bu \\ y &= Cx + Du \end{aligned} \tag{3.20}$$

$$\begin{pmatrix} A - \lambda_i I & B \\ KC & -I \end{pmatrix} \begin{pmatrix} Z_i \\ P_i \end{pmatrix} s_{ri} = \begin{pmatrix} 0 \\ 0 \end{pmatrix}, \quad i = 1, \cdots, k_i \tag{3.21}$$

Where k_i eigenvalues are assigned and s_{ri} is a vector that selects the appropriate right eigenvector z_i form the eigenspace Z_i. Subsequently, the eigenstructure problem may be stated as

> For a specified eigenspectrum Λ, find a gain matrix K that will satisfy the k_i equations in equation (3.21) for a selected right eigenvector set $Z = z_i(i = 1, 2., k_i)$.

Corresponding to the right eigenvector, there are also left eigenvectors. Therefore the problem could also be clarified in terms of left eigenvectors.

$$\begin{pmatrix} A' - \lambda_i I & C' \\ K'C' & -I \end{pmatrix} \begin{pmatrix} V_i \\ Q_i \end{pmatrix} s_{ri} = \begin{pmatrix} 0 \\ 0 \end{pmatrix}, \quad i = 1, \cdots, k_m \tag{3.22}$$

The number $m + l$ is the maximum number of pairs of eigenvalue and eigenvector which could be assigned. If $m + l > n$ the whole eigenspectrum can be assigned by output feedback. There are 4 major algorithms to solve eigenstructure assignment problem: the protection methods, the parametric methods, the projection methods and the orthogonal eigenvetor methods. The choice of eigenvector is the central issue for the majority of the algorithms.

3.2.2 Linear quadratic optimal control

Linear quadratic optimal control dates back to the 1960s whose development coincided with large research programs and considerable funding in the United States and the former Soviet Union on space related problems [16]. Since then, many books have been written on this subject such as Anderson and Moore (1989) and Kwakernaak and Sivan (1972).

This technique enable the designer to consider both the requirements on the amplitude of the control inputs and the settling time of the state variables. Furthermore, the resulting closed-loop of LQ control exhibits very good multivariable stability margins when considering infinite horizon optimization and the weighting matrices are suitably chosen [17]. LQ theory has many applications in aeronautical field among which the most important application is definitely the design of flight control system of AFTI/F-16 aircraft. When the state variables are not available, the Kalman filter can be used to design an observer of state variables which is called LQR. However, the robustness margins are no longer guaranteed in the presence of an observer [17].

3.2.3 H_∞

H_∞ has been established since the 1980s, motivated by shortcoming of LQG (Linear Quadratic Gaussian) control technique and designing multi-variable robust controllers. As described in reference [17], 'the approach is based on minimising over frequency the peak values of certain system transfer functions that can be chosen by the design engineer to represent design objectives'. More explicitly, the standard H_∞ optimisation problem is to find a stabilising controller K which is proper

and minimises the supremum (lowest upper bound) over frequence of the maximum singular value of T_{zr}, the transfer function from the reference inputs to the output errors or costs. That is, to minimise

$$\|T_{zr}\|_\infty = \sup_{\mathrm{Re}(s) > 0} \bar{\sigma}\left[T_{zr}\left(s\right)\right] \tag{3.23}$$

A stabilizing controller achieving the minimum closed loop norm, $\|T_{zr}\|_\infty = \gamma_{opt}$, is said to be optimal. This can be solved efficiently using the algorithm of Doyle et al. (1989), and be reducing γ iteratively, an optimal solution is approached [16].

Chapter 4

Nonlinear control technique introduction

4.1 Overview

Airplane is a inherently nonlinear system resulting from the nonlinear aerodynamics, nonlinear properties of some components of flight control system such as the saturation of actuators. In order to describe the aircraft, several types of aircraft model are invented based on which different flight control methods could be applied. First of all, let us introduce a general taxonomy of nonlinear state-space dynamic models as indicated in figure 4.1.

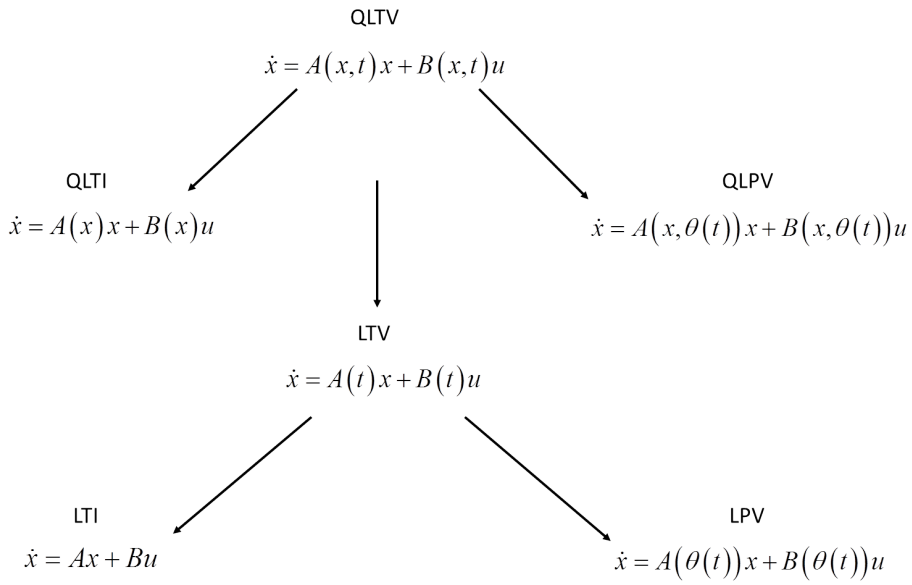

Figure 4.1: Dynamics of system models and their relationships; $x = x(t)$ is the state, $u = u(t)$ the input and $\theta = \theta(t)$ external parameters (variables different from x and u). Source: [1]

As illustrated in the above picture, reference [1] states that 'the LTI (linear time invariant) model arises from Taylor linearization around a single flight condition and is excellent for linear controller design, but has rather limited applicability for the whole flight envelope'. A more precise model called LPV (linear parameter varying) model, locating in the bottom right corner of figure 4.1, attracted a lot interests recently due to the preservation of transparency of linear controllers design and yet presentation of the rapidly changing dynamics. In the LPV model, the A, B, C matrix are varying according to the external parameter θ which is different from x and u. Nevertheless, the LPV model is still a collection of linear designs and it is impossible to distinguish between the real disturbance and the manifestation of nonlinearity [1]. The controller design based on LPV model still cannot cope with the whole flight envelope especially for high angle of attack. For presenting explicitly the nonlinearity of the aircraft, a general model is developed which is quasi-linear time varying (QLTV). The A, B, C matrix are varying along not only the state variables x but also the time t. Two special cases of this general form are generized as QLTI (quasi-linear time invariant) and QLPV (quasi-linear parameter varying).

The traditional gain scheduling technique designs the controller based on a set of LTI models and many linear control methods can be applied based on LPV model. Recently, some control methods are used for QLPV model to achieve better performance at the present of nonlinearity. Moreover, the Lyapunov stability theory could also be used to design nonlinear controller subject to certain types of aircraft models. The difficulties for application of this method is to find suitable Lyapunov functions [18].

4.2 Gain scheduling

A practical way to handle the nonlinear aircraft model is called gain scheduling which linearises the nonlinear model at a set of flight points and then designs a locally linear controller for each linearized aircraft model. Finally schedules the controllers' gains throughout the overall flight envelop. In gain scheduling scheme, the global controller gains are varying according to a specific function with respect to scheduling parameters such as speed and altitude which means the global controller gain switches to the corresponding local controller when the airplane is approaching that point in the data space. After that, the regime between design points should be verified to be stable and assessed for performance.

For normal airplane and limited flight envelope whose nonlinearities is mild and sufficiently smooth, this method have been proven successful [18]. However, Gain scheduling is usually cumbersome and time consuming since a set of local controller needs to be designed. Furthermore, Gain schedule can not cope with the conditions when high maneuver occurs or excessive range of flight envelope is required which means heavy nonlinearities might occur.

4.3 A approach based on Quasi-Linear-Parameter-Varying Model

As the previous section describes, the nonlinear system could be linearized at a single equilibrium point, obtaining linear time invariant (LTI) model to enable linear controller design. For capturing the nonlinearities of the system, a more precise model called linear parameter varying (LPV) model is developed by retaining higher order terms while processing linearization. Furthermore, the nonlinear system model could be explicitly described by so-called Quasi-Linear-Parameter-Varying Model without any approximation. The QLPV model can be developed by using Barbashin method. Based on the QLPV model, the applicability of linear control design method is preserved while retaining the nonlinearities of the full system dynamics [19]. An application of nonlinear controller design using polynomial eigenstructure assignment based on QLPV model is presented in [19].

For LPV model, adaptive control theory could also be used to obtain a gain scheduling controller $K(p)$ for the overall flight envelop.

4.4 Backstepping

Backstepping is a recursive, Lyapunov-based nonlinear design method, which could be applied to nonlinear system in a lower-triangular form. It is emerged in recent years. This nonlinear design method have shown great potential due to its flexibility and avoiding cancellation of useful nonlinearities [20]. However, it also has a drawback that a Lyapunov function has to be found in order to apply this method [21].

The idea of backstepping is that a controller is designed recursively by considering some of the state variables as 'virtual controls' and designing intermediate control laws for them using Lyapunov-based design method. Hence, Sonneveldt, L. [22] stated that the backstepping control law is recursively constructed, along with a control Lyapunov function (clf) to guarantee global stability. Considering following system model with lower-triangular form

$$\dot{x}_1 = f(x_1) + g(x_1)\, x_2 \tag{4.1}$$

$$\dot{x}_2 = u \tag{4.2}$$

First of all, consider x_2 as the virtual control of the x_1-subsystem and find a virtual control law $\alpha_1(x_1)$ that stabilizes the subsystem by using the control Lyapunov function $V_1(x_1)$.

$$V_1(x_1) = \frac{1}{2} x_1^2 \tag{4.3}$$

The virtual control law

$$x_2 = \alpha_1(x_1)$$

is selected to guarantee the time derivative of this clf is negative definite shown as follows.

$$\dot{V}_1 = \frac{\partial V_1}{\partial x_1}(x_1)\left(f(x_1) + g(x_1)\,\alpha_1(x_1)\right) < 0, \qquad x \neq 0 \tag{4.4}$$

Secondly, define the error between x_2 and its desired value as

$$z = x_2 - \alpha_1(x_1) \tag{4.5}$$

and rewrite the system (4.1) in terms of error state.

$$\dot{x}_1 = f(x_1) + g(x_1)\left(\alpha_1(x_1) + z\right) \tag{4.6}$$

$$\dot{z} = u - \frac{\partial \alpha}{\partial x_1}(x_1)\left(f(x_1) + g(x_1)\left(\alpha_1(x_1) + z\right)\right) \tag{4.7}$$

Now, the clf (4.4) can be expanded with a term penalizing the error state z

$$V_2(x_1, z) = V_1(x_1) + \frac{1}{2}z^2 \tag{4.8}$$

The time derivative of V_2 is equal to

$$\dot{V}_2 = \frac{\partial V_1}{\partial x_1}\left(f + g\left(\alpha_1 + z\right)\right) + z\left(u - \frac{\partial \alpha}{\partial x_1}\left(f + g\left(\alpha_1 + z\right)\right)\right) \tag{4.9}$$

$$= \frac{\partial V_1}{\partial x_1}\left(f + g\alpha_1\right) + z\left(\frac{\partial V_1}{\partial x_1}g + u - \frac{\partial \alpha}{\partial x_1}\left(f + g\left(\alpha_1 + z\right)\right)\right) \tag{4.10}$$

which can be rendered negative definite with the control law

$$u = -cz + \frac{\partial \alpha}{\partial x_1}\left(f + g\left(\alpha_1 + z\right)\right) - \frac{\partial V_1}{\partial x_1}g, \qquad c > 0$$

In short, starting with the triangular form of the nonlinear system, each step of the backstepping, namely designing a control law for the virtual control, can be divided into three parts [22]:

- Introduce a virtual cotnrol α and an error state z, and rewrite the current state equation in terms of these,
- Choose a clf for system, treat it as a final stage,
- Choose a control law for the virtual control that makes the clf stable.

These three actions should be carried out for each backstepping step. Thus, it could be argued that backstepping technique is a recursive control design method.

Chapter 5

Flying and handling quality criteria

5.1 American military standard

DEF-STAN 00-970 and MIL-F-8785C are flying and handling quality requirements to cope with conventional aircraft whose short period mode behaviour is second order like. However, they are not appropriate for highly augmented advanced aircraft. Along with people's understanding of handling quality is improving, Hoh et al.'s report provided a proposal which could be applied to evaluate the flying quality of highly augmented aircraft in 1982. His report is included into American military standard MIL-STD-1797A. It is a considerable progress for handling quality used for highly augmented aircraft from DEF-STAN 00-970 and MIL-F-8785C to MIL-STD-1797A [1]. And MIL-STD-1797A still includes most stability requirement for classical aircraft in DEF-STAN 00-970 and MIL-F-8785C.

MIL-F-8785C categorizes the degrees of flying quality to 3 levels: 1, 2 and 3, according to specific aircraft class and flight phase. The aircraft are divided into 4 classes: I, II, III and IV, while the flight phases are sorted in 3 categories: A, B and C.

The table below shows the requirements for short period mode damping.

Table 5.1: Short period mode damping. Source:[2]

Flight phase	Level 1		Level 2		Level 3
	$\zeta_s$min	$\zeta_s$max	$\zeta_s$min	$\zeta_s$max	$\zeta_s$min
CAT A	0.35	1.3	0.25	2	0.1
CAT B	0.3	2	0.2	2	0.1
CAT C	0.5	1.3	0.35	2	0.25

Table 5.2: Phugoid damping ratio. Source:[2]

Level of flying qualities	Minimum damping ratio
1	0.04
2	0
3	Unstable, period $T_p > 55s$

The short period frequency requirements are clarified relating to n_α, namely normal load factor per unit angle of attack. Low speed is coincidence with low value of n_α. In general, low speed requires low frequency, while at high speed, the frequency should be higher. For example, the requirement of short period frequency for flight phase category B is shown in figure 5.1. The requirements for lateral dynamic stability could be found in MIL-F-8785C as well. It is no longer presented here.

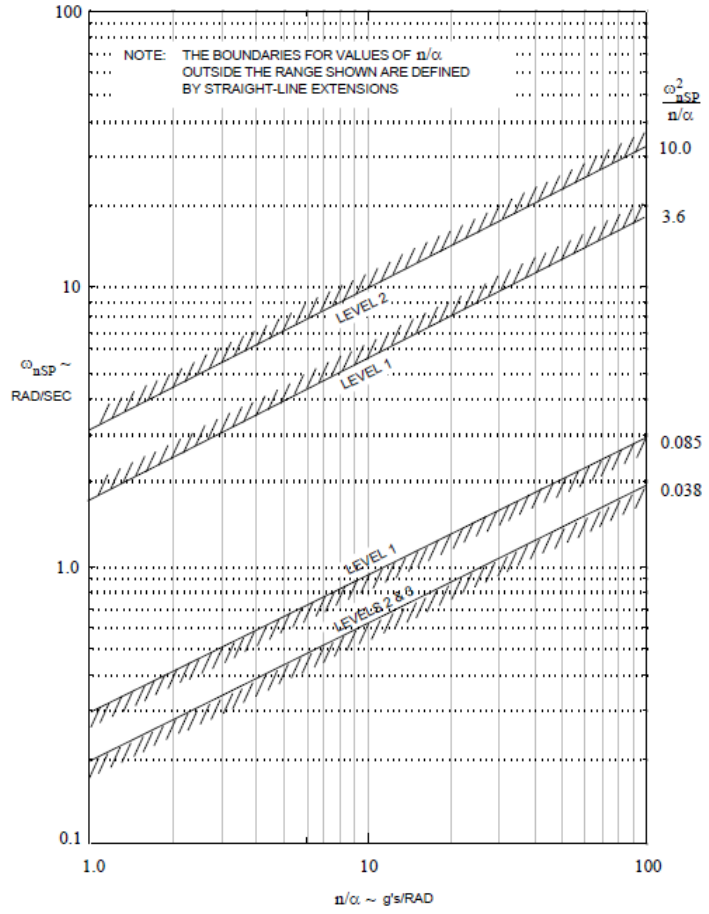

Figure 5.1: frequency requirement for category B flight phase Source: [2]

5.2 C* criteria

In above section the C* controller has been introduced, and here we will give a brief definition of C* criterion. C* criterion give two boundaries for time response of C* for 1 step elevator input. These two boundaries are named category 1 and 4 corresponding to category A and category C flight phase. The category 1 is used for tracking task meanwhile the category 4 is applied when perform take-off and landing task. C* criterion is derived from extensive flight tests and flight experiences. The C* criteria in the time domain is indicated in following figure. C* criteria is more

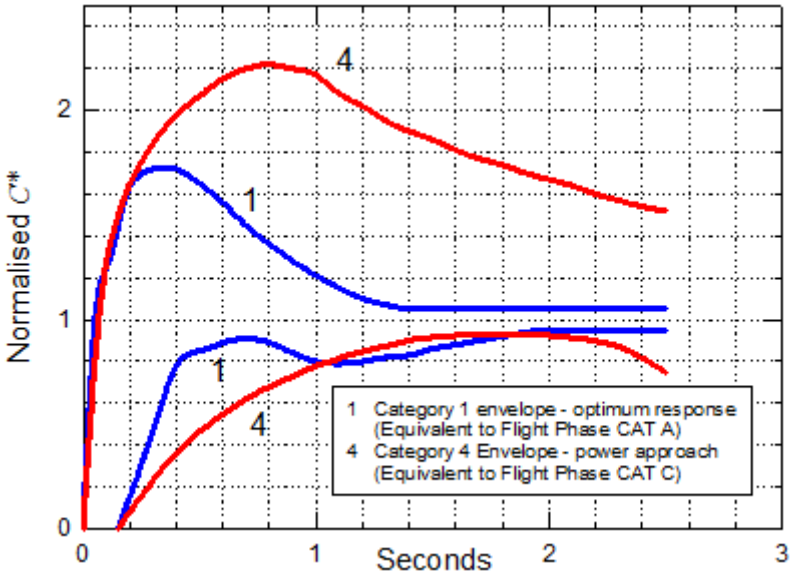

Figure 5.2: C* criteria in time domain. Source:[3]

often applied in the frequency domain as it is difficult to evaluate in the time domain. C* criteria in a form of Bode diagram is shown below.

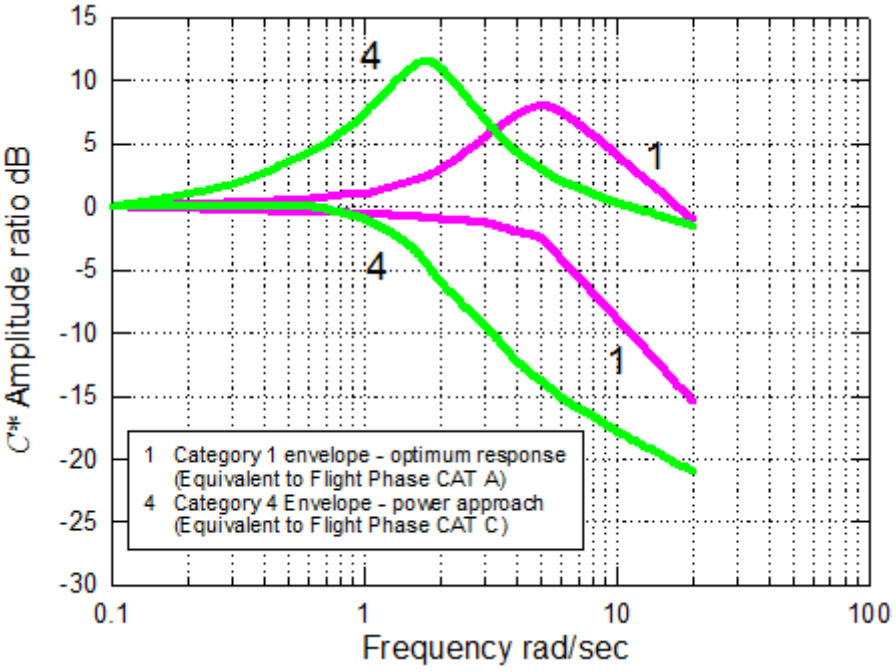

Figure 5.3: C* criteria in frequency domain. Source:[3]

5.3 Gibson criteria

Traditional flying and handling quality criteria are concerned with short period damping ratio and frequency. For a typical second order like aircraft, this could guarantee a good response of angle of attack α, normal acceleration a_z and q. However, there is no direct attention paid to responses of pitch attitude and fly path which are also significant in pilot perception of handling quality. Gibson [3] pointed that although the short period damping and undamped natural frequency are well designed to meet the traditional handling quality requirement the pitch attitude and fly path responses may still be unacceptable. There might be following three reasons given in M. Cook's lecture notes [3]:

1. For highly augmented airplane, the airplane behaves less like a second order system;
2. Since pitch attitude is not a design target parameter for traditional handling quality requirements, it is easily changed without intention.
3. For classical aircraft, the time lag T_θ remain constant because of the limitation of flight envelop. However, T_θ variation could be found in the aircraft operating in large envelope or the aircraft using direct lift control (DLC). It is T_θ variation that could cause handling qualities problems.

Thereby, Gibson criteria concerned more on pitch attitude and fly path response. The Gibson criteria consists of two criteria relating to longitudinal handling qualities: Dropback criterion and Phase rate criterion [3].

Dropback criterion is concerned with two parameters of pitch attitude response and pitch rate response: $q_m/q_s$and DB/q_s. q_m is the peak of q response and q_s is the steady state of q response. Attitude Dropback namely DB is defined as the displacement from the linear part of the real attitude response to the line $\theta(t) = q_s \cdot t$. Dropback criterion and phase rate criterion are illustrated in figure 5.4 and figure 5.5 below.

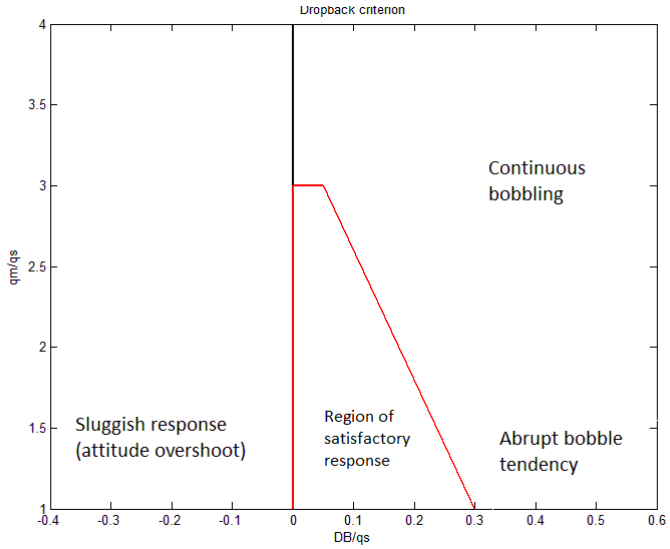

Figure 5.4: Dropback criterion. Source: [3]

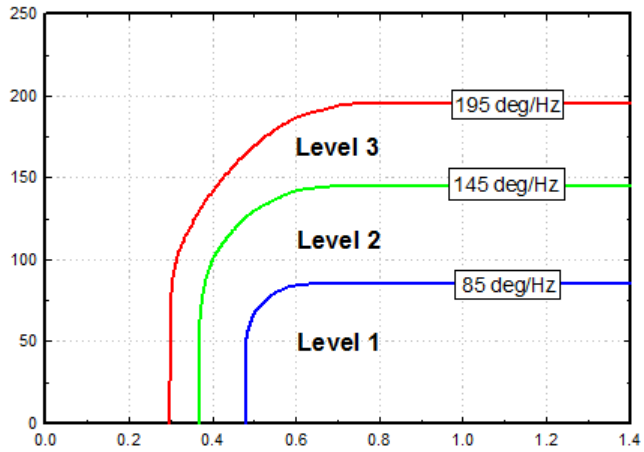

Figure 5.5: Phase rate criterion. Source: [3]

Chapter 6

Nonlinear dynamic inversion (NDI)

6.1 NDI theory introduction

Dynamic inversion synthesis is a controller design technique which is able to cancel out the original plant dynamic that is deficient or undesirable, and replace it by desirable dynamics. This method is realized by carefully selecting the feedback function. Dynamic inversion can be used in both state feedback and output feedback. The basic assumption is that the plant dynamic is known exactly and can be completely cancelled out. However, in practical application, plant dynamic model is impossible to be perfect, therefore robust ability is usually required for dealing with possible uncertainties. [23, p.7]

Since the dynamic of aircraft is inherently nonlinear, the linear design tools have to design a feedback gains for each operating point based on the linear model, and then schedule all these gains for the overall flight envelop. However, nonlinear dynamic inversion theory allows to directly design control system for nonlinear model through cancelling out the aircraft dynamic. Thus, dynamic inversion technique has been becoming popular in aircraft industry in recent years.[12, p.484-485]

Nonlinear dynamic inversion is based on developments of two vital aspects of control theory which are feedback linearization and non-interacting control law. Feedback linearization is a technique that could algebraically transform the nonlinear dynamic system into an equivalent linear system through exact state transformation rather than by linear approximations of dynamics [23, p.1] [24, p.207]. The basic theory of nonlinear dynamic inversion could be found in many books such as [24], [17] and [25].

Below introduction to nonlinear dynamic inversion theory is represented in reference [24]. Consider following nonlinear system described by companion form:

$$\begin{aligned} \dot{x} &= f(x) + g(x)\,u \\ y &= h(x) \end{aligned} \tag{6.1}$$

Take time derivative of y trying to find the relationship between output y and input

u, since y is not directly related with u in above dynamic equations. As a result, an equation is given as follow.

$$\dot{y} = \frac{\partial h}{\partial x} \cdot \frac{\partial x}{\partial t} = \nabla h \left(f + gu \right) = L_f h \left(x \right) + L_g h \left(x \right) u \tag{6.2}$$

Where $L_f h(x) = \nabla h f$ is known as the first order Lie derivative vector [9] and $L_g h(x) u = \nabla h g u$. If $L_g h(x) u \neq 0$, then the input transformation can be introduced such that lead to a simple linear dynamic.

$$v = L_f h \left(x \right) + L_g h \left(x \right) u \tag{6.3}$$

Then

$$\dot{y} = v \tag{6.4}$$

This is a very simple linear system behaving like a pure first order integral.

If $L_g h(x) u = 0$, more time derivative of y is required until this term is nonzero. If we need to differentiate the output equation r times to get the explicit relationship between output and input, r is defined as 'relative degree' of the system. This relative degree is equal to the excess of poles over zeros for the linear system. Assuming that r times derivatives are required for the output equation, namely $L_g L_f^{r-1} h \left(x \right) \neq 0$, the following outcome is yielded.

$$y^{(r)} = L_f^r h \left(x \right) + L_g L_f^{r-1} h \left(x \right) u \tag{6.5}$$

Let $v = L_f^r h \left(x \right) + L_g L_f^{r-1} h \left(x \right) u$ then $y^{(r)} = v$ is gained. The system becomes a pure r order integrator as a result of the introduction of new input v. Then

$$u = \left(L_g L_f^{r-1} h \left(x \right) \right)^{-1} \left(v - L_f^r h \left(x \right) \right) \tag{6.6}$$

The method processed above is technically known as 'input-output linearization'. If n times derivative of y are needed to let u appear in equation (8), which is equal to the order of system, the system can be linearized using 'input-state linearization' methods, where $\{ y, \dot{y}, \ddot{y}, \cdots, y^{(n-1)} \}$ is set to be new state vector. It means that the nonlinear system is fully linearized by input-state linearization, which means there is no internal dynamic exists.

Once the nonlinear system has been linearized by feedback linearization, becoming a very simple linear dynamic, all the linear control techniques may be applied to achieve the control objectives, such as pole placement. A general NDI controller structure is shown below. The inner loop is feedback linearization loop which functions linearization of the system. The outer loop is feedback control loop which is responsible for stabilization of the new linear system. Thus the NDI control law comprises of two parts: feedback linearization control law and the outer loop stabilization linear control law [24]. Regarding stability augmentation problem, the control law is

$$v = -k_0 y - k_1 \dot{y} - \ldots - k_{r-1} y^{(r-1)} \tag{6.7}$$

With k_i is chosen so that the characteristic equation $p^n + k_{n-1} p^{n-1} + \ldots + k_1 \dot{p} + k_0$ has all its poles on the left-hand side of the complex plane, leads to the exponentially stable dynamics.

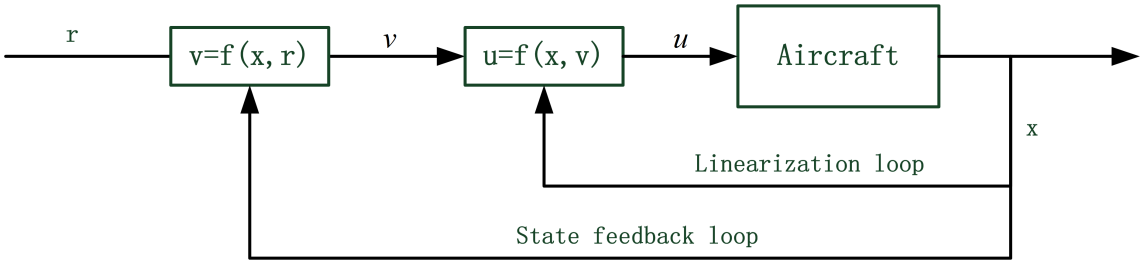

Figure 6.1: Basic structure of dynamic inversion

For command tracking control problem, the control law

$$v = y_c^{(r)} - k_0 e - ... - k_{n-1} e^{(r-1)} \tag{6.8}$$

Where $e = y - y_c$ is the tracking error, leads to an exponentially convergent tracking error dynamics, namely $e(t) \to 0$.

The NDI theory could be also easily applied in linear system. Considering a linear aircraft model

$$\begin{aligned} \dot{x} &= Ax + Bu \\ y &= Cx \end{aligned} \tag{6.9}$$

Taking time derivative of y, yields

$$\dot{y} = C\dot{x} = C\left(Ax + Bu\right) = CAx + CBu \tag{6.10}$$

For aircraft, CB is usually nonzero. Then, a new input is defined as follow.

$$v = CAx + CBu \tag{6.11}$$

Then the real input could be calculated as

$$u = \left(CB\right)^{-1}\left(v - CAx\right)$$

So that we have $\dot{y} = v$, that behaves like a pure integrator. v is also the first order derivative of the control variable. For rotation angular rate control, v are $\{\dot{p}, \dot{q}, \dot{r}\}$. For control tracking problem, the control law

$$v = \dot{y}_c - ke$$

Where $e = y - y_c$, is simply chosen. k is selected so that the error dynamic is stable which implies $e\left(t\right) \to 0$. A general dynamic inversion controller structure for linear aircraft model is manifested as below.

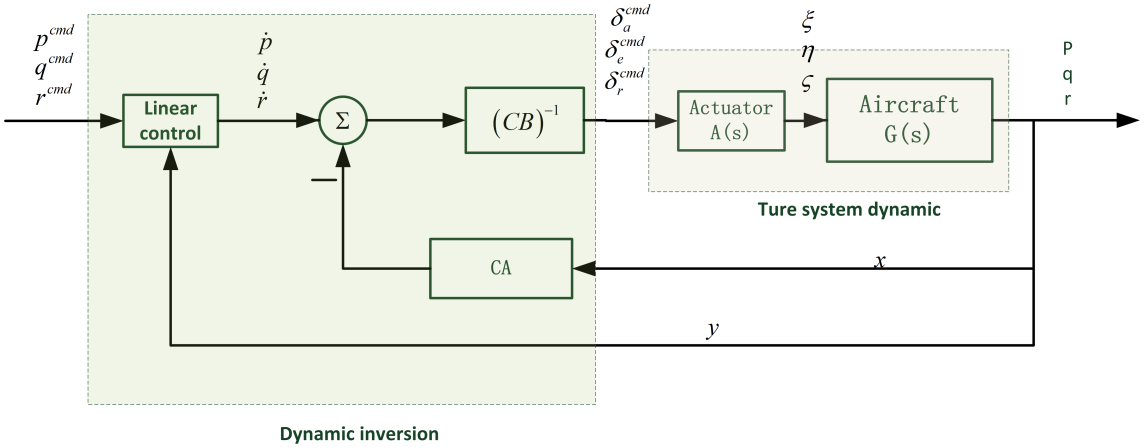

Figure 6.2: Linear system dynamic inversion controller structure

6.2 Nonlinear aircraft model

The coupled nonlinear equations of motion of an aircraft with body axes are generalized in M. Cook's book [9] as follows

$$\begin{aligned} m\left(\dot{U} - rV + qW\right) &= X_a + X_g + X_c + X_d \\ m\left(\dot{V} - pW + rU\right) &= Y_a + Y_g + Y_c + Y_d \\ m\left(\dot{W} - qU + pV\right) &= Z_a + Z_g + Z_c + Z_d \end{aligned} \tag{6.12}$$

$$\begin{aligned} I_x\dot{p} - (I_y - I_z)\,qr - I_{xz}\,(pq + \dot{r}) &= L_a + L_g + L_c + L_d \\ I_y\dot{q} + (I_x - I_z)\,pr + I_{xz}\,(p^2 - r^2) &= M_a + M_g + M_c + M_d \\ I_z\dot{r} - (I_x - I_y)\,pq + I_{xz}\,(qr - \dot{p}) &= N_a + N_g + N_c + N_d \end{aligned} \tag{6.13}$$

With

$$\begin{aligned} U &= U_e + u \\ V &= V_e + v \\ W &= W_e + w \end{aligned}$$

where the p, q and r are the components of the angular velocity about the body axes; U, V and W are components of velocity of aircraft about body axes. Subscript a, g, c, p and d respectively denote aerodynamic force, gravity, control force, thrust and disturbance force. L, M and N denote moments about three body axes. I means the inertia. [9, p.72-73]

In regards to nonlinear dynamic inversion application, the three moment equations should be used. Keep time derivatives of angular rate at left side, and move all other items to right side, below equations are derived from 6.44 given in reference [23].

$$\begin{aligned} \dot{p} &= \tfrac{I_zL + I_{xz}N}{I_xI_z - I_{xz}^2} + \tfrac{I_{xz}(I_x - I_y + I_z)pq}{I_xI_z - I_{xz}^2} + \tfrac{\left[I_z(I_y - I_z) - I_{xz}^2\right]qr}{I_xI_z - I_{xz}^2} \\ \dot{q} &= \tfrac{1}{I_y}\left[M + (I_z - I_x)\,pr + I_{xz}\,(r^2 - p^2)\right] \\ \dot{r} &= \tfrac{I_{xz}L + I_xN}{I_xI_z - I_{xz}^2} - \tfrac{I_{xz}(I_x - I_y + I_z)qr}{I_xI_z - I_{xz}^2} + \tfrac{\left[I_x(I_x - I_y) + I_{xz}^2\right]pq}{I_xI_z - I_{xz}^2} \end{aligned} \tag{6.14}$$

Where L, M and N are respectively the total moments about three axes. Since the body coordinate origin coincides with the gravity center, it is said that in [9]

$$L_g = M_g = N_g = 0 \tag{6.15}$$

$$\begin{aligned} X_g &= -mg\sin\theta_e - mg\theta\cos\theta_e \\ Y_g &= mg\psi\sin\theta_e + mg\phi\cos\theta_e \\ Z_g &= mg\cos\theta_e - mg\theta\sin\theta_e \end{aligned} \tag{6.16}$$

Primary control surfaces of aircraft are aileron, elevator and rudder. Control surfaces deflections change the aerodynamic condition, in turn give rise to producing moments and forces. Thus, it is normal to calculate the forces and moments produced by control surfaces by aerodynamic control derivatives. One thing should be stressed is that all following equations are expressed in terms of normalized American derivatives notation.

$$\begin{aligned} X_c &= m\left(X_{\delta_e}\delta_e + X_{\delta_{th}}\delta_{th}\right) \\ Y_c &= m\left(Y_{\delta_a}\delta_a + Y_{\delta_r}\delta_r\right) \\ Z_c &= m\left(Z_{\delta_e}\delta_e + Z_{\delta_{th}}\delta_{th}\right) \end{aligned} \tag{6.17}$$

The moment items due to control surface could be written in form of concise American normalized derivatives according to reference [9] as follows:

$$\begin{aligned} M_c &= M_{\delta_e}\delta_e + M_{\delta_{th}}\delta_{th} \\ L_c &= L'_{\delta_a}\delta_a + L'_{\delta_r}\delta_r \\ N_c &= N'_{\delta_a}\delta_a + N'_{\delta_r}\delta_r \end{aligned} \tag{6.18}$$

With respect to the forces and moments generated by aerodynamic force, an approximation is usually used, omitting the high order items of the Taylor series [9].

$$\begin{aligned} X_a &= mg\sin\theta_e + m\left(X_u u + X_{\dot{w}}\dot{w} + X_w w + X_q q\right) \\ Z_a &= -mg\cos\theta_e + m\left(Z_u u + Z_{\dot{w}}\dot{w} + Z_w w + Z_q q\right) \\ Y_a &= m\left(Y_v v + Y_p p + Y_r r\right) \end{aligned} \tag{6.19}$$

Same as before, the moment items contributed by aerodynamic forces could be rewritten in form of American normalized derivatives according to reference [9] as follows:

$$\begin{aligned} M_a &= M_u u + M_{\dot{w}}\dot{w} + M_w w + M_q q \\ L_a &= L'_v v + L'_p p + L'_r r \\ N_a &= N'_v v + N'_p p + N'_r r \end{aligned} \tag{6.20}$$

Assume that all moments and force caused by disturbance are zero. Thus substitute equations from (6.15) to (6.20) into equations (6.12) and (6.13), following nonlinear motion equations are gained.

For longitudinal mode:

$$\begin{aligned} \dot{u} &= X_u u + X_{\dot{w}}\dot{w} + X_w w + \left(X_q - W_e\right) q + X_{\delta_e}\delta_e + X_{\delta_{th}}\delta_{th} - g\theta\cos\theta_e + \left(rV_e + rv - qw\right) \\ \dot{w} &= Z_u u + Z_{\dot{w}}\dot{w} + Z_w w + \left(Z_q + U_e\right) q + Z_{\delta_e}\delta_e + Z_{\delta_{th}}\delta_{th} - g\theta\sin\theta_e + \left(qu - pV_e - pv\right) \\ \dot{q} &= M_u u + M_{\dot{w}}\dot{w} + M_w w + M_q q + M_{\delta_e}\delta_e + M_{\delta_{th}}\delta_{th} + \frac{(I_z - I_x)pr + I_{xz}\left(r^2 - p^2\right)}{I_y} \\ \dot{\theta} &= q \end{aligned} \tag{6.21}$$

With an alternative expression for w

$$\alpha = \frac{w}{V_{TO}}$$

For lateral mode:

$$\begin{aligned}
&\dot{v} = Y_v v + (Y_p + W_e)\, p + (Y_r - U_e)\, r + Y_{\delta_a}\delta_a + Y_{\delta_r}\delta_r + g\phi\cos\theta_e + g\psi\sin\theta_e + pw - ru \\
&\dot{p} = L'_v v + L'_p p + L'_r r + L'_{\delta_a}\delta_a + L'_{\delta_r}\delta_r + \frac{I_{xz}(I_x - I_y + I_z)pq + \left[I_z(I_y - I_z) - I_{xz}^2\right]qr}{I_x I_z - I_{xz}^2} \\
&\dot{r} = N'_v v + N'_p p + N'_r r + N'_{\delta_a}\delta_a + N'_{\delta_r}\delta_r + \frac{-I_{xz}(I_x - I_y + I_z)qr + \left[I_x(I_x - I_y) + I_{xz}^2\right]pq}{I_x I_z - I_{xz}^2} \\
&\dot{\phi} = p + rtg\,(\theta_e) \\
&\dot{\psi} = r/\cos\,(\theta_e)
\end{aligned} \tag{6.22}$$

With alternative expression for v

$$\beta = \frac{v}{V_{TO}}$$

Then the lateral mode could be rewritten as

$$\begin{aligned}
\dot{\beta} =& Y_v\beta + \frac{1}{V_{TO}}(Y_p + W_e)\, p + \frac{1}{V_{TO}}(Y_r - U_e)\, r + Y^*_{\delta_a}\delta_a + Y^*_{\delta_r}\delta_r \\
&+ \frac{1}{V_{TO}}(g\phi\cos\theta_e + g\psi\sin\theta_e + pw - ru)
\end{aligned} \tag{6.23}$$

$$\begin{aligned}
\dot{p} =& L'_\beta\beta + L'_p p + L'_r r + L'_{\delta_a}\delta_a + L'_{\delta_r}\delta_r \\
&+ \frac{I_{xz}(I_x - I_y + I_z)pq + \left[I_z(I_y - I_z) - I_{xz}^2\right]qr}{I_x I_z - I_{xz}^2}
\end{aligned} \tag{6.24}$$

$$\begin{aligned}
\dot{r} =& N'_\beta\beta + N'_p p + N'_r r + N'_{\delta_a}\delta_a + N'_{\delta_r}\delta_r \\
&+ \frac{-I_{xz}(I_x - I_y + I_z)qr + \left[I_x(I_x - I_y) + I_{xz}^2\right]pq}{I_x I_z - I_{xz}^2}
\end{aligned} \tag{6.25}$$

Where

$$\begin{array}{ll}
Y^*_{\delta_a} = \frac{Y_{\delta_a}}{V_{TO}} & Y^*_{\delta_r} = \frac{Y_{\delta_r}}{V_{TO}} \\
L'_\beta = L'_v V_{TO} & N'_\beta = N'_v V_{TO}
\end{array}$$

For easier comparison between coupled nonlinear motion equations and decoupled linear motion equations, the decoupled linear motion equations are given as below.

Longitudinal mode:

$$\begin{aligned}
&\dot{u} = X_u u + X_{\dot{w}}\dot{w} + X_w w + (X_q - W_e)\, q + X_{\delta_e}\delta_e + X_{\delta_{th}}\delta_{th} - g\theta\cos\theta_e \\
&\dot{w} = Z_u u + Z_{\dot{w}}\dot{w} + Z_w w + (Z_q + U_e)\, q + Z_{\delta_e}\delta_e + Z_{\delta_{th}}\delta_{th} - g\theta\sin\theta_e \\
&\dot{q} = M_u u + M_{\dot{w}}\dot{w} + M_w w + M_q q + M_{\delta_e}\delta_e + M_{\delta_{th}}\delta_{th} \\
&\dot{\theta} = q
\end{aligned} \tag{6.26}$$

Lateral mode:

$$\begin{aligned}
&\dot{v} = Y_v v + (Y_p + W_e)\, p + (Y_r - U_e)\, r + Y_{\delta_a}\delta_a + Y_{\delta_r}\delta_r + g\phi\cos\theta_e + g\psi\sin\theta_e \\
&\dot{p} = L'_v v + L'_p p + L'_r r + L'_{\delta_a}\delta_a + L'_{\delta_r}\delta_r \\
&\dot{r} = N'_v v + N'_p p + N'_r r + N'_{\delta_a}\delta_a + N'_{\delta_r}\delta_r \\
&\dot{\phi} = p + rtg\,(\theta_e) \\
&\dot{\psi} = r/\cos\,(\theta_e)
\end{aligned} \tag{6.27}$$

It is easily seen that all the coupled items and the insignificant items are omitted such that these equations become decoupled and linear.

However, these aerodynamic coefficients do not remain constant throughout the entire flight envelop, varying according to flight conditions. Thus, it is necessary that the NDI controller should take the variations of aerodynamic coefficients into account. Updating the controller by all data of every individual operation point is not a practical way to do it, which is replaced by making an approximation for the variations of these aerodynamic coefficient. Below approximations called least-squares aerodynamic model are given.

Longitudinal:

$$C_i = K_1(\alpha)\frac{\bar{c}}{2V}q + K_2(\alpha)\delta_e + K_3(\alpha), \quad i = D, L, m \tag{6.28}$$

Lateral:

$$C_i = K_4(\alpha)\beta + K_5(\alpha)\frac{b}{2V}p + K_6(\alpha)\frac{b}{2V}r + K_7(\alpha)\delta_a + K_8(\alpha)\delta_r, i = Y, l, n \tag{6.29}$$

With

$$\begin{aligned} C_m &= M/qS\bar{c} \\ C_n &= N/qSb \\ C_l &= L/qSb \end{aligned}$$

All the K_s are functions of angle of attack only.

6.3 Feedback linearization for nonlinear aircraft equations

Feedback linearization could be done based on above nonlinear motion equations. In general, nonlinear dynamic motion equations could be written as [26].

$$\begin{bmatrix} \dot{p} \\ \dot{q} \\ \dot{r} \end{bmatrix} = \begin{bmatrix} f_p(x) \\ f_q(x) \\ f_r(x) \end{bmatrix} + g(x) \begin{bmatrix} \delta_a \\ \delta_e \\ \delta_r \\ \delta_{th} \end{bmatrix} \tag{6.30}$$

Where

$$x = [\psi, \theta, \phi, p, q, r, u, v, w]$$

$$g(x) = \begin{bmatrix} g_{p_{\delta a}}(x) & 0 & g_{p_{\delta r}}(x) & 0 \\ 0 & g_{q_{\delta e}}(x) & 0 & g_{q_{\delta th}}(x) \\ g_{r_{\delta a}}(x) & 0 & g_{r_{\delta r}}(x) & 0 \end{bmatrix}$$

For example

$$\begin{aligned} f_p(x) &= L'_v v + L'_p p + L'_r r + \frac{I_{xz}(I_x - I_y + I_z)pq + \left[I_z(I_y - I_z) - I_{xz}^2\right]qr}{I_x I_z - I_{xz}^2} \\ g_{p_{\delta a}} &= L'_{\delta_a} \end{aligned} \tag{6.31}$$

Therefore, the general expression of nonlinear dynamic inversion is given as

$$\begin{bmatrix} \delta_a \\ \delta_e \\ \delta_r \\ \delta_{th} \end{bmatrix} = g^{-1}(x) \left(\begin{bmatrix} \dot{p} \\ \dot{q} \\ \dot{r} \end{bmatrix} - \begin{bmatrix} f_p(x) \\ f_q(x) \\ f_r(x) \end{bmatrix} \right) \tag{6.32}$$

In this case, the control matrix must be invertible for all existing admissible values of x. However, according to Jennifer Georgie And John Valasek [27], $g(x)$ is not invertible for so-called differentially non-flat systems, whose control variables are more than the control inputs. Hence, the number of system control variable is required less or equal to the number of control inputs, otherwise the system is underactuated and not invertible. Even if the control matrix $g(x)$ is invertible but the magnitude of $g(x)$ is very small, this may give rise to control ineffectiveness, in other words, control surface will become unbounded, in turn this may cause actuator saturation. Such a problem is underwent when use NDI controller to control angle of attack, as the elevator have very little influence on angle of attack namely the $g(x)$ magnitude is very small in this case. A technique called time-scale separation method is invented to resolve this problem [27].

The entire control variables of aircraft are sorted as two groups which are fast dynamic variables and slow dynamic variables. This separation of fast dynamic variables and slow dynamic variables is called two-time-scale separation method. With application of this method, the system could be written as two general differential equations such that the control inputs appear in only one equation.

$$\begin{aligned} \dot{x}_1 &= \bar{f}_1(x_1) + \hat{B}_1(x_1)\, x_2 \\ \dot{x}_2 &= \bar{f}_2(x_1, x_2) + \hat{B}_2(x_1, x_2)\, \bar{u} \end{aligned} \tag{6.33}$$

First, the desired is generated by linear control law such as $\dot{x}_{1d} = g(x_{1c} - x_1)$. Then the command value of x_{2c} could be computed from the equation (6.33) as below.

$$x_{2c} = \hat{B}_1^{-1}(x_1) \left[\dot{x}_{1d} - \bar{f}_1(x_1) \right] \tag{6.34}$$

Afterward, repeat above inversion process again to obtain input by following two equations:

$$\dot{x}_{2d} = g(x_{2c} - x_2) \tag{6.35}$$

$$\bar{u} = \hat{B}_2^{-1}(x_1, x_2) \left[\dot{x}_{2d} - \bar{f}_2(x_1, x_2) \right] \tag{6.36}$$

In aircraft design application, if the slow state variable is chosen as control variable, two-Time-scale separation method divides the inversion process into two steps. One step is so-called slow dynamic inversion which is from time derivatives of attitude angle such as $\dot{\theta}_d$, $\dot{\beta}_d$ and $\dot{\phi}_d$ to calculate attitude angle rate p, q, and r command. The second step is the inversion from time derivatives of attitude angle rate to yield the surface deflections δ_e, δ_r, δ_r command or thrust vector command. [28]

An example of entire structure of 2 time-scale inversion is illustrated in figure 6.3.

An alternative way is that using a second order dynamic inversion control law directly yields input u from desired time derivatives of attitude angle. For example, input δ_e is calculated from $\ddot{\alpha}_d$ by a second order inversion, although δ_e have little effect on $\dot{\alpha}$. [4]

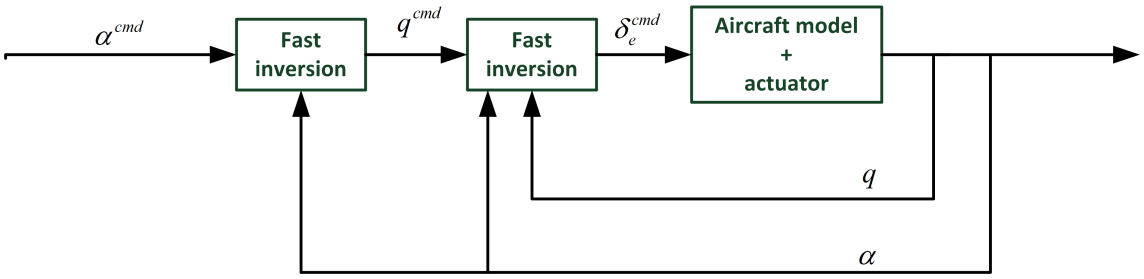

Figure 6.3: 2 time-scale inversion method

6.4 Internal dynamic

If the relative degree is equal to system order n, the feedback linearization is called input-state feedback linearization which entirely linearizes system via transform system states into a new state space. However, the system is merely partly linearized if the relative degree r is less than system order n, which is called input-output feedback linearization. In this case, the new linearized system only have r order, therefore n-r states are missing which are considered 'unobservable' in the input-output linearization. This part of the dynamics is called internal dynamics since it cannot be seen from the external outputs.

The NDI controller stability and performance could be dramatically deteriorated by the instability of internal dynamics. The stability of these n-r poles could be easily checked through zero-dynamic technique. Let us introduce zero-dynamics as follows.

When the relative degree r is defined and $r < n$, $y, \dot{y}, \cdots, y^{r-1}$can be found as part of the new state components of the linearized system. Let

$$\mu = (\mu_1, \mu_2, \cdots, \mu_r)^T = (y_1, \dot{y}, \cdots, y^{r-1})^T \tag{6.37}$$

In a neighborhood Ω of point x_0 be the part state space of the linearized system. According to the lemma in Slotine and Li's book, there exist a $n - r$ order vector $\psi = (\psi_1, \psi_2, \cdots, \psi_{n-r})$, such that the vector μ and ψ are combined as a new state space which is so-called normal coordinates or normal states in Ω. Then the system could be rewritten as

$$\dot{\mu} = \begin{pmatrix} \mu_2 \\ \cdots \\ \cdots \\ \mu_r \\ a(\mu, \psi) + b(\mu, \psi)u \end{pmatrix} \tag{6.38}$$

$$\dot{\psi} = w(\mu, \psi) \tag{6.39}$$

with the output defined as

$$y = \mu_1 \tag{6.40}$$

The dynamics of ψ is considered as internal dynamics. If we keep the outputs of the original system zero, then we have a dynamic shown as below which is zero-

dynamics. The zero-dynamics is defined to be the internal dynamics of the system when the system output is kept at zero by the input [24].

Zero-dynamics have advantage of only containing internal state variables comparing to internal dynamics. Thus, the stability of internal dynamics could be easily verified by verifying the stability of zero-dynamics. NDI controller is feasible on condition that the zero-dynamic of nonlinear system is stable. A system has unstable zero-dynamic which implies that internal dynamic is unstable amount to the system having non-minimum phase which is as a result of positive zeros. The zero-dynamic is different due to different output y, so the zero-dynamic could be ensured stable by carefully selecting output y [24].

6.5 Desired dynamic

In this section, some methods of designing the desired dynamic which is the most significant part in NDI are introduced. After dynamic inversion, the aircraft model has become a pure integrator. Therefore performance of the controller is completely depended on the control law of the desired dynamic. Georgie and Valasek [27] gave us some 4 methods to design desired dynamics for dynamic inversion controller. They are: proportional control law, PI (proportional plus integral) control law, dynamics satisfying various flying quality levels and dynamics corresponding to passenger ride quality. Here 3 of them are introduced and there are also many other control laws for desired dynamic design and some of them are revealed in the NDI application review section.

The first one is proportional dynamics which is the simplest one. The control law is given as

$$C\dot{V}_{des} = K_p \left(CV_{cmd} - CV\right) \tag{6.41}$$

where CV is the control variable of NDI controller. Below chart shows the overall structure of proportion control law for desired dynamics based on angular rate control variables. Gain Kp simply amplifies the error between commands and feed-

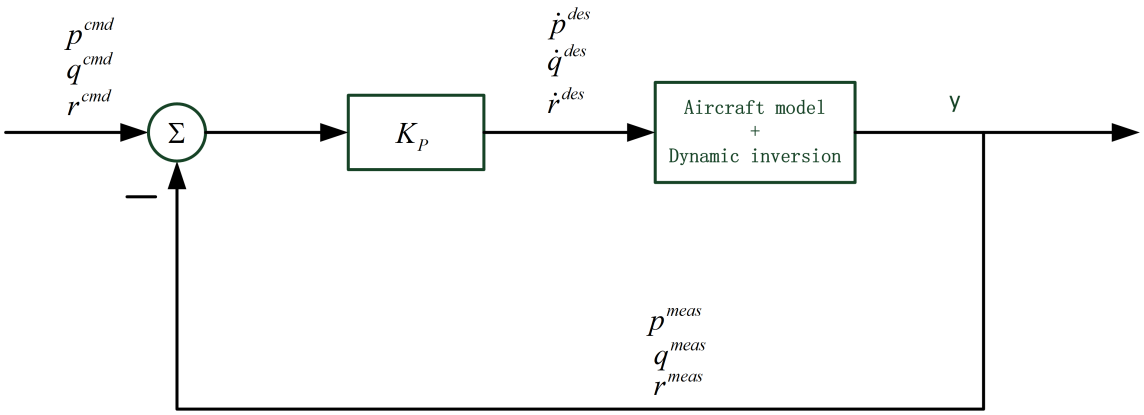

Figure 6.4: Proportion desired dynamic

back items. If dynamic inverted aircraft model is treated approximately as a pure integrator, the close loop transfer function can be calculated as

$$\frac{CV}{CV_{cmd}} = \frac{K_p}{s + K_p} \tag{6.42}$$

It is a first order transfer function, hence the output exponentially converge to the steady state. The convergence speed is controlled by the pole position $-K_p$.

The proportional integral (PI) control law is considerably popular in fighter design. The general PI control law is written as

$$C\dot{V}_d = K_p \left(CV_c(t) - CV(t)\right) + K_i \int_0^t \left(CV_c(t) - CV(t)\right) dt \tag{6.43}$$

The close loop transfer function of PI control law could be derived.

$$\frac{CV}{CV_{cmd}} = \frac{K_p\left(s + \frac{K_i}{K_p}\right)}{s^2 + K_p s + K_i} \tag{6.44}$$

The close loop transfer function has following properties:

$$\varsigma_s = \frac{K_p}{2\sqrt{K_i}}, \omega_{ns} = \sqrt{K_i}, T_\theta = \frac{K_p}{K_i}$$

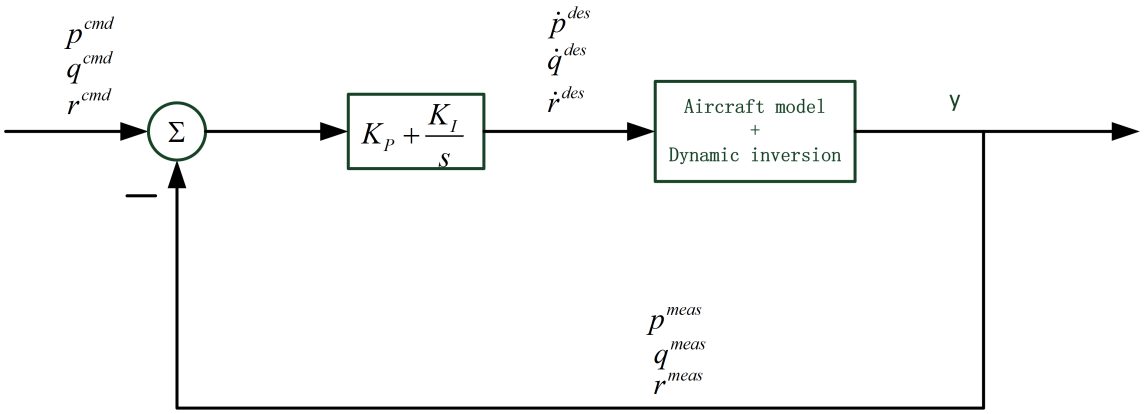

Figure 6.5: Proportion plus integral desired dynamic

This method is aiming to meet the flying quality requirement Mil-STD-1797A [2] which contains requirements about damping and natural frequency according to flight phase and aircraft type. The value of gain K_p, K_i could be selected according to these requirements meanwhile the value of time lag T_θ must be considered as well.

With respect to ride qualities (RQ), the desired dynamic could be designed in form of below equation.

$$C\dot{V}_{des} = \frac{K_{RQ}}{s + b}\left(CV_{cmd} - CV\right) \tag{6.45}$$

Then the close transfer function can be written as

$$\frac{CV}{CV_{cmd}} = \frac{K_{RQ}}{s^2 + bs + K_{RQ}} \tag{6.46}$$

The constant b and K_{RQ} are selected to obtain desired damping ratio and value of CAP in order to meet the ride qualities requirement. The CAP is calculated by

$$CAP = \frac{\omega_n^2}{n_\alpha} \tag{6.47}$$

CAP is a parameter used in high augmented aircraft to describe the flying quality requirements instead of natural frequency. Thus, both constant b and gain K_{RQ} could be determined by desired damping ratio and CAP.

Then performances of all these three desired dynamics are contrasted in terms of time domain response and frequency domain response in reference [27]. The flying quality is checked in time domain whereas the robust stability and performance are verified in frequency domain. Moreover, the quadratic cost and passenger ride comfort index are evaluated for all desired dynamics in reference [27].

6.6 Robustness

Robustness is an essential issue for NDI controller since NDI controller is based on assumption that the dynamic model of aircraft is entirely exact. However, this is not the case in reality, therefore the NDI controllers are very sensitive to uncertainties. As a result, the performance of NDI controller perhaps deteriorates when encounter uncertainties. If the responses of a control system are bounded in the specific required scope under a certain range of uncertainties, the control system is robust. Thus, it may be suggested that robust control law could be applied in desired dynamic control law design so as to endow the aircraft with desired robustness and performance properties. Quantitative feedback control (QFC), structured singular values (μ) synthesis, Sliding mode control and adaptive control could be employed for desired dynamic design to guarantee robust properties. There are two types of uncertainties which are parametric uncertainty and unmodeled dynamics. Adaptive control method is promising for dealing with uncertainties in constant or slow-varying parameter [24]. In this thesis, adaptive control technique is implemented to solve robustness problem which is illustrated in detail in chapter 9.

6.7 NDI applications review

Nonlinear dynamic inversion is quite popular in recent years as it could directly deal with nonlinear systems, and much research has been done in this area. Most of them concern the control of supermaneuver fighter in case of operation at very high angle of attack or having large operation envelop. Some of them involve trust vectoring control (TVC) except for the normal control surface [28] [5].

A general coupled nonlinear dynamic motion equation is given in Campbell's paper [29] as

$$\dot{\omega} = A(t)\,\omega + G(t)\,z + B(t)\,u \tag{6.48}$$

ω is denoted as the vector of roll, pitch and yaw rate. z represents for a nonlinear combination of ω, such as $pq, qr, pr, (p^2 - q^2), (r^2 - p^2)$ and $q^2 - r^2$. Therefore, the general expression of nonlinear dynamic inversion is given as

$$u = \hat{B}(t)^{-1}\left(\dot{\omega}_d - \hat{A}(t)\,\omega - \hat{G}(t)\,z\right) \tag{6.49}$$

In different applications, the control inputs are different. In some high performance fighters, the control inputs are not only the normal control surface, but also the

thrust vector. Usually these two control surfaces are not activated at the same time. The thrust vectoring control is only active at high angle of attack where the conventional control surfaces become extremely inefficient. A control surface allocation method between conventional control surfaces and thrust vectoring control surface is introduced in Atesoglu and Ozgoren's paper [28].

With respect to the inner-loop linearization, the so called time-scale separation method [28] [4] [26] is normally used, which separates the dynamic inversion into two steps: one is fast state variable inversion; the other is slow state variable inversion. A seconder order inversion is also used for angle of attack control problem in the inner-loop design to replace above method [4] [10].

In terms of the outer loop design, the out-loop control law is considerably crucial for NDI technique on which the performance of whole controller depends. The simple control laws for desired dynamic are proportional and proportional plus integral control law. The proportional and PI (proportion plus integral) control laws application are introduced in [28], [4] and [29]. Some robust control design techniques are applied such as quantitative feedback control (QFC) [4] and structured singular value (μ) synthesis [5] [30] [31], aiming to endow the airplane robustness performance since the NDI is very sensitive with uncertainties and does not guarantee any robustness. Moreover, a method called linear quadratic full state feedback with loop shaping [32] based on linear quadratic regulator theory (LQR) is carried out for desired dynamic design. This method achieves robust properties by possessing proper gain and phase margin.

The picture Below shows how the Quantitative feedback control law co-operates with nonlinear dynamic inversion.

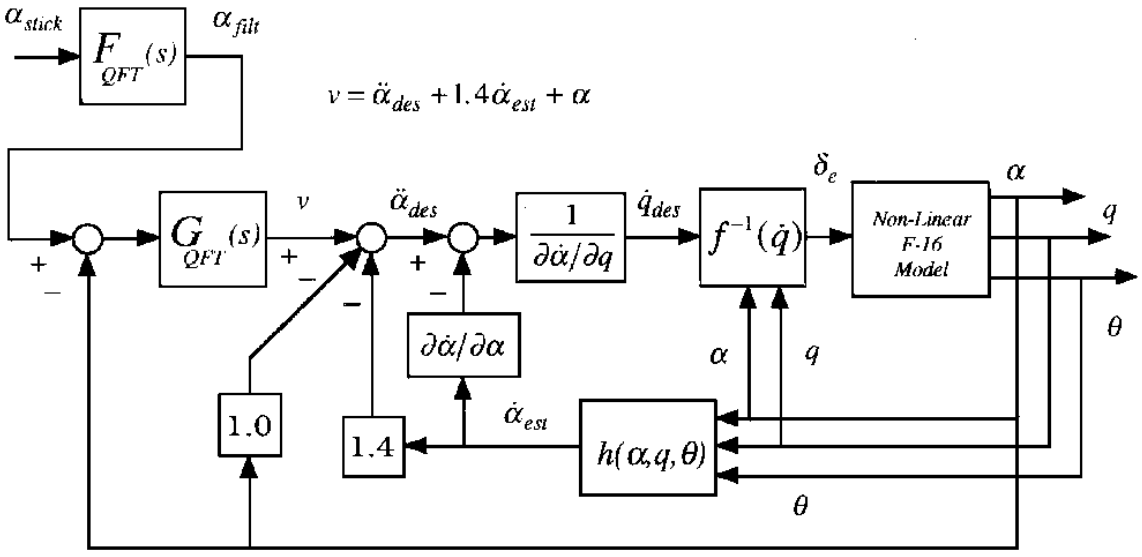

Figure 6.6: Overall controller structure of quantitative feedback control law co-operates with nonlinear dynamic inversion. Source: [4]

In the above design, angle of attack is the control output, and input u is replaced by

pseudoinput v. After dynamic inversion inner loop is done, the outer loop control law should be designed to obtain the $\ddot{\alpha}_{des}$. The $F_{QFT}(s)$ and $F_{QFT}(s)$ are quantitative feedback control law. And another control law between pseudo input v and $\ddot{\alpha}_{des}$ is added as well. One idea is that $v = \ddot{\alpha}_{des}$, namely $P_{DI}(S) = \frac{\alpha(s)}{v(s)} = \frac{1}{s^2}$. In this paper, the relationship is selected as $v = \ddot{\alpha}_{des} + 1.4\dot{\alpha}_{des} + \alpha$. The general form of P is as follows:

$$P_{DI}(s) = \frac{(1+\varepsilon_1)}{(s+\varepsilon_2)(s+\varepsilon_3)} \tag{6.50}$$

Where the ε are caused by uncertainties in the state equations. A basic rule of select P is that it should have stable poles having the same magnitude as the poles of linearizations of the open-loop aircraft system.

For structure singular value (μ) synthesis application in outer loop design, reference [5] gives the introduction. At first, the system uncertainty should be modeled as figure 6.7 shown.

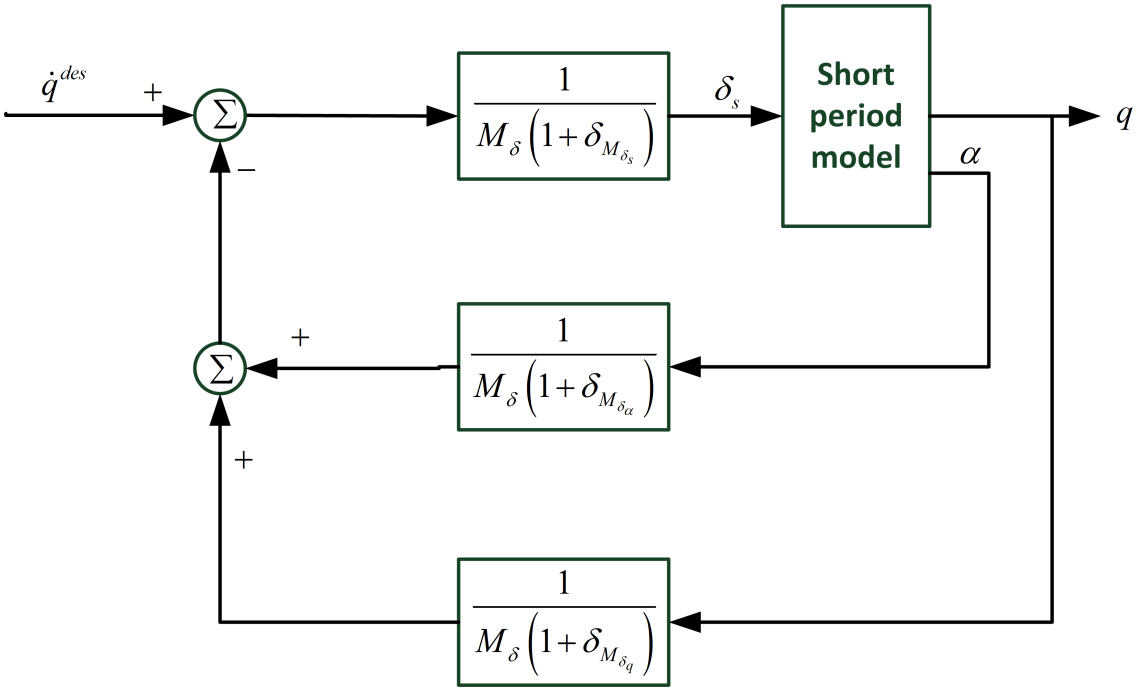

Figure 6.7: Uncertainty model of aircraft. Source: [5]

Above model considers both uncertainties in aerodynamic coefficients and the errors in the measurements. The set of possible transfer functions between $\dot{q}$ and $\dot{q}_d$ are described by $(1.04 + 0.21\delta_2)/(s + 1.2\delta_1)$ with $-1 \leq \delta_1 and \delta_2 \leq 1$. The term δ_1 refer to pole variations and δ_2 refers to the gain variations in the linearized transfer function models. The overall structure of μ synthesis combined with dynamic inversion is illustrated as below. The D-K iteration is a practical approach to find a stabilizing controller K.

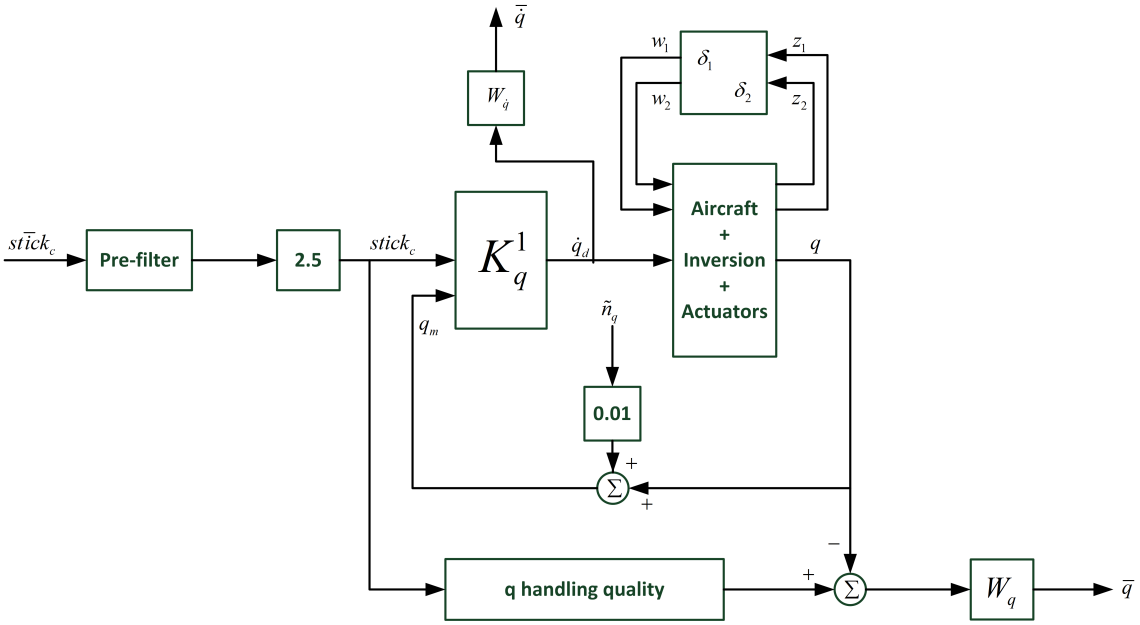

Figure 6.8: Overall structure of μ synthesis combined with dynamic inversion. Source: [5]

Chapter 7

Nonlinear dynamic inversion controller design for Boeing747

7.1 Nonlinear coupling B747 model

The nonlinear coupling B747 model is based on the nonlinear motion equation (6.21) and (6.22) introduced in section 6.2. It can be seen that the aircraft models become coupled by introducing p and r items in longitudinal mode and q items in lateral mode. Moreover, the nonlinear features are generated by the nonlinear items including mass inertial. All stability derivative data are obtained from NASA CR-2144 [13, p.230].

The longitudinal and lateral aircraft nonlinearity coupled parameter varying Simulink models which are both modified based on the linear parameter varying (LPV) aircraft Simulink model provided by Dr Mudassire Lone are respectively provided in appendix A.

7.2 Actuator model

The control surface actuators of Boeing 747 are modelled as second order transfer functions which are linked with motion rate limiting and deflection saturation. The following elevator model is used:

$$\frac{\delta_e}{\delta_{ec}} = \frac{450}{s^2 + 30s + 450} \tag{7.1}$$

Below rudder and aileron model are used from [33, p.8-9]:

$$\frac{\delta_a}{\delta_{ac}} = \frac{-1.77s + 399}{s^2 + 48.2s + 399} \tag{7.2}$$

$$\frac{\delta_r}{\delta_{rc}} = \frac{12.6s^2 - 1185s + 27350}{s^3 + 77.7s^2 + 3331s + 27350} \tag{7.3}$$

The rate limits and deflection limits are shown respectively in the table below.

Table 7.1: Actuator limits

	Rate rang	Deflection rang
Elevator	$\pm 60^o/s$	$\pm 35^o$
Aileron	$\pm 60^o/s$	$\pm 40^o$
Rudder	$\pm 60^o/s$	dynamic

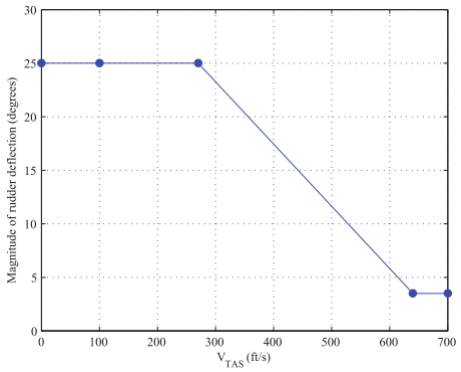

Figure 7.1: Rudder actuator dynamic saturation schedule

7.3 Inner loop feedback linearization

In this case, three angular rates about 3 body axes are chosen as control variables. Therefore, motion equations of these three parameters should be inversed to calculate three control surface deflections. Two-time-scale separation method is not needed for this case as the control variables are equal to control inputs. In dynamic inversion, actuator dynamic is ignored since the frequency of actuator is much higher than aircraft frequency. All the control surface deflection commands are calculated according to equation (6.32) by substituting all the $f(x)$ and $g(x)$.

$$\delta_e = \frac{1}{M_{\delta_e}}\left(\dot{q}_{des} - M_u u - M_{\dot{w}}\dot{w} - M_w w - M_q q - M_{\delta_{th}}\delta_{th} - \frac{(I_z - I_x)pr + I_{xz}\left(r^2 - p^2\right)}{I_y}\right)$$

$$\begin{bmatrix} \delta_a \\ \delta_r \end{bmatrix} = \begin{bmatrix} L'_{\delta_a} & L'_{\delta_r} \\ N'_{\delta_a} & N'_{\delta_r} \end{bmatrix}^{-1} \left(\begin{bmatrix} \dot{p}_{des} \\ \dot{r}_{des} \end{bmatrix} - \begin{bmatrix} L'_\beta & L'_p & L'_r \\ N'_\beta & N'_p & N'_r \end{bmatrix} \begin{bmatrix} \beta \\ p \\ r \end{bmatrix} - \begin{bmatrix} \frac{I_{xz}(I_x - I_y + I_z)pq + \left[I_z(I_y - I_z) - I_{xz}^2\right]qr}{I_x I_z - I_{xz}^2} \\ \frac{-I_{xz}(I_x - I_y + I_z)qr + \left[I_x(I_x - I_y) + I_{xz}^2\right]pq}{I_x I_z - I_{xz}^2} \end{bmatrix} \right) \tag{7.4}$$

Equation (7.4) is the flight control law of Boeing 747 which varies according to different types of desired dynamics. The overall structure of NDI controllers for

Boeing 747 longitudinal and lateral mode attitude rate control are depicted as figure 7.2.

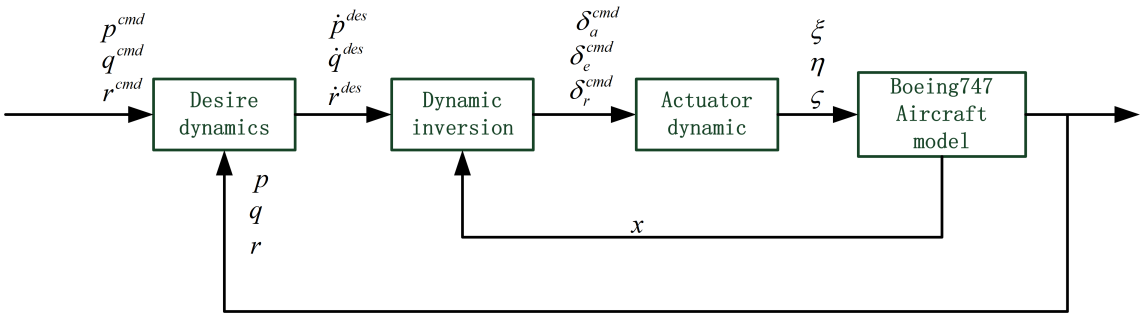

Figure 7.2: The overall structure of NDI controllers of Boeing 747

After feedback linearization, the whole system should become a pure integrator if there is no desired dynamic. Figure 7.3 shows the response of aircraft model for 1 deg/s q command after dynamic inversion linearization at a chosen flight point (Mach 0.9 and Altitude 40000ft). It is obvious that the response is similar with a response of integrator within first 5 seconds , but not a pure integrator as the influence of actuator. After first a few seconds the response goes quickly down because both Mach number and altitude have been changed considerably, in turn give rise to the discrepancies of aerodynamic derivatives resulting in incomplete cancellation of the aerodynamic of the aircraft. The variations of Mach number and Altitude are also illustrated by figures 7.4 and 7.5. With respect to lateral direction attitude angular rate, the roll rate and yaw rate have similar case with pitch rate after inner loop feedback linearization.

A wrong way of doing nonlinear dynamic inversion linearization was done prior to the above way, which is feeding back all aerodynamic derivatives computed by the measured Mach number and Altitude. This method is based on pre-known aerodynamic derivatives data and, more importantly, cannot guarantee system stability in case of disturbances and measurement noise being presented.

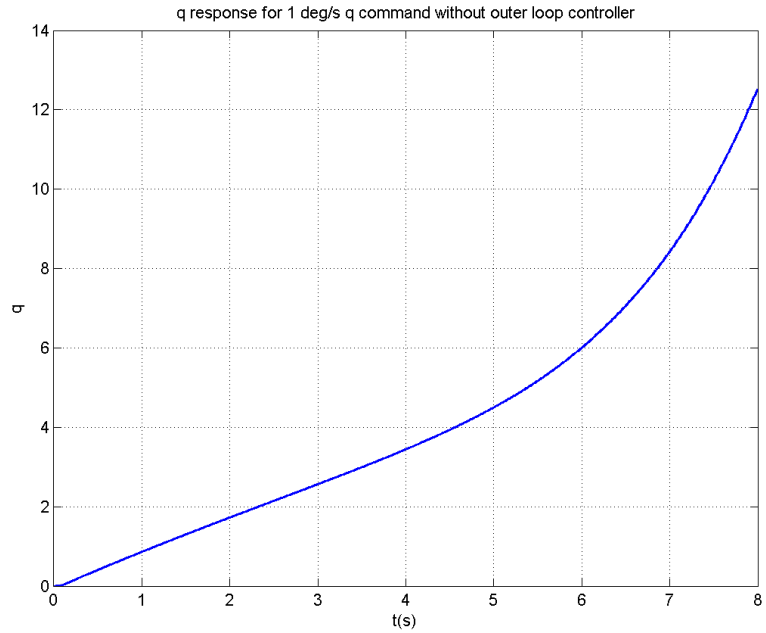

Figure 7.3: q response for 1 deg/s q command without outer loop controller

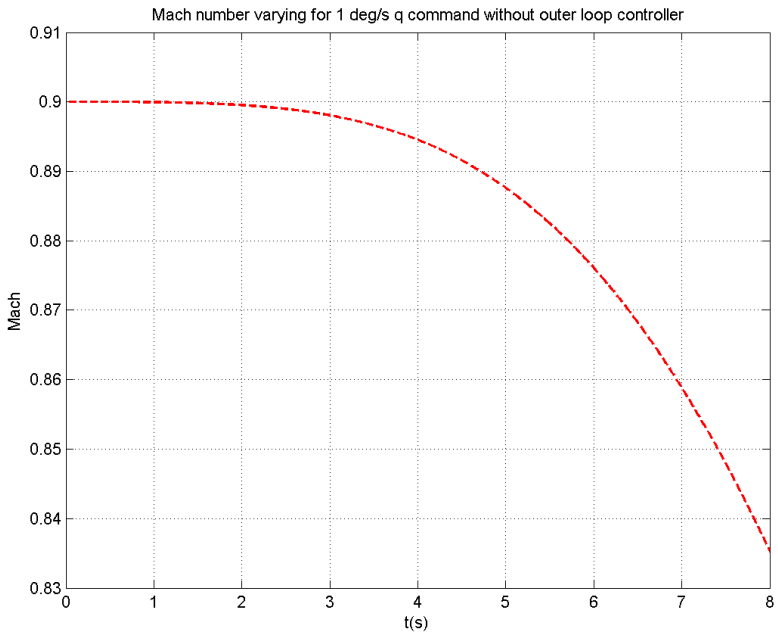

Figure 7.4: Mach varying for 1 deg/s q command without outer loop controller

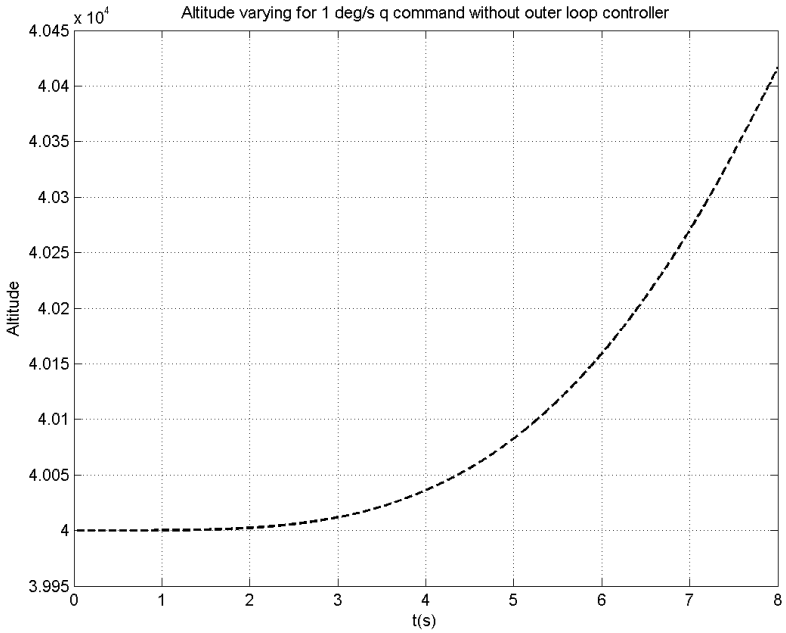

Figure 7.5: Altitude varying for 1 deg/s q command without outer loop controller

7.4 Internal dynamics stability verification

In this section, the stability of the internal dynamics of the feedback linearization of Boeing 747 is verified. Firstly, the state space equation should be transformed to normal form. Then to obtain the zero-dynamics by setting all the element of μ to be zero. Finally, check the stability of zero-dynamics.

The aircraft model is approximated as two decoupled modes which are longitudinal mode and lateral mode for the internal dynamics verification. Therefore the internal dynamics stability are separately verified with respect to longitudinal mode and lateral mode. For simplification reason, some small items are eliminated such as $X_{\dot{w}}$. Following equations (7.5) and (7.6) illustrate the simplified decoupled longitudinal and lateral dynamics.

$$\begin{bmatrix} \dot{u} \\ \dot{w} \\ \dot{q} \\ \dot{\theta} \end{bmatrix} = \begin{bmatrix} X_u u + X_w w - Wq - g\cos(\theta_e)\theta \\ (Z_u u + Z_w w + q(Z_q + U) - g\sin(\theta_e)\theta)/(1 - Z_{\dot{w}}) \\ M_u u + M_w w + M_q q \\ q \end{bmatrix} + \begin{bmatrix} X_{\delta_e} \\ Z_{\delta_e}/(1 - Z_{\dot{w}}) \\ M_{\delta_e} \\ 0 \end{bmatrix} \cdot \delta e \tag{7.5}$$

$$\begin{bmatrix} \dot{v} \\ \dot{p} \\ \dot{r} \\ \dot{\phi} \\ \dot{\psi} \end{bmatrix} = \begin{bmatrix} Y_v v + Wp - Ur + g(\cos(\theta_e)\phi + \sin(\theta_e)\psi) \\ L_r r + L_p p + L_\beta v/U \\ N_\beta v/U + N_r r + N_p p \\ p + r\tan(\theta_e) \\ r/\cos(\theta_e) \end{bmatrix} + \begin{bmatrix} Y_{\delta_r} & 0 \\ L_{\delta_r} & L_{\delta_a} \\ N_{\delta_r} & N_{\delta_a} \\ 0 & 0 \\ 0 & 0 \end{bmatrix} \cdot \begin{bmatrix} \delta r \\ \delta a \end{bmatrix} \tag{7.6}$$

The outputs of longitudinal mode and lateral mode are respectively indicated below.

$$y = q \quad for\, longitudinal\, mode;$$
$$y = \begin{cases} p \\ r \end{cases} \quad for\, lateral\, mode.$$

First of all, we verify the internal stability of the longitudinal mode through zero-dynamics. In order to achieve that, the normal form of the longitudinal mode should be established. The output q , dented as μ defined in section 6.4, is chosen as the first state of the normal states since the relative degree of the output is 1, provided that

$$\mathbf{g_{\delta e}} = \begin{bmatrix} X_{\delta_e} \\ Z_{\delta_e}/(1 - Z_{\dot{w}}) \\ M_{\delta_e} \\ 0 \end{bmatrix}$$
$$\nabla q \cdot \mathbf{g} \neq 0$$

After that, the remaining 3 states $Z_j (j = 1, 2, 3)$ should be found which should satisfy

$$\nabla Z_j \cdot \mathbf{g} = 0 \tag{7.7}$$

which means that all the vector Z_j are within the hyperplane orthogonal to $\mathbf{g}$. Therefore, all the states Z_j are linearly independent of q and linearly independent of each other. The existence of Z_j is proofed in [24, p.251].

The solution of (7.7) could be found as below.

$$\begin{bmatrix} Z_1 \\ Z_2 \\ Z_3 \end{bmatrix} = \begin{bmatrix} \theta \\ \frac{u}{X_{\delta_e}} - \frac{q}{M_{\delta_e}} \\ \frac{u}{X_{\delta_e}} - \frac{w(1-Z_{\dot{w}})}{Z_{\delta_e}} \end{bmatrix} \tag{7.8}$$

The normal states are formed as a blend of output q and internal dynamics states Z_j, namely $[\mu, Z_j]$. The derivatives of the normal states could be computed

$$\begin{bmatrix} \dot{\mu} \\ \dot{Z}_1 \\ \dot{Z}_2 \\ \dot{Z}_3 \end{bmatrix} = \begin{bmatrix} \dot{q} \\ \dot{\theta} \\ \frac{\dot{u}}{X_{\delta_e}} - \frac{\dot{q}}{M_{\delta_e}} \\ \frac{\dot{u}}{X_{\delta_e}} - \frac{\dot{w}(1-Z_{\dot{w}})}{Z_{\delta_e}} \end{bmatrix} \tag{7.9}$$

Furthermore, the expressions of the original states with respect to the normal states are calculated as shown below.

$$\begin{bmatrix} u \\ w \\ q \\ \theta \end{bmatrix} = \begin{bmatrix} (X_{\delta_e}(\mu + M_{\delta_e} Z_2))/M_{\delta_e} \\ -(Z_{\delta_e}(\mu + M_{\delta_e} Z_2 - M_{\delta_e} Z_3))/(M_{\delta_e}(Z_{\dot{w}} - 1)) \\ \mu \\ Z_1 \end{bmatrix} \tag{7.10}$$

Thus, by substituting (7.10) into (7.9), the normal form of the longitudinal mode dynamic is obtained. Intuitively, the internal dynamics is gained as well in form of

$$\dot{\mathbf{Z}} = \mathbf{Z}(\mu, \mathbf{Z}) \tag{7.11}$$

The right side of the equation exclude input δ_e. Now, set μ as 0, as a result the zero-dynamics is obtained as:

$$\dot{\mathbf{Z}} = \mathbf{Z}(0, \mathbf{Z}) \tag{7.12}$$

Above zero-dynamics could be rewritten as

$$\dot{\mathbf{Z}} = A\mathbf{Z} + B \tag{7.13}$$

We could obtain the stability of zero-dynamics by checking the eigenvalues of matrix A in equation (7.13), namely the poles of the dynamics. If all the eigenvalues of A are all at the left side plane, the zero-dynamics is stable. As a result, the zero-dynamics of the longitudinal mode is verified stable throughout the entire flight profile. The calculation of internal dynamics verification of both longitudinal mode and lateral mode in Matlab are shown in Appendix B.

The internal dynamics of the lateral mode could be processed in a similar way. The key difference is that the lateral mode is a MIMO system, with 2 inputs. As a result, the internal states $\mathbf{Z}$ have to be orthogonal to both vectors $\mathbf{g}(x)$ of δ_r and δ_a. Here we just show the key results of the verifications for no repetition. The internal dynamics states should verify the following equations

$$\mathbf{g}_{\delta_\mathbf{a}} = \begin{bmatrix} 0 & L_{\delta_a} & 0 & N_{\delta_a} & 0 \end{bmatrix}^T \tag{7.14a}$$

$$\mathbf{g}_{\delta_\mathbf{r}} = \begin{bmatrix} Y_{\delta_r} & L_{\delta_r} & 0 & N_{\delta_r} & 0 \end{bmatrix}^T \tag{7.14b}$$

$$\nabla Z_j \cdot \mathbf{g} = 0 \tag{7.15}$$

The normal states are selected as indicated in equation (7.16).

$$\begin{bmatrix} \mu_1 \\ \mu_2 \\ Z_1 \\ Z_2 \\ Z_3 \end{bmatrix} = \begin{bmatrix} p \\ r \\ \phi \\ \psi \\ \frac{v}{Y_{\delta_r}} + \frac{p}{L_{\delta_a}} - \frac{r}{N_{\delta_a}} \end{bmatrix} \tag{7.16}$$

Consequently, the zero-dynamics could be yield via setting all the outputs $\mu = 0$, shown in the form below.

$$\dot{\mathbf{Z}} = \mathbf{Z}(0, \mathbf{Z}) \tag{7.17}$$

The stability of this zero-dynamics of lateral mode for the entire flight profile is verified stable, in turn the internal dynamics of lateral mode is stable. In summary, based on above analysis, the internal dynamics of Boeing 747 aircraft model is stable throughout the entire flight envelop.

7.5 Desired dynamic design

As previous section 6.5 discussed, desired dynamic are the key part of NDI controller which determined the stability and control performance of system. Four types desired dynamics are applied for Boeing 747 model to meet the handling quality requirements.

Boeing 747 is a large civil transport for which there are specific handling quality requirements. Performance requirements (derived from [17]): the close loop systems should be able to track pitch angle command with a rise time $t_s < 5s$, and a setting time $t_r < 20s$ (within 99% of the demand value). The overshoot of any control variable should be very little (<5%) at above 305 m whereas may increase to 30% below that altitude in order to obtain higher tracking performance. Moreover, the pitch rate response should be minimized to provide better passenger comfort. Control activity should be minimized, more specifically, under moderate turbulence conditions the mean actuator rate of the elevator must be less than 33% of the maximum rate.

First of all, the proportional desired dynamic, as described in 6.5, is applied at cruise condition (Mach 0.85, Altitude 36000 ft). Setting the proportional gain at 3, following closed loop transfer function is obtained. The response of NDI controller with proportional law exponentially converges to the demand value.

$$\frac{q}{q_{cmd}} = \frac{K_p}{s + K_p} = \frac{3}{s + 3} \tag{7.18}$$

The second desired dynamic is proportion and integral control law. Setting $K_I = 4, K_P = 4$, the closed loop transfer function of NDI controller with PI desired control law is given below.

$$\frac{q}{q_{cmd}} = \frac{K_P\left(s + \frac{K_I}{K_P}\right)}{s^2 + K_P s + K_I} = \frac{4\,(s+1)}{s^2 + 4s + 4} \tag{7.19}$$

with

$$\varsigma = 1, \omega_n = 2rad/s, T_\theta = \frac{K_P}{K_I} = 1s$$

The third desired dynamic is called RQ (ride quality) control law. By setting $K_{RQ} = 9$ and $b = 4.2$, the close loop transfer function is provided as

$$\frac{q}{q_{cmd}} = \frac{K_{RQ}}{s^2 + bs + K_{RQ}} = \frac{9}{s^2 + 4.2s + 9} \tag{7.20}$$

with

$$\varsigma_s = 0.7, \omega_n = 3rad/s$$

The last desired dynamic is introduced previously in form of equation (6.8), named tracking desired dynamic. For Boeing 747 longitudinal mode q command control, the relative degree is 1 and if chose the $k = 3$, results in the following close loop dynamic

$$\dot{e} + 3e = 0 \tag{7.21}$$

The solution of the above equation is

$$e = e^{-3t} \tag{7.22}$$

It is evident that the error converges to zero exponentially is exactly the same with the desired proportional dynamics. Fugyre 7.6 illustrates the q responses of these 4 desired dynamics for 1 deg/s q command at cruise condition.

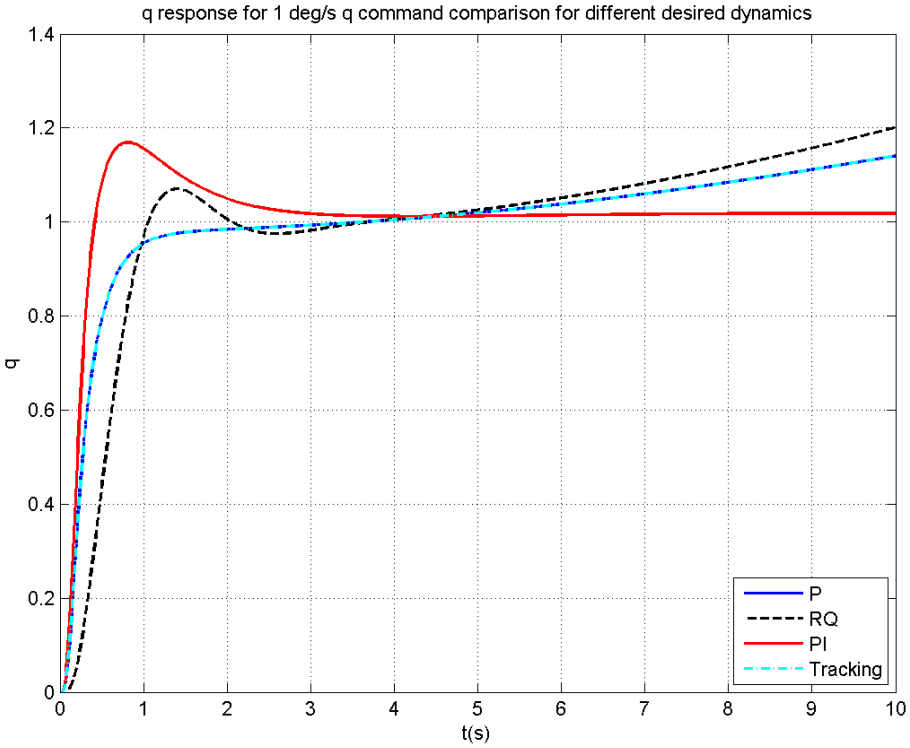

Figure 7.6: q response of different desired dynamics for 1 deg/s q command

Let us assess the time responses of pitch rate with respect to military requirement. In Mil-STD-1797A [22], for class III aircraft B flight phase, following requirements should be satisfied.

$$\begin{aligned} &0.3 \leq \varsigma_s \leq 2 \\ &0.7 rad/s \leq \omega_{ns} \leq 4.2 rad/s \end{aligned} \tag{7.23}$$

In time domain, above requirements could be converted to time response requirements as below, based on the methods introduced in reference [34].

Table 7.2: The requirements in time domain for Military requirements

Parameters	Definition	Value
t_d	The time first arrive half of steady state value	2.6s
t_r	The time response rise from 10% to 90%	5s
t_p	The time first arrive at peak	5.3s
t_s	The time response settled in the ±5% error	16.7s
Overshoot	The discrepancy between peak and steady state value	37%

Superimpose above requirements on the same chart of the 4 types of desired dynamics NDI controllers.

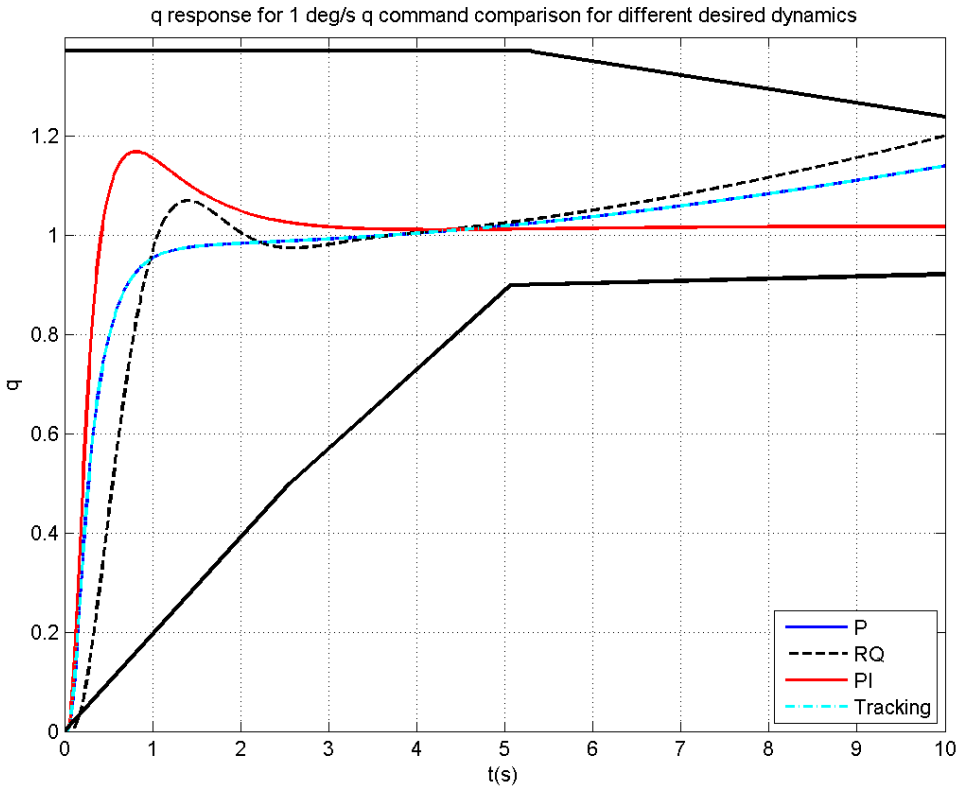

Figure 7.7: Desired dynamics assessed by military requirement

From figure 7.7, It is implied that the desired proportional dynamic (P) and the tracking desired dynamic both eventually make the whole controller first order transfer function whose behaviour is exponential convergence in the first 5 seconds. The final controller of PI desired dynamic looks like a second order transfer function as previously described. The close loop controller of RQ desired dynamic operate exactly as we expect, a second order system with desired damping ratio and natural frequency. It is evident that PI controller could entirely satisfy the military requirements but cannot meets the civil aircraft overshoot requirement (<5%). P and

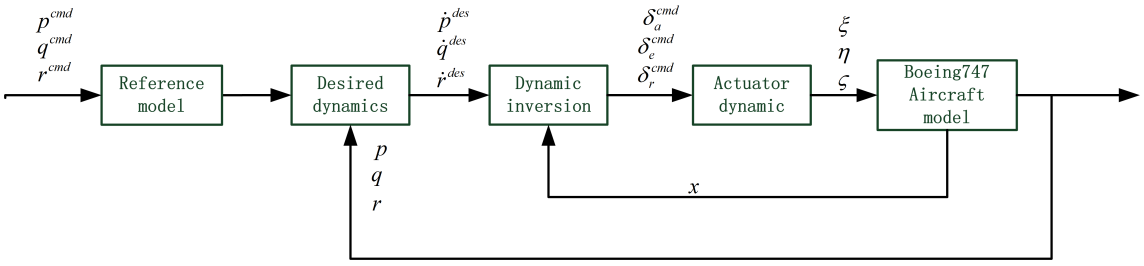

Figure 7.8: The overall structure of NDI controllers of Boeing 747 with reference model

tracking desired dynamics almost fulfill the military requirements apart from last few seconds when the responses diverges due to the incomplete cancellation. The RQ desired dynamic meets the military requirements very well but has the same problem with P desired control law.

However, the tracking desired dynamic is different from the proportional dynamic if we add a reference model before desired dynamics, indicated as figure 7.8. For example, the following reference model is selected, and then the responses of pitch rate step command of 4 types desired dynamic are shown in figure 7.9.

$$G_{ref} = \frac{64}{s^2 + 16s + 64}, \quad with\ \varsigma = 1 \quad \omega = 8rad/s \tag{7.24}$$

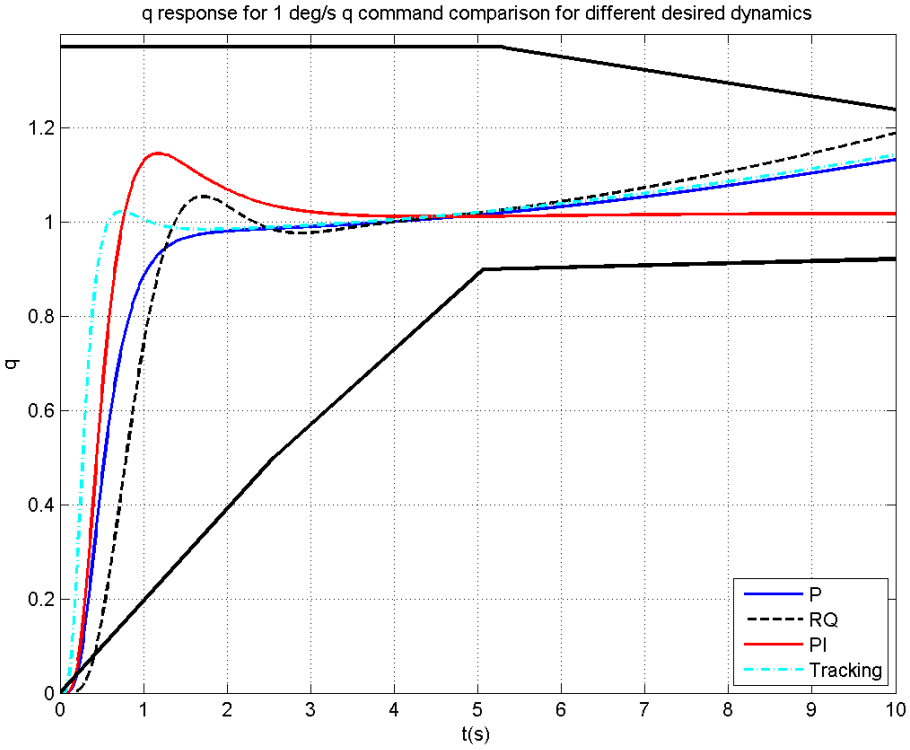

Figure 7.9: The q responses for 4 types of desired dynamic NDI controller adding reference model

7.6 Design point selection

One of the major advantages of nonlinear dynamic inversion is dealing with nonlinear system with less gain schedule or without gain schedule. Therefore, the design point of NDI controller should be carefully selected to meet the handling quality requirements in large range of flight conditions. It should also be taken into account that the handling requirements in different flight phase are different. Table 7.3 manifests the test flight conditions of each flight phase. For example, the design

Table 7.3: Typical flight points in different flight phase for Boeing 747. Source: [6] [7]

	Mach	Altitude (ft)
Climb	0.76	25000
Cruise	0.85	36000
Decent	0.5	20000
Approach	0.25	8000

point is chosen at cruise flight condition (Mach 0.85 and Altitude 36000ft), where the airplane staies for the longest time. The q response at other flight phases could be obtained by simulation. Four NDI controllers with different desired dynamics are assessed for above 4 flight conditions. The results are indicated as figure 7.10.

From figure 7.10, it is can be drawn the conclusion that the PI controller has the best robustness performance since all the response could converge towards to demand value and maintain at a value with small steady state error. Whereas, all other three desired dynamics cannot retain good stability characteristic and control performance in case of non-design point. More other flight points are taken into account as the design points. The assessments of controllers with design points at decent, climb and approach are shown respectively as figure 7.11, figure 7.12 and figure 7.13.

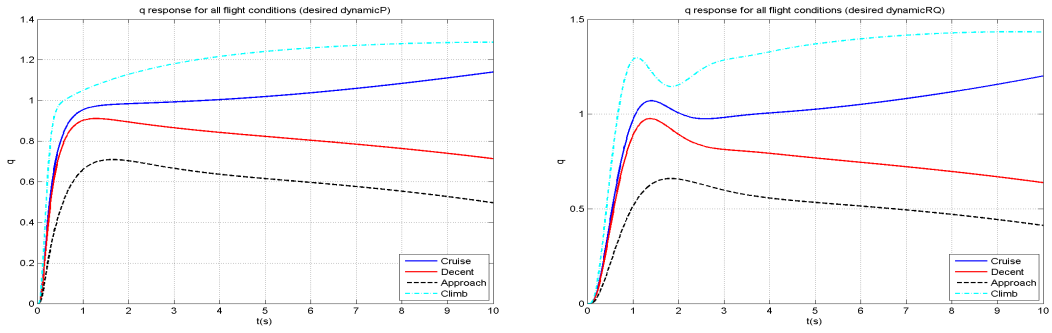

(a) P desired dynamics (b) RQ desired dynamics

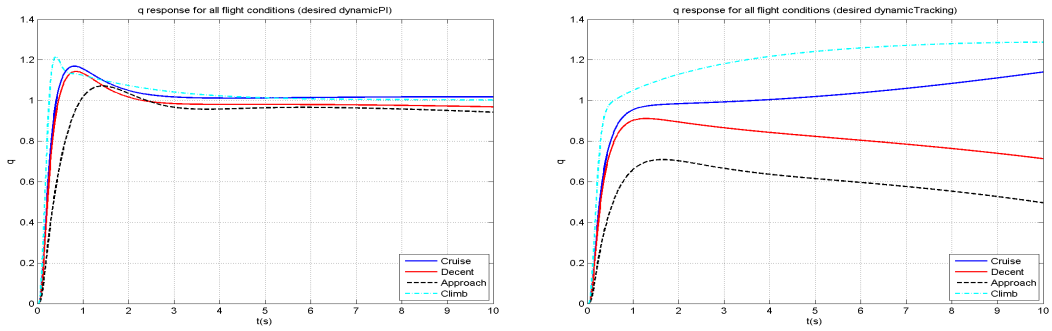

(c) PI desired dynamics (d) Tracking desired dynamics

Figure 7.10: Assessments of 4 NDI controllers with design point at cruise condition for overall flight envelop

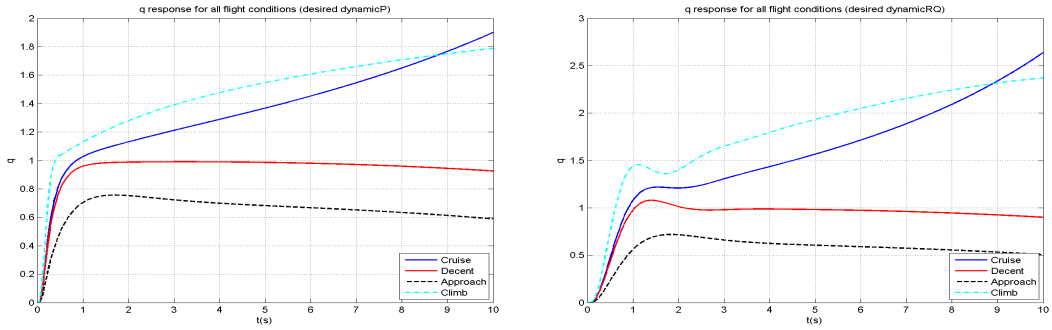

(a) P desired dynamics (b) RQ desired dynamics

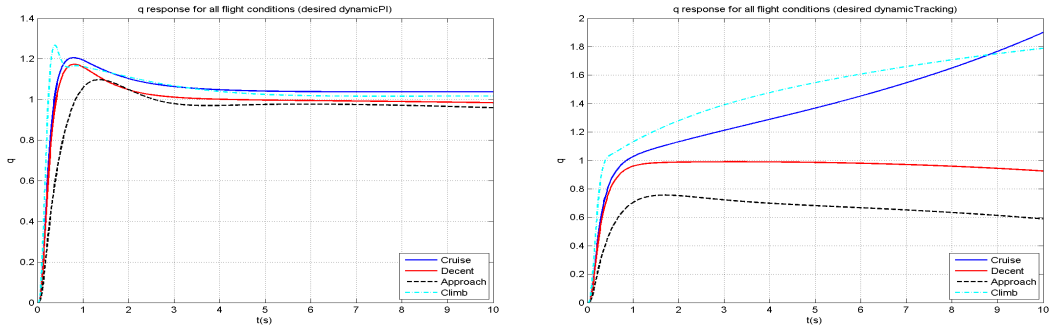

(c) PI desired dynamics (d) Tracking desired dynamics

Figure 7.11: Assessments of 4 NDI controllers with design point at decent condition for overall flight envelop

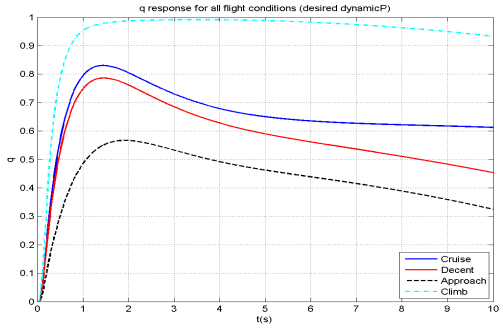

(a) P desired dynamics

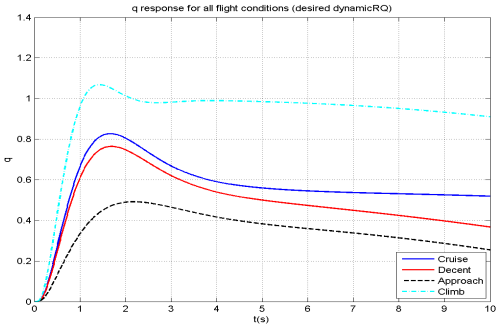

(b) RQ desired dynamics

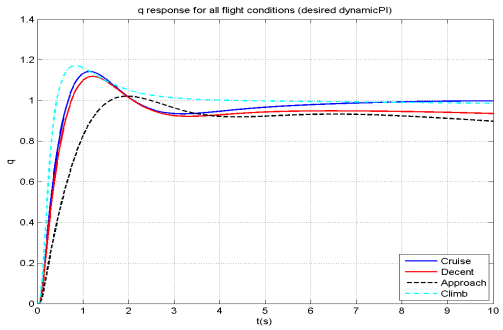

(c) PI desired dynamics

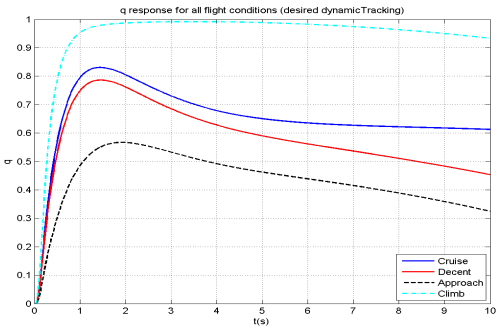

(d) Tracking desired dynamics

Figure 7.12: Assessments of 4 NDI controllers with design point at climb condition for overall flight envelop

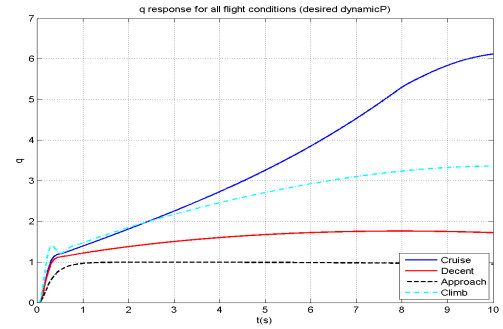

(a) P desired dynamics

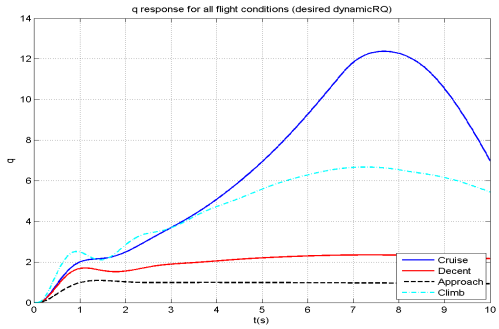

(b) RQ desired dynamics

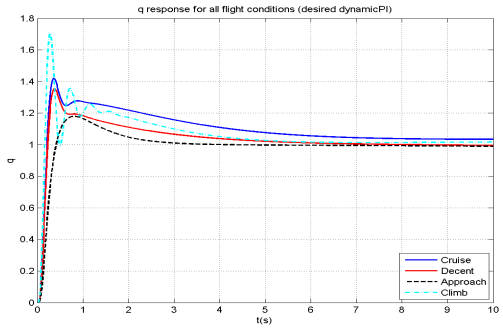

(c) PI desired dynamics

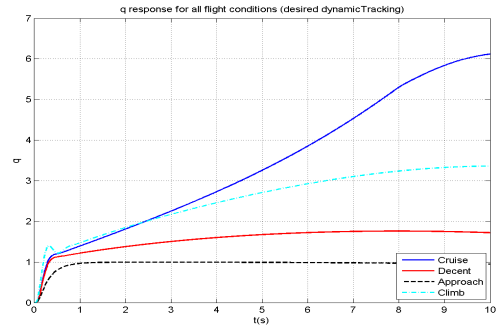

(d) Tracking desired dynamics

Figure 7.13: Assessments of 4 NDI controllers with design point at approach condition for overall flight envelop

Above figures show the assessments of NDI controllers with 4 types of desired dynamics in case of different design points. Some conclusions might be drawn as below:

- Each type of desired dynamic exhibits similar response when the test flight condition is the same as the design point; For example, the response of P desired control law at the cruise point provided that the design point in cruise point is similar with the response at the decent based on design point at decent point.

- PI desired control law has relatively high robustness performance whereas other desired control laws cannot cope with large flight envelop no matter what design point the NDI controller is.

- For PI desired control law, the performance of controllers with design points at cruise and decent have smaller overshoot, short settle time and less steady state error comparing to the other two design points. For P , tracking and RQ desired control law, the performances of controllers with design point at cruise, decent and climb have no substantial discrepancies, but the performance is much poorer when design point is at approach point.

In summary, the controller design point should be set at cruise condition where the airplane stay longest time. In addition, PI control law should be selected as the desired dynamic of NDI controller due to the best robustness performance. In chapter 9, an adaptive control technique is applied in order to improve the robustness capacity of NDI controller in the presence of parameter uncertainty.

7.7 Lateral mode NDI controller design

The NDI controller design in lateral mode of Boeing 747 is similar with longitudinal mode. The NDI control law of roll rate control and heading rate control are described as (7.4). Analogizing with longitudinal mode, lateral mode could also have several types of desired dynamics such as proportional, proportional plus integral and ride quality. The controller parameters should be tuned according to the lateral dynamics and the lateral handling and flight quality requirements.

The design results of roll rate control are indicated in table 7.4 and figure 7.14. In analogy to longitudinal mode control, P and Tracking desired dynamics have the same response. From figure 7.14, it is can be seen that P, RQ and Tracking desired dynamics have reasonable rise time and little overshoot whereas PI desired control law have relatively high overshoot. In addition, PI desired control have the smallest steady state error meanwhile P, Tracking and RQ desired dynamics have bigger steady state error. All responses of 4 types of desired dynamics retain at command value very well.

Table 7.4: Controller gain values for roll rate control

Desired dynamics	Parameters value
P	$K_P = 3$
PI	$K_P = 2, K_I = 2$
RQ	$K_{RQ} = 3.2, b = 4$
Tracking	$k = 3$

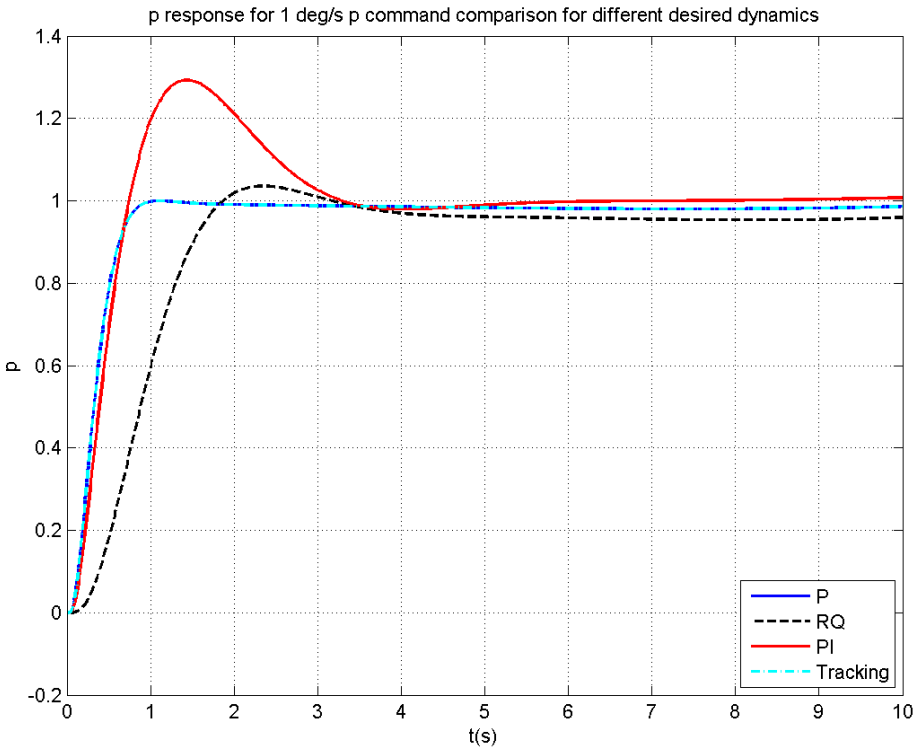

Figure 7.14: p response of different desired dynamics for 1 deg/s p command at cruise condition

The design results of heading rate control are illustrated as table 7.5 and figure 7.15. Referring to figure 7.15, all 4 types of desired dynamic have the similar properties with that of roll rate control. Yet, all responses diverge at the last 2 seconds due to the incomplete dynamic cancellation. It might be drawn the conclusion that the feedback linearization works well to cancel out the original aircraft dynamics and each desired dynamic functions as expected. Furthermore, the controller parameters need to be tuned to meet the explicit lateral flying and handling quality requirements.

Table 7.5: Controller gain values for heading rate control

Desired dynamics	Parameters value
P	$K_P = 3$
PI	$K_P = 2, K_I = 2$
RQ	$K_{RQ} = 9, b = 4.8$
Tracking	$k = 3$

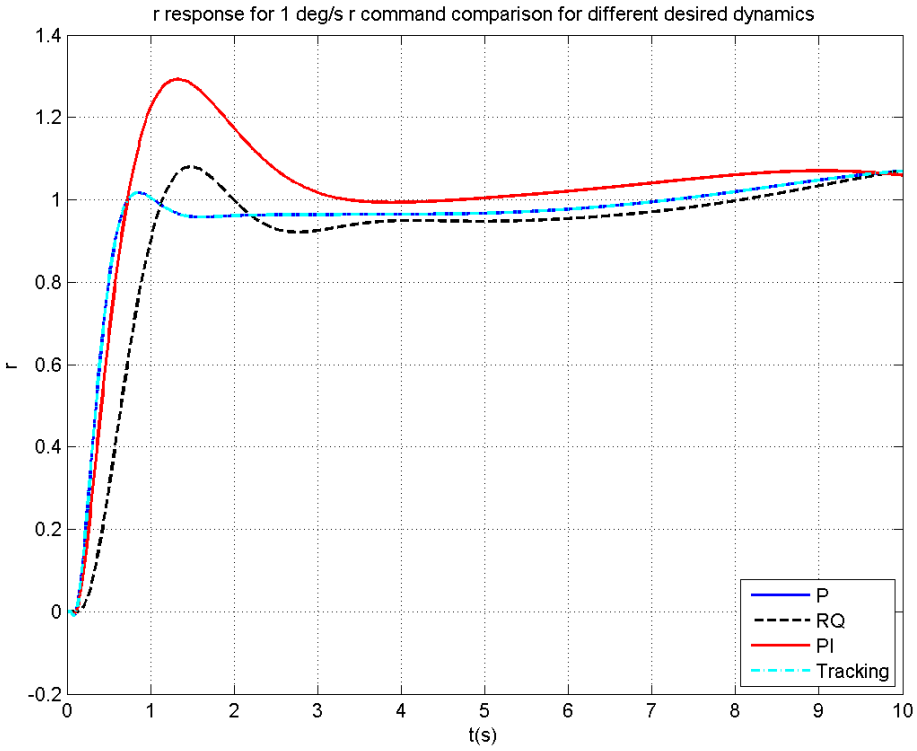

Figure 7.15: r response of different desired dynamics for 1 deg/s r command at cruise condition

7.8 Summary

The development of NDI control law of Boeing 747 is accomplished in this chapter. Four types of desired dynamics are accessed and the internal dynamics of both longitudinal and lateral mode are verified to be stable. The PI desired control law could overcome the incomplete dynamic cancellation and maintain at command value all the time while the other 3 types of desired dynamic diverge at last several seconds resulting from the assessment.

The cruise condition is selected as the design point after 4 different flight points at 4 flight phases are evaluated. The evaluation implies that the PI desired control law

has the best robustness property contrast to other 3 control laws.

The lateral mode NDI controllers are also designed in the last section. Roll rate and heading rate are chosen as the control variable and the feedback linearization works well. Four types of desired dynamic function are evaluated for roll rate and heading rate control.

In order to improve the robustness performance, adaptive control technique is applied to recursively estimate the varying parameters of the aircraft system and then the NDI controller is adjusted according to the estimates of the varying parameters.

Chapter 8

Sliding mode control

8.1 Sliding mode control theory introduction

As we discussed earlier, modeling inaccuracies and parametric uncertainty can have strong adverse effects on NDI controller, in other words, performance of the NDI controller deteriorates dramatically in case of uncertainty presented. Sliding mode control is known as a method to deal with the control problem for time invariant system subject to parameter uncertainty, unmodeling uncertainty and system perturbations. This chapter introduces the sliding mode control theory and the SMC controller design for Boeing 747 airplane. The concept of SMC is that the system states are forced to reach and remain on a predefined surface which presents the desired dynamics within the states space. The principal advantages of SMC are: reducing system order and insensitive to matched uncertainty. Designing a SMC controller is usually partitioned into two steps; firstly, design the sliding surface and then design the control law to maintain state trajectory on the sliding surface. The dynamic behaviour when confine to the surface is called sliding motion which is the desired dynamics of the system. The control law functions to make the system trajectory move towards the sliding surface and retain it on the surface. The brief description of SMC is given as following, and more detail informations are provided in [35] and [24].

Consider a uncertain linear time invariant system with m inputs given by

$$\dot{x}(t) = Ax(t) + Bu(t) + f(t, x, u) \tag{8.1}$$

where $A \in \mathbf{R}^{n\times n}$ and $B \in \mathbf{R}^{n\times m}$ with $1 \leq m < n$. The function f is assumed to be unknown but bounded by some known functions of state. Let $s : \mathbf{R}^n \to \mathbf{R}^m$ be a linear function represented as

$$s(x) = Sx \tag{8.2}$$

where $S \in \mathbf{R}^{m\times n}$ is of full rank and define a hyperplane

$$\sigma = \{x \in \mathbf{R}^n : s(x) = 0\} \tag{8.3}$$

If the system trajectory is forced onto and remained on the hyperplane σ after t_s, an ideal sliding motion is said to be taking place for all $t > t_s$. In addition, function $s(t) = Sx(t)$ is called switching function.

8.1.1 Properties of sliding motion

As previously mentioned, the major two merits are that of order reduction and invariance towards matched uncertainty. Now, let us have an insight look at these two properties. These two properties are given in [35] as proposition 3.1 and theorem 3.1.

Order reduction: In sliding motion, the *nth order* system is reduced by dimension of input vector, m, to an $(n-m)^{th}$ order system and the eigenvectors associated with any nonzero eigenvalues of the system matrix

$$A_{eq} = \left(I_n - B(SB)^{-1}S\right) A \tag{8.4}$$

belong to the null space of the matrix S.

m of the states can be expressed as a linear combination of the remaining $n-m$ states resulting from the fact that $S \in \mathbf{R}^{m\times n}$ is full rank. Thus, the sliding motion only depends on the dynamics of these $n-m$ states and a order reduction is taken place.

Invariance: The ideal sliding motion is totally insensitive to the matched uncertainty.

The uncertainty, given as form a of $D\xi(t,x)$, is described as matched uncertainty if $\mathcal{R}(D) \subset \mathcal{R}(B)$. An uncertainty which does not lie within the range space of the input distribution matrix is described as unmatched uncertainty. From invariance property, it follows that the reduced order motion is completely insensitive to matched uncertainty.

8.1.2 Sliding surface design

So far, the SMC control problem and the properties of SMC controller has been stated, and then the two steps of designing a SMC controller as mentioned above should be carried out. First of all, the switching function should be designed so that the motion of dynamic system could meet the control requirements. Several methods could be applied to accomplish this job, such as robust eigenstructure assignment and quadratic minimisation introduced in [35].

It becomes simple to design the switching function provided that system is of the so-called regular form [36, p.60]. Following description of the regular form is introduced in [35]. Consider the nominal form of the system (8.1)

$$\dot{x}\left(t\right) = Ax\left(t\right) + Bu\left(t\right) \tag{8.5}$$

where $rank(B) = m$ and (A, B) is a controllable pair. Define an associated switching function

$$s(t) = Sx(t) \tag{8.6}$$

The nominal system (8.5) and switching function (8.6) could be expressed in the regular form

$$\dot{z_1}(t) = A_{11}z_1(t) + A_{12}z_2(t) \tag{8.7}$$
$$\dot{z_2}(t) = A_{21}z_1(t) + A_{22}z_2(t) + B_2u(t) \tag{8.8}$$

with the switching function given as

$$s(t) = S_1z_1(t) + S_2z_2(t) \tag{8.9}$$

The coordinate transformation is written as below defined by an orthogonal matrix T_r.

$$z(t) = T_rx(t) \tag{8.10}$$

The matrix sub-blocks in (8.7) and (8.8) can be obtained in terms of the original pair (A, B) from

$$T_rAT_r^T = \begin{bmatrix} A_{11} & A_{12} \\ A_{21} & A_{22} \end{bmatrix} \qquad T_rB = \begin{bmatrix} 0 \\ B_2 \end{bmatrix} \tag{8.11}$$

In analogy with above, the elements of the switching function in (8.9) satisfy

$$ST_r^T = \begin{bmatrix} S_1 & S_2 \end{bmatrix} \tag{8.12}$$

It can be seen that the system is split into two connected subsystem. The first one is independent of control input meanwhile the dimension of the second subsystem is corresponding to the input dimension m. When sliding motion is taking place, we have following equation

$$S_1z_1(t) + S_2z_2(t) = 0 \tag{8.13}$$

Therefore

$$\begin{aligned} z_2 &= -S_2^{-1}S_1z_1(t) \\ &= -Mz_1(t) \end{aligned} \tag{8.14}$$

where $M \in \mathbf{R}^{m\times(n-m)}$ is defined to be

$$M = S_2^{-1}S_1 \tag{8.15}$$

The new states z_2 is obviously linearly dependent on the z_1 partition. Hence, the sliding motion is governed by equations (8.8) and (8.14). This can be seen as a $(n-m)th$ order system with z_2 as a linear full-state feedback control signal. Closing the loop with the full states feedback, the closed loop system equation is obtained as below.

$$\dot{z}_1(t) = (A_{11} - A_{12}M)\, z_1(t) \tag{8.16}$$

Now the control problem becomes that of designing matrix M to ensure above $(n-m)th$ order system (8.16) stable and meet the control performance.

8.1.3 Control law design

A control law should be constructed to direct the system trajectory towards to the sliding surface and remain it on the surface after a sliding surface is given. Once the trajectory reaches the surface, the sliding motion is taking place, providing the robustness for all the matched uncertainty. In order to ensure the sliding motion is reachable, the reachability condition should be holding, in other words, the sliding surface has to be locally attractive. A common condition for existence of sliding motion is given as

$$s\dot{s} < 0 \tag{8.17}$$

However, this condition could only require that the system trajectory move towards to sliding surface asymptotically [24]. A stronger condition is introduced in [24], called the η-reachability condition:

$$s\dot{s} < -\eta|s| \tag{8.18}$$

This stronger condition guarantees that the sliding surface is reached within

$$t_s < \frac{|s\,(0)|}{\eta} \tag{8.19}$$

So far, the reachability condition has been already given as above, and then a variable control law structure need to be established to meet the reachability condition. It is commonplace to consider following control structure

$$u(t) = u_{eq} + u_n \tag{8.20}$$

where u_{eq} is called equivalent control law which guarantee the system states trajectory remaining on the sliding surface without introduction of any uncertainty, whereas the item u_n is a non-linear switching control rejecting the matched uncertainty and requiring the system trajectory approaching towards sliding surface. u_{eq} could be calculated from the nominal form (8.5) by letting $\dot{s}\,(t) = S\dot{x}\,(t) = 0$. u_n is commonly chosen as

$$u_n\,(t) = -\rho\,(t, x)\,\mathrm{sgn}\,(s) \tag{8.21}$$

provided that

$$\rho\,(t, x) \geq \left|\sum_{i=1}^{n} \Delta_i\,(t)\,x_i\,(t)\right| + \eta \quad for\ all\ t, x \tag{8.22}$$

This discontinuous control signal introduces chattering which is not expected in mechanical system. Therefore, in order to smooth the control action, the discontinuous sign function could be replaced by a saturation function so that the system trajectory is confined within a limited boundary layer of the sliding face. The width of the layer is determined by the saturation function.

8.2 Sliding mode control law design and evaluation for Boeing747 model

8.2.1 Regular form of the longitudinal Boeing 747 model

For sliding mode control design of Boeing 747 aircraft, let us consider the decoupled longitudinal system model. The system longitudinal model becomes following referring to (6.21) by neglecting the p and r coupling items, small state product items and the δ_{th}.

$$\begin{aligned}
\dot{u} &= X_u u + X_{\dot{w}}\dot{w} + X_w w + (X_q - W_e)\, q - g\theta\cos\theta_e + X_{\delta_e}\delta_e \\
\dot{w} &= Z_u u + Z_{\dot{w}}\dot{w} + Z_w w + (Z_q + U_e)\, q - g\theta\sin\theta_e + Z_{\delta_e}\delta_e \\
\dot{q} &= M_u u + M_{\dot{w}}\dot{w} + M_w w + M_q q + M_{\delta_e}\delta_e \\
\dot{\theta} &= q
\end{aligned} \tag{8.23}$$

Above equation could be rewritten into state space form with respect to state variables $x = [u, w, \theta, q]$, shown as below. Some derivative coefficients disappear due to the lack of data of Boeing 747, such as X_q, $X_{\dot{w}}$.

$$\begin{bmatrix} \dot{u} \\ \dot{w} \\ \dot{\theta} \\ \dot{q} \end{bmatrix} = \begin{bmatrix} X_u & X_w & -g\cos\theta & -W_e \\ \frac{-Z_u}{Z_{\dot{w}}-1} & \frac{-Z_w}{Z_{\dot{w}}-1} & \frac{g\sin\theta_e}{Z_{\dot{w}}-1} & \frac{-(Z_q+U_e)}{Z_{\dot{w}}-1} \\ 0 & 0 & 0 & 1 \\ M_u - \frac{M_{\dot{w}}Z_u}{Z_{\dot{w}}-1} & M_w - \frac{M_{\dot{w}}Z_w}{Z_{\dot{w}}-1} & \frac{M_{\dot{w}}g\sin\theta_e}{Z_{\dot{w}}-1} & M_q - \frac{M_{\dot{w}}(Z_q+U_e)}{Z_{\dot{w}}-1} \end{bmatrix} \begin{bmatrix} u \\ w \\ \theta \\ q \end{bmatrix} + \begin{bmatrix} X_{\delta_e} \\ \frac{-Z_{\delta_e}}{Z_{\dot{w}}-1} \\ 0 \\ M_{\delta_e} - \frac{M_{\dot{w}}Z_{\delta_e}}{Z_{\dot{w}}-1} \end{bmatrix} \delta_e \tag{8.24}$$

It is convenient to design the sliding mode control when the model is converted to a so-called regular form [35]. Since $rank(B) = m$, there exists an invertible matrix of elementary row operations $T_r \in \mathbf{R}^{n\times n}$ such that

$$T_r B = \begin{bmatrix} 0 \\ B_2 \end{bmatrix} \tag{8.25}$$

where $B_2 \in \mathbf{R}^{m\times m}$ and is nonsingular. After the transformation, the system model can be expressed in the regular form

$$\begin{aligned}
\dot{z}_1(t) &= A_{11} z_1(t) + A_{12} z_2(t) \\
\dot{z}_2(t) &= A_{21} z_1(t) + A_{22} z_2(t) + B_2 u(t)
\end{aligned} \tag{8.26}$$

The new variables $z(t)$ are defined by

$$z(t) = T_r x(t) \tag{8.27}$$

The matrix sub-blocks in (8.26) are obtained in terms of the original pair (A, B) from (8.28) and (8.25).

$$T_r A T_r^{-1} = \begin{bmatrix} A_{11} & A_{12} \\ A_{21} & A_{22} \end{bmatrix} \tag{8.28}$$

For the case of Boeing 747, select the T_r so that the new B matrix becomes

$$T_r B = \begin{bmatrix} 0 \\ 0 \\ 0 \\ M_{\delta_e} - \frac{M_{\dot{w}} Z_{\delta_e}}{Z_{\dot{w}} - 1} \end{bmatrix} \tag{8.29}$$

and z_2 is still q. Thus, z_2 expressed in terms of new state variables $z(t)$ is equal to the original one, the second equation in (8.24) expressed by the original state variables $x(t)$.

8.2.2 Sliding mode control law design for Boeing 747

This section describes the derivation of the SMC controller for Boeing 747. Consider the regular form of Boeing 747 longitudinal airplane model at presence of parametric uncertainty.

$$\begin{aligned} \dot{z}_1(t) &= A_{11} z_1(t) + A_{12} q(t) \\ \dot{q}(t) &= A_{21} z_1(t) + A_{22} q(t) + B_2 u(t) \end{aligned} \tag{8.30}$$

First of all, let us consider how to design the sliding surface. The sliding surface could be traditionally defined as

$$s_i = \sum_{j=0}^{r_i - 1} c_{ij} e_i^{(j)} = 0 \quad \forall i = 1 \sim m \tag{8.31}$$

where superscript j represents jth derivative, and vector $r = r_1, r_2, \ldots, r_m{}^T$ is a vector relative degree of the system (8.30). The coefficients $c_{ij} \forall i = 1 \sim m, \forall j = 0 \sim r_i - 1$ must be defined to provide the desired dynamics of system to meet the handling quality requirements [37]. For the Boeing 747 aircraft longitudinal mode control problem, which is a single input, elevator command δ_e, and single output, pitch rate command q, system, the sliding surface could be defined as (8.32) by above method (8.31).

$$s = e \tag{8.32}$$

where $e = q - q_d$. Since the relative degree of output q is 1 the $j = 0$ is obtained in (8.31). The dynamics of the sliding motion make the output q track the desired command q_d. The sliding mode control law could reject the matched uncertainty which means the uncertainty in the input channel.

Whence the reachability condition is

$$e \cdot \dot{e} < 0 \tag{8.33}$$

Rewrite the second equation of (8.30) as below form

$$\dot{q} = f(x) + g(x) u \tag{8.34}$$

where f and g is the real value of aircraft which are varying along flight conditions. The mismatch between the real flight condition and the nominal condition (design point) is treated as uncertainty which is a parametric uncertainty. The uncertainty on f is bounded by some known function $F = F(x)$ and the boundary of g is also defined by (8.35). The nominal value of f and g are denoted respectively as f^* and g^* which stand for controller design point.

$$\begin{aligned} &|f^* - f| < F \\ &|g^* - g| < G \\ &g_{\min} < g^* < g_{\max} < 0 \end{aligned} \tag{8.35}$$

Consider the nominal form of model to calculate the equivalent control law u_{eq}. Set $\dot{e} = 0$, therefore

$$\begin{aligned} &\dot{e} = 0 \\ &\Rightarrow \dot{y} - \dot{y}_d = 0 \\ &\Rightarrow L_{f^*}h(x) + L_{g^*}h(x)\, u_{eq} - \dot{y}_d = 0 \\ &\Rightarrow u_{eq} = (L_{g^*}h(x))^{-1} (\dot{y}_d - L_{f^*}h(x)) \end{aligned} \tag{8.36}$$

Thus u_{eq} is the equivalent control law which could maintain the system trajectory on the sliding surface in nominal condition, namely the controller design point. Contrasting to NDI control law, it is evident that the u_{eq} is equal to the feedback linearization in NDI control law. As discussed before, u_n is commonly chosen as $-ksgn(e)$, therefore below sliding control law is obtained.

$$u = (L_{g^*}h(x))^{-1} (\dot{y}_d - k\mathrm{sgn}(e) - L_{f^*}h(x)) \tag{8.37}$$

Then substitute sliding control law (8.37) into $\dot{y}$ based on the parameter varying airplane model, we have

$$\dot{y} = L_f h(x) + L_g h(x) (L_{g^*}h(x))^{-1} (\dot{y}_d - k\mathrm{sgn}(e) - L_{f^*}h(x)) \tag{8.38}$$

For Boeing 747 model, $h(x)$ is identity matrix. Besides, following concise denotation are made for simplification.

Table 8.1: Abbreviation

Original denotation	Abbreviation	Expression in Boeing 747 model
$L_f h(x)$	f	$M_u u + M_{\dot{w}}\dot{w} + M_w w + M_q q$
$L_{f^*}h(x)$	f^*	$\hat{M}_u u + \hat{M}_{\dot{w}}\dot{w} + \hat{M}_w w + \hat{M}_q q$
$L_g h(x)$	g	M_{δ_e}
$L_{g^*}h(x)$	g^*	$\hat{M}_{\delta_e}$

After simplification, we have

$$\begin{aligned} \dot{y} &= f + gg^{*-1} (\dot{y}_d - k\mathrm{sgn}(e) - f^*) \\ &= f + \dot{y}_d - f^* + \left(gg^{*-1} - 1\right) (\dot{y}_d - f^*) - gg^{*-1} k\mathrm{sgn}(e) \end{aligned} \tag{8.39}$$

Then

$$\begin{aligned} \dot{y} - \dot{y}_d &= f - f^* + \left(gg^{*-1} - 1\right)\left(\dot{y}_d - f^*\right) - gg^{*-1}k\mathrm{sgn}\left(e\right) \\ \dot{e} &= f - f^* + \left(gg^{*-1} - 1\right)\left(\dot{y}_d - f^*\right) - gg^{*-1}k\mathrm{sgn}\left(e\right) \end{aligned} \tag{8.40}$$

Equation (8.40) is the expression of $\dot{e}$. Next step is to calculate the condition of k to satisfy the reachability condition (8.33). For simplification, denote $f - f^* + \left(gg^{*-1} - 1\right)\left(\dot{y}_d - f^*\right)$ as H.

$$\begin{aligned} & e \cdot \dot{e} < 0 \\ \Rightarrow & e\left(H - g^{*-1}gk\mathrm{sgn}\left(e\right)\right) < 0 \\ \Rightarrow & eH - g^{*-1}gk\mathrm{sgn}\left(e\right)e < 0 \\ \Rightarrow & eH - g^{*-1}gk\left|e\right| < 0 \\ \Rightarrow & k > g^*g^{-1}\frac{eH}{|e|} \\ \Rightarrow & k > g^*g^{-1}|H| \end{aligned} \tag{8.41}$$

Thereby, the error will converge to 0 as long as we keep k satisfying above condition. Because the boundary of f and g is already known, the maximum value of the right hand side of above inequality equation (8.41) could be calculated. A alternative stronger reachability condition called $\eta-$ reachability condition is given below

$$e \cdot \dot{e} \leq -\eta|e| \tag{8.42}$$

where η is a small positive value, then the time required to hit the sliding surface $e = 0$ could be calculated as

$$t_{reach} \leq \frac{\left|s\left(0\right)\right|}{\eta} \tag{8.43}$$

Thus, the condition of k becomes

$$k \geq g^*g^{-1}Hsgn(e) + g^*g^{-1}\eta \tag{8.44}$$

Therefore, first of all the maximum value of the right hand side of (8.41) which could be denoted as Q, should be calculated.

$$\begin{aligned} g^*g^{-1}|H| &= g^*g^{-1}\left|f - f^* + \left(gg^{*-1} - 1\right)\left(\dot{y}_d - f^*\right)\right| \\ &\leq g^*g^{-1}\left(\left|f - f^*\right| + \left|g^{*-1}\left(g - g^*\right)\left(\dot{y}_d - f^*\right)\right|\right) \\ &= g^*g^{-1}\left(\left|f - f^*\right| + \left|g^{*-1}\left(\dot{y}_d - f^*\right)\right|\left|g - g^*\right|\right) \\ &\leq \frac{|g^*|}{|g|_{\min}}\left(F + \left|g^{*-1}\left(\dot{y}_d - f^*\right)\right|G\right) \end{aligned} \tag{8.45}$$

From the scopes of all the aerodynamic derivatives data given as below table 8.2, the $F(x)$ and G could be computed as (8.46) and (8.47).

Table 8.2: Scope of aerodynamic derivatives

Aerodynamic derivatives	Scope	
	Max	Min
M_u	0.000259	-0.000199
$M_{\dot{w}}$	-0.0000905	-0.000246
M_w	-0.00101	-0.00262
M_q	-0.284	-0.925
M_{de}	-0.378	-2.08

$$
\begin{aligned}
|f - f^*| &= \left|\left(M_u - \hat{M}_u\right) u + \left(M_{\dot{w}} - \hat{M}_{\dot{w}}\right) \dot{w} + \left(M_w - \hat{M}_w\right) w + \left(M_q - \hat{M}_q\right) q\right| \\
&< \left|\left(M_{u_{\max}} - M_{u_{\min}}\right) u\right| + \left|\left(M_{\dot{w}_{\max}} - \hat{M}_{\dot{w}_{\min}}\right) \dot{w}\right| \\
&\quad + \left|\left(M_{w_{\max}} - \hat{M}_{w_{\min}}\right) w\right| + \left|\left(M_{q_{\max}} - \hat{M}_{q_{\min}}\right) q\right| \\
&= |0.000458u| + |0.0001555\dot{w}| + |0.0016w| + |0.641q| \qquad (8.46)
\end{aligned}
$$

$$
|g - g^*| \leq 1.602 \qquad (8.47)
$$

For an impulse command of q of 1 deg/s for 5 seconds, the value of Q is given as picture below .

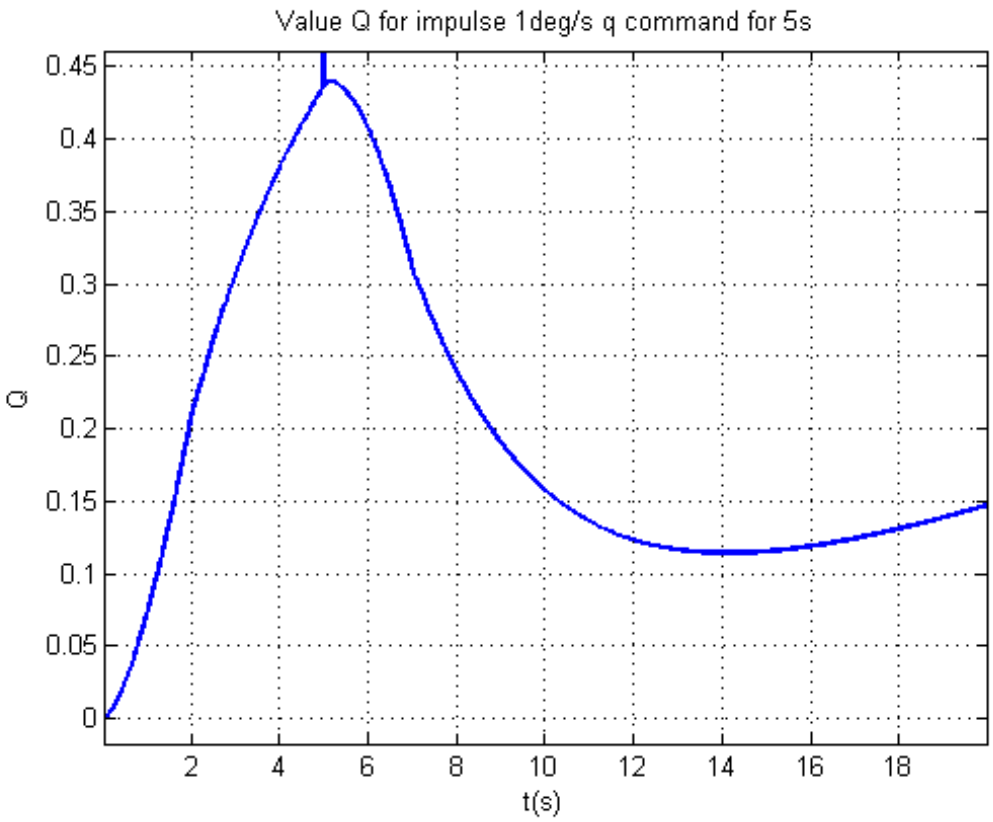

Figure 8.1: Value Q for impulse 1deg/s q command for 5s

It is evident that the maximum value of $Q < 0.45$. Based on above derivation, following sliding mode controller is developed, with constant gain k provided that reachability condition is satisfied which means $k \geq Q$.

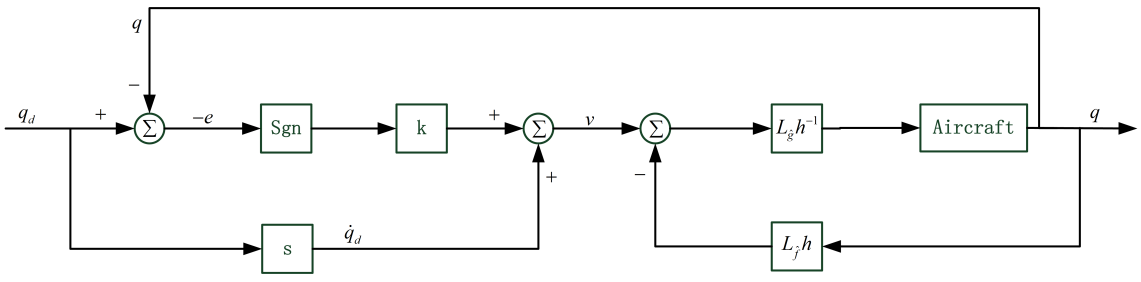

Figure 8.2: Sliding mode controller with constant gain k

Let us set sliding mode controller gain as 0.45, then following results are obtained.

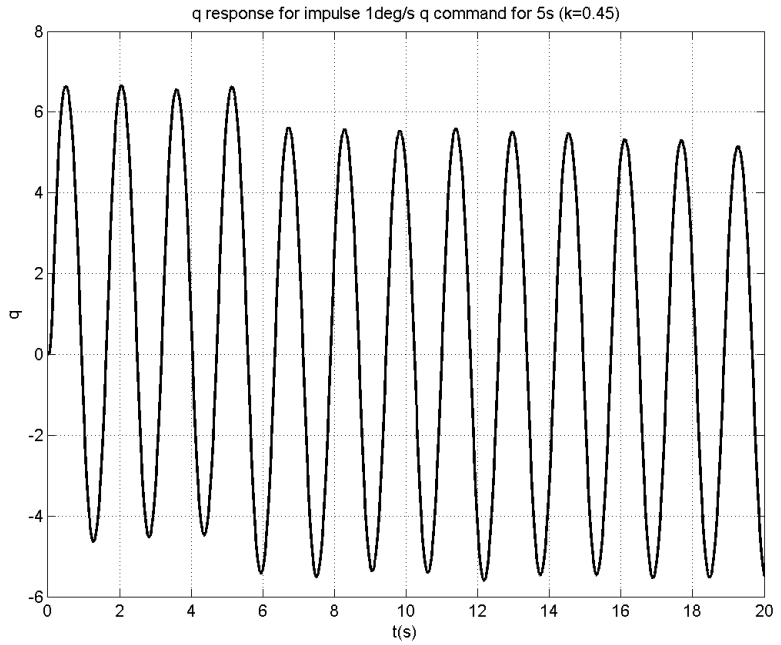

Figure 8.3: q response for impulse 1deg/s q command for 5s (k=0.45)

Obviously, the response is not good. The reason might be that the calculated boundary of uncertainty is much higher than the real uncertainty away from the nominal condition so that the magnitude of chattering is far away from the reasonable extent. In order to reduce the boundary of value Q, some assumption might be hold under certain circumstances. In case of that the flight condition is equal to controller design point, for example controller design point is selected at cruise point, Mach number 0.85 and Altitude 40000ft, the value of g does not vary too much, therefore an assumption that

$$g = g^* \Rightarrow G = 0 \tag{8.48}$$

is reasonably made. Consequently,

$$g^* g^{-1} |H| = F \tag{8.49}$$

For an impulse command of q of 1 deg/s for 5 seconds, the value of $F(x)$ is calculated as shown in figure 8.4.

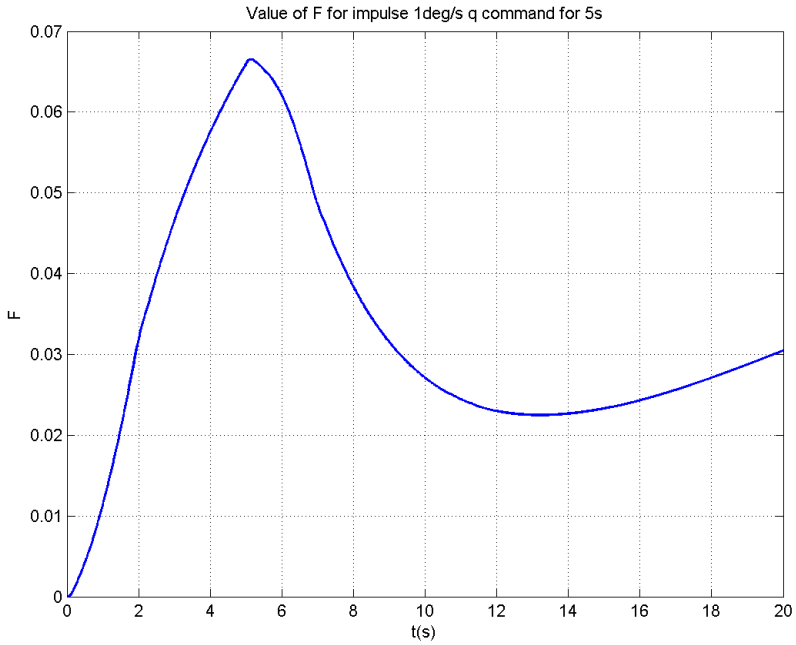

Figure 8.4: Value of F for impulse 1deg/s q command for 5s

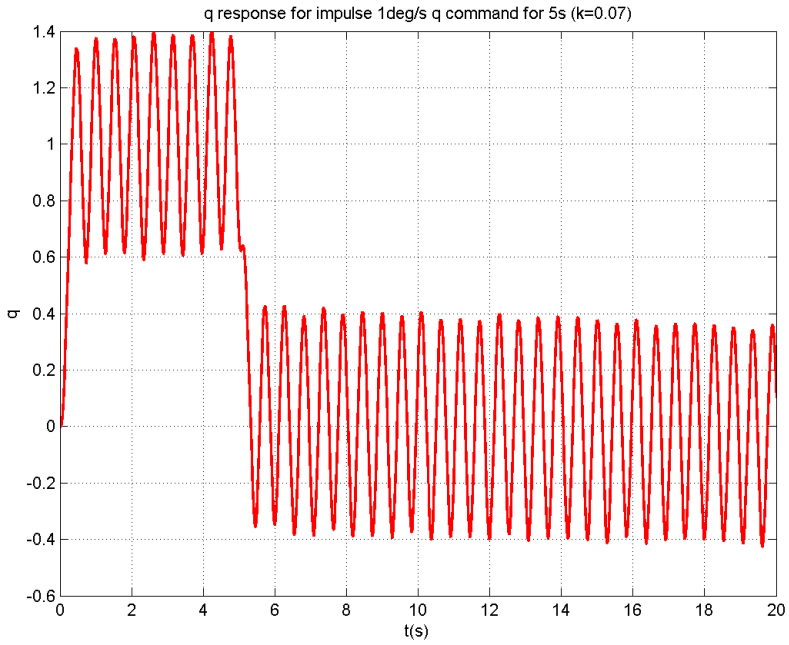

Figure 8.5: q response for impulse 1deg/s q command for 5s (k=0.07)

From the result, it is seen that $F < 0.07$. Setting SMC controller gain at 0.07, result is shown in figure 8.5. The result is still not good enough but it becomes more reasonable. It could be implied that the value of F should be very small at

the beginning due to all the small deviations of aerodynamic derivatives from the nominal condition and all the small values of state variables. Thus, let us assume that the value of Q less than 0.01 at cruise condition for a 1deg/s q common for 5 seconds. Setting $k = 0.01$ following results are gained.

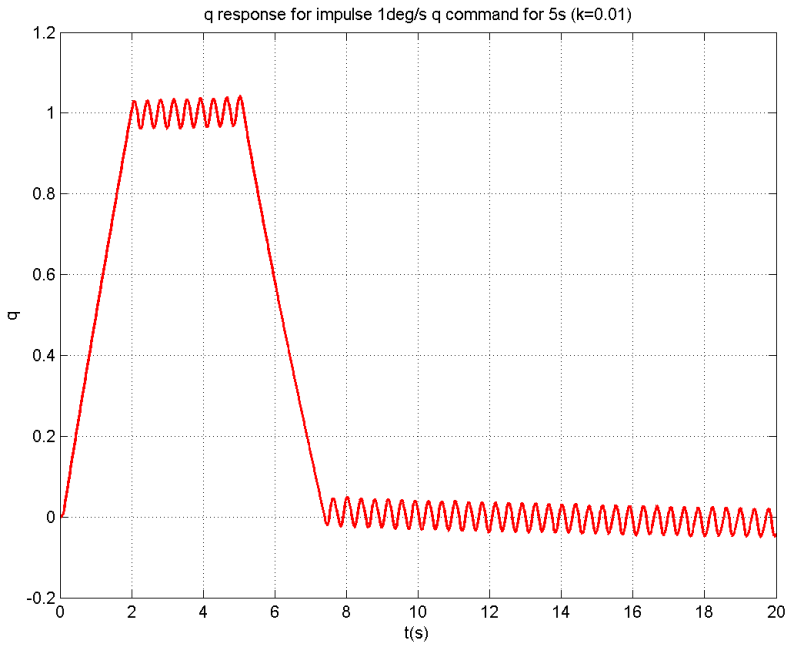

Figure 8.6: q response for impulse 1deg/s q command for 5s (k=0.01)

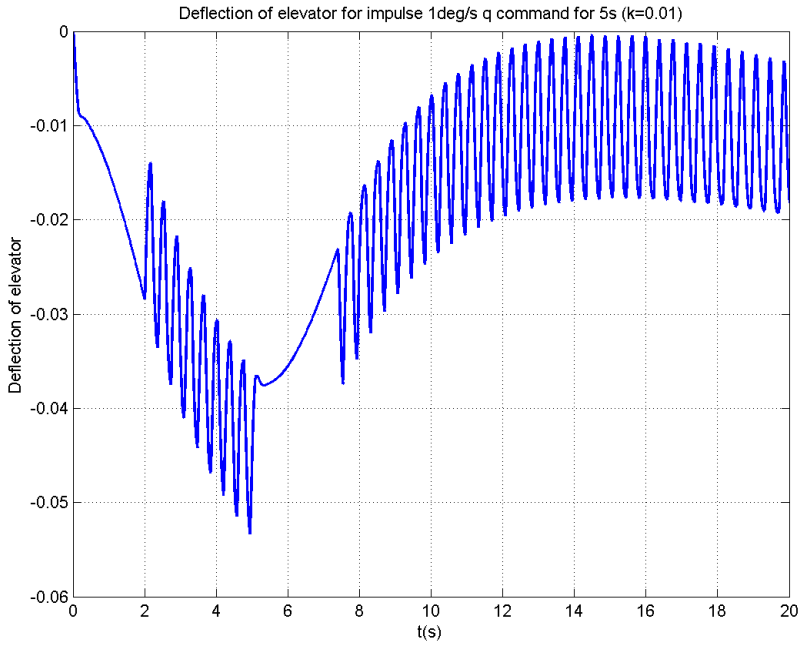

Figure 8.7: Deflection of elevator for impulse 1deg/s q command for 5s for smoothed SMC (k=0.01)

Above result provided acceptable converge speed and less than 5% chattering is much better than previous ones and does not diverge which proves above assumption is satisfied. By comparing figure 8.3, figure 8.5 and figure 8.6, two conclusions might be drawn that:

- The magnitude of chattering is proportional to the value of sign function gain k;
- The settle time is inversely proportional to the value of sign function gain k since the η increase as the control gain rising, consequently the settle time is reduced.

Other flight conditions are assessed for controller gain at 0.01 for the same q command shown below. From figure 8.8, it can be seen that the response can not reach the command value at approaching flight condition meanwhile converge speed slow down at decent flight point at which the response start to diverge at the last second. Intuitively, the SMC controller gain should be enlarged to cope with bigger uncertainty throughout the overall flight profile. Figure 8.9 indicates the evaluation results obtained for SMC controller gain $k = 0.03$. It is evident that all the chattering become larger although responses of all flight condition could converge to command value and settling time are shorter. Thus improvements are needed in order to handle all flight conditions and at the same time, trying to maintain desired performance.

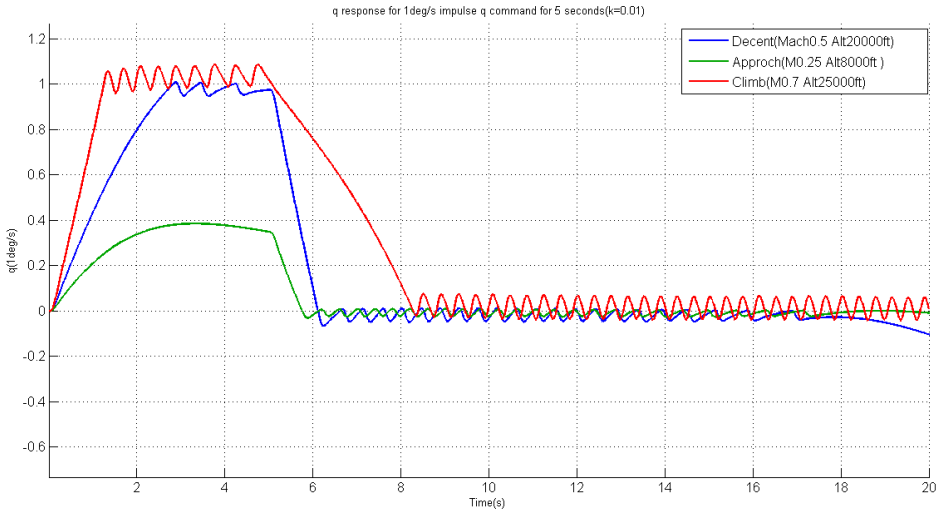

Figure 8.8: q response for 1deg/s impulse q command for 5 seconds at other flight points (k=0.01)

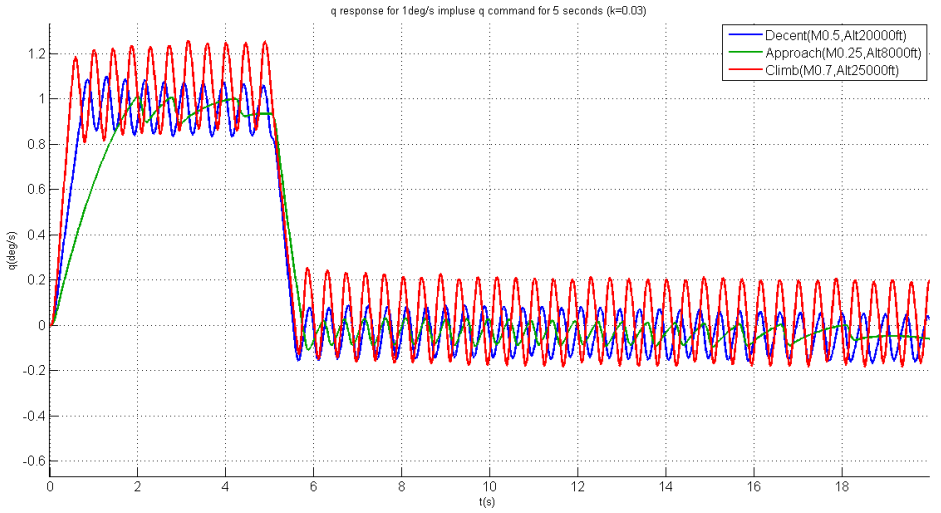

Figure 8.9: q response for 1deg/s impulse q command for 5 seconds at other flight points (k=0.03)

8.2.3 Smoothing the control action

As illustrated in previous section, there is some chattering in all outputs since the controller cannot maintain the system trajectory exactly on the sliding surface. This chattering, in turn, causes undesired high discontinuous control activity (as shown in figure 8.7) and further may excite high-frequency dynamics neglected in modeling [24].Hence, it is intuitive to smooth at the control inputs.

An easy way to achieve this is to replace the sign function by a saturation function in SMC control law. The idea is that once the system trajectory goes inside a boundary layer along sliding surface the control inputs are smoothed by a saturation function of s rather than the discontinuous sign function of s. The original sliding mode control law (8.37) is replaced by

$$u = \left(L_{g^*}h\left(x\right)\right)^{-1}\left(\dot{y}_d - k\text{sat}(e) - L_{f^*}h\left(x\right)\right) \tag{8.50}$$

The control input is smoothed as indicated in figure 8.10.

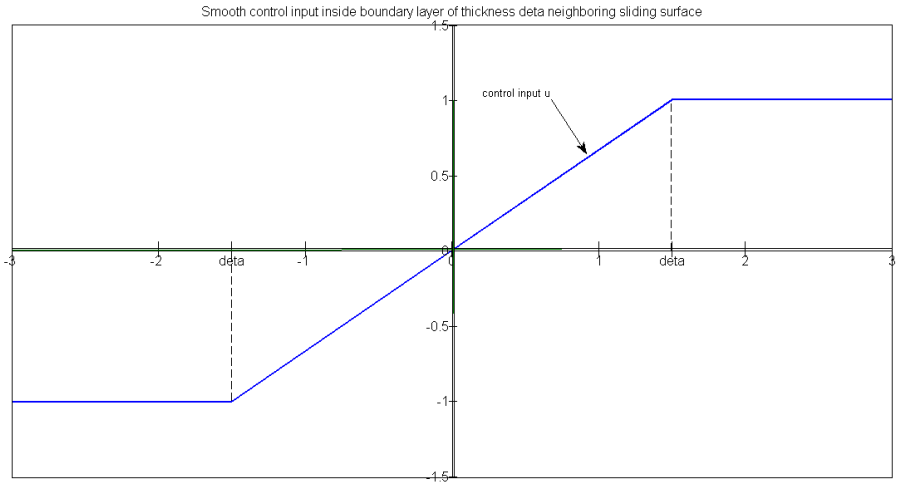

Figure 8.10: Control interpolation in the boundary layer

However, this replacement could give rise to somewhat steady state error that might be eliminated by introduction of an integral term in the sliding surface [37]. The choice of boundary thickness δ is critical since small values of δ may not solve the chattering problem whereas large values may increase the steady state error, thus it requires a compromise choice when selecting the boundary layer thickness [38]. Here the boundary layer is chosen as 5% of the command value so that the steady state error is not too much. For 1deg/s q impulse command, the value of boundary thickness δ is

$$\delta = 1 \times pi/180 \times 5\% = 8.75e^{-4} \tag{8.51}$$

Thus, the continuous SMC control law is obtained as below

$$u = \left(L_{g^*}h\left(x\right)\right)^{-1}\left(\dot{y}_d - k\text{sat}(\frac{e}{\delta}) - L_{f^*}h\left(x\right)\right) \tag{8.52}$$

The same command as shown in the last section, 1deg/s impulse q command for 5 seconds, is taken for the smoothed SMC control law with design point at cruise condition (Mach 0.85, Altitude 40000ft), providing following evaluation result (figure 8.11). The response is very good which has rise time of 2 seconds , settle time of 2 seconds, rather small overshoot of 2% and very little steady state error. In addition,

the input signal, namely deflection of the elevator, is smooth and without high frequency oscillation, indicated in figure 8.12.

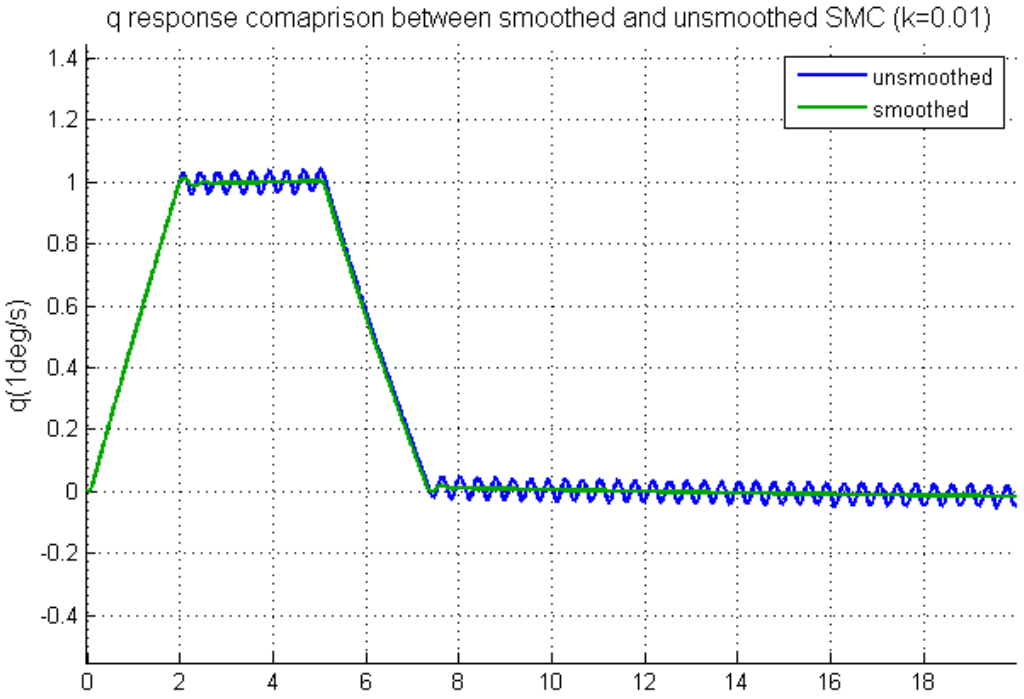

Figure 8.11: q response comparison between smoothed and unsmooth SMC (k=0.01) for impulse 1deg/s q command for 5s

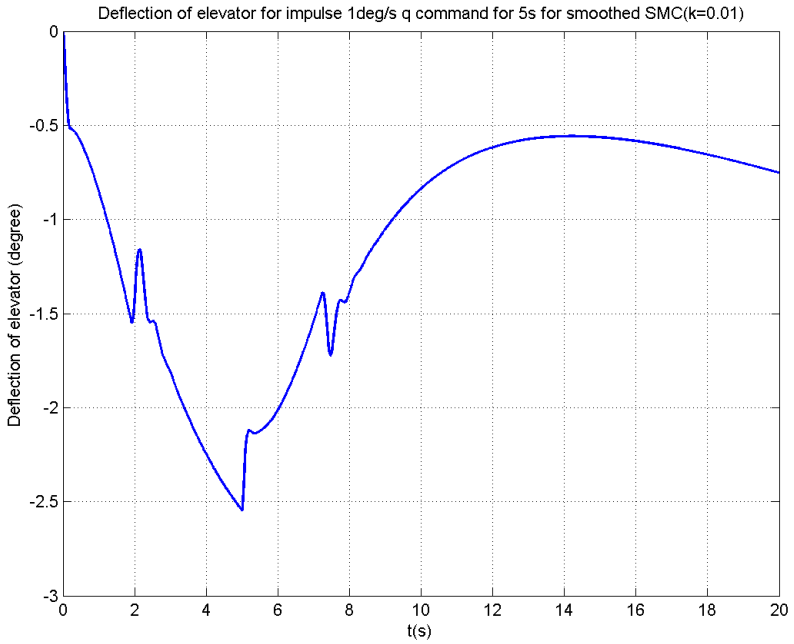

Figure 8.12: Deflection of elevator for impulse 1deg/s q command for 5s for smoothed SMC(k=0.01)

8.2.4 Variation of Sliding mode control law

By analogy with the desired dynamic of NDI controller, SMC also could have some variations of the control law, for example adding a proportional term to the SMC control law (8.52). However, it should be noticed that the desired dynamics of the system is defined by sliding surface (8.32) after the system trajectory has arrived on the sliding surface whereas the variations of the SMC control law could only change the mean of convergence to the sliding surface.

For instance, if we add a proportional term $k_p e$ in the SMC control law (8.52), the following is obtained.

$$u = \left(L_{g^*} h\left(x\right)\right)^{-1} \left(\dot{y}_d - L_{f^*} h\left(x\right) - k\mathrm{sat}(\frac{e}{\delta}) - k_p e\right) \tag{8.53}$$

Then (8.40) becomes

$$\dot{e}{=}f - f^* + \left(g g^{*-1} - 1\right)\left(\dot{y}_d - f^*\right) - g g^{*-1} k\mathrm{sgn}\left(e\right) - g g^{*-1} k_p e \tag{8.54}$$

If substitute (8.54) into the reachability condition (8.33)

$$\begin{aligned} e \cdot \dot{e} &= e\left(H - g g^{*-1} k\mathrm{sgn}\left(e\right) - g g^{*-1} k_p e\right) && (8.55)\\ &= -g g^{*-1} k_p e^2 - e\left(H - g g^{*-1} k\mathrm{sgn}\left(e\right)\right) && (8.56) \end{aligned}$$

where $-g g^{*-1} k_p e^2 < 0$, if k_p is positive and $e\left(H - g g^{*-1} k\mathrm{sgn}\left(e\right)\right)$ is negative on condition that

$$k > g^{-1} g^* \left|H\right| \tag{8.57}$$

which is the same with (8.41). Thus, in other words, the reachability condition is hold as long as k meets the original condition (8.41). Yet, the convergence speed is different since the following equation is gained.

$$e \cdot \dot{e} < -g g^{*-1} k_p e^2 \tag{8.58}$$

where $g g^{*-1} k_p$ is a positive value. It could be interpreted that the system trajectory of the new SMC control law goes to sliding surface much faster than that of original control law with the same value of k. If k_p is chosen as 1, the responses of these two SMC control laws are compared in the figure below.

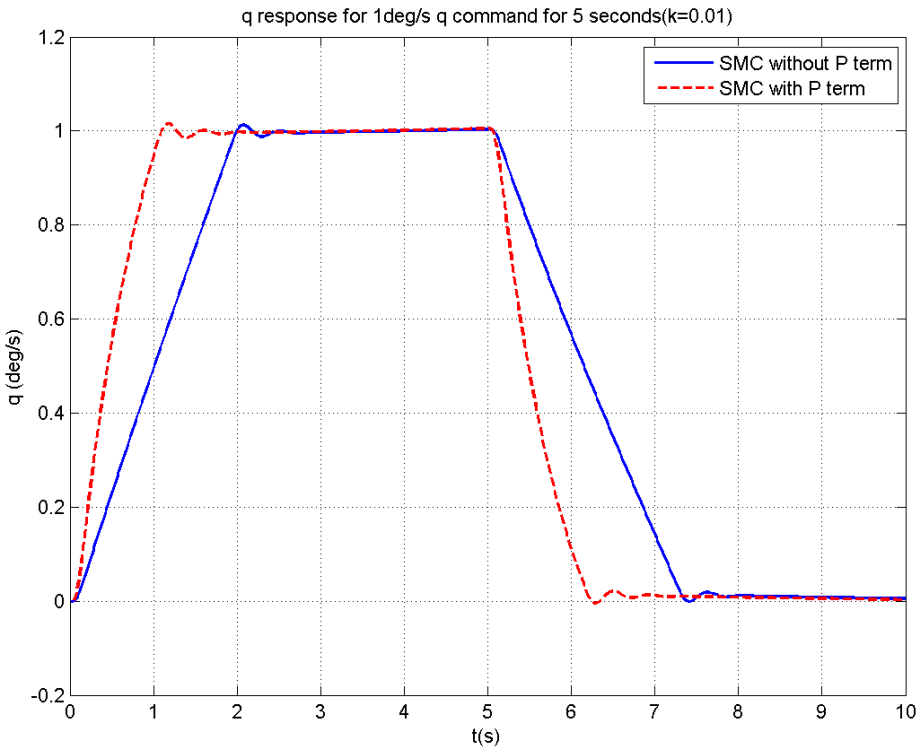

Figure 8.13: Comparison between SMC with P term and without P term

As Shown in the above figure 8.13, it is obvious that the convergence speed of SMC with proportional term is much faster than that of SMC without proportional term. The meaning of this is that the convergence speed could be increased without changing value of k, namely without increasing the magnitude of chattering, referring to the first conclusion drawn in section 8.2.2.

Next, let us stress that both the proportion term and integral term are added into the SMC control law, providing following control law.

$$u = \left(L_{g^*}h\left(x\right)\right)^{-1}\left(\dot{y}_d - L_{f^*}h\left(x\right) - k\mathrm{sgn}\left(e\right) - k_p e - k_i\int edt\right) \tag{8.59}$$

Substituting control law (8.59) in to system (8.34), the equation (8.40) becomes

$$\dot{e}{=}f - f^* + \left(gg^{*-1} - 1\right)\left(\dot{y}_d - f^*\right) - gg^{*-1}k\mathrm{sgn}\left(e\right) - gg^{*-1}k_p e - gg^{*-1}k_i\int edt \tag{8.60}$$

In the next chapter, the disturbance expression is given as below based on the control law (8.59), analogizing with 9.41.

$$\begin{aligned} d &= \Delta f + \Delta g u \\ &= \Delta f + \Delta g g^{*-1}\left(\dot{q}_d - f^*\right) - \Delta g g^{*-1}k\mathrm{sgn}\left(e\right) - \Delta g g^{*-1}k_i\int edt \end{aligned} \tag{8.61}$$

Thus, the equation (8.60) can be rewritten as

$$\dot{e}{=}\ \mathrm{d} - k\mathrm{sgn}\left(e\right) - k_p e - k_i\int edt \tag{8.62}$$

The dynamics of e is ensured stable as long as the term $\mathrm{d} - k\mathrm{sgn}\,(e)$ is negative value and the control gain k_p and k_i are both positive value. Hence, the sliding surface is able to be reached in finite time.

The integral term sums the instantaneous error over time and gives the accumulated offset that have been corrected previously. Therefore, the integral term is able to help driving the error to zero ($e = 0$ is sliding surface) quickly but may cause overshoot as an adverse effect. In addition, assuming that the proportional term and the value k together are not sufficient to drive e towards sliding surface when facing big disturbance, e will increase and move away from the sliding surface. Then the integral action will increase the control action accordingly and become sufficient to force the trajectory to move back to the sliding surface after a period of time, satisfying the reaching condition $e \cdot \dot{e} < 0$ [39]. In this sense, integral term reinforces the robustness performance of the controller to some extent.

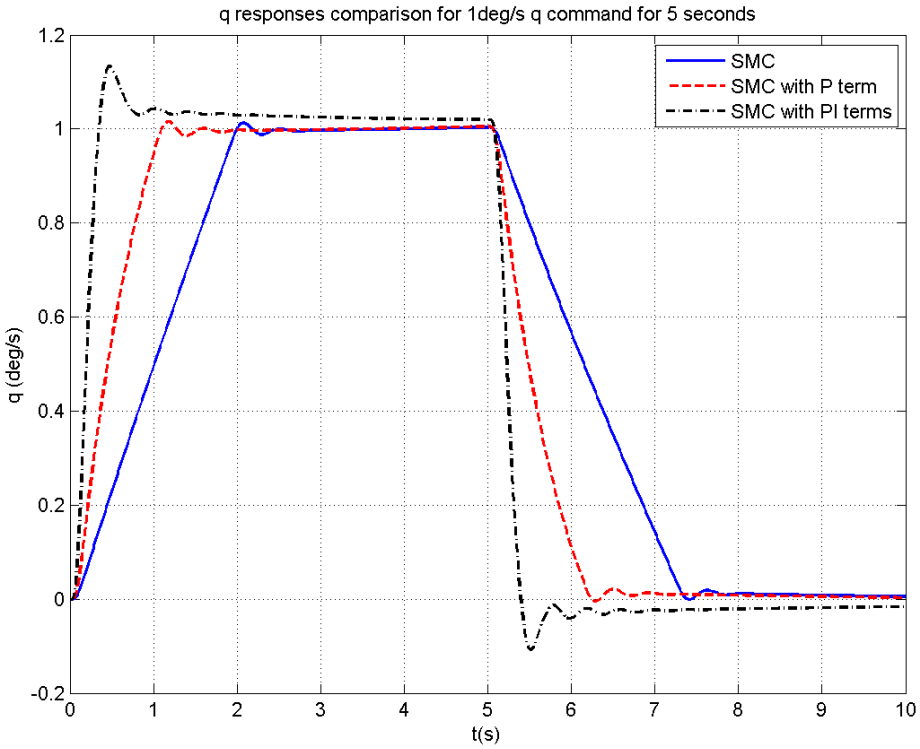

Figure 8.14: q responses comparison between SMC, SMC with P term and SMC with PI term for 1 deg/s impulse input for 5 seconds

A PI SMC control law is designed providing that the proportional term gain and integral term gain is selected the same with PI NDI control law in section 7.5 ($k_p = 4$ and $k_i = 4$) and the value of k retain at 0.01. Above figure 8.14 illustrates the results of smoothed SMC, P SMC and PI SMC at design point, implying that integral term significantly decreases the rise time but causes a big overshoot at the same time.

The PI SMC control law and PI NDI control law are also contrasted for cruise point in the chart below. As expected, the PI SMC controller has slightly shorter rise time

and settle time than PI NDI controller. Furthermore, the PI SMC controller has less overshoot than the PI NDI controller. Meanwhile, the steady state error of PI SMC controller keeps the same with that of PI NDI controller. More flight points are assessed for PI NDI controller and PI SMC controller, provided in appendix C.

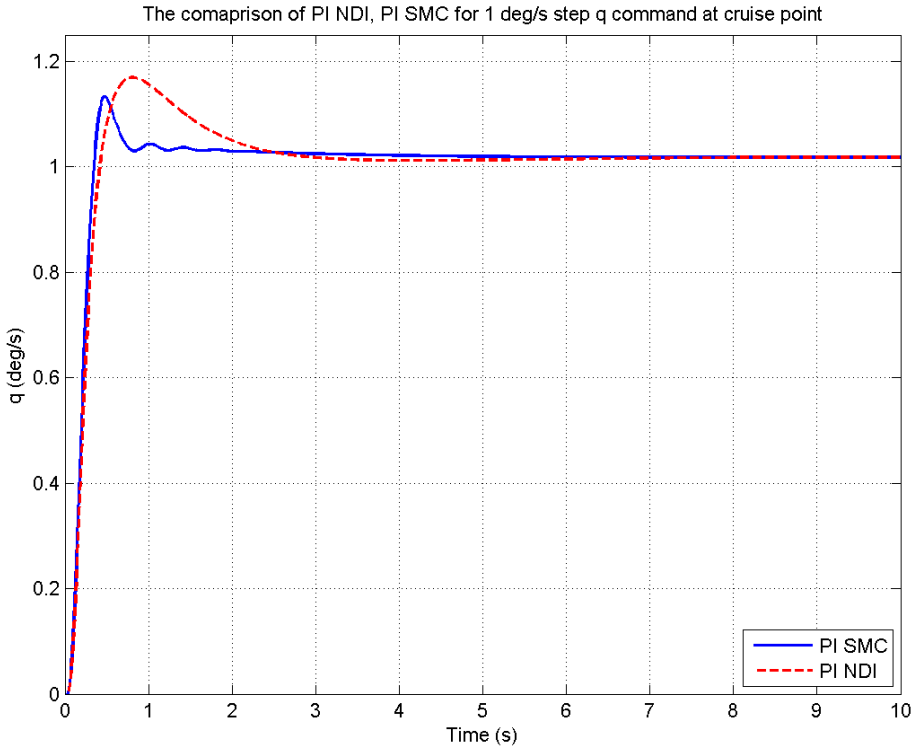

Figure 8.15: The comaprison of PI NDI, PI SMC for 1 deg/s step q command at cruise point

8.2.5 Assessment for the overall flight profile

In this section, all these 3 types of smoothed SMC control law are evaluated at 4 typical flight points. These 3 types of smoothed SMC control laws are shown as below.

1. Smoothed SMC control law

$$u = g^{*-1}\left(\dot{y}_d - f^* - k\text{sat}(\frac{e}{\delta})\right) \quad k = 0.01,\ \delta = 8.75e^{-4} \tag{8.63}$$

2. Smoothed SMC with proportional term

$$u = g^{*-1}\left(\dot{y}_d - f^* - k\text{sat}(\frac{e}{\delta}) - k_p e\right) \quad k = 0.01,\ k_p = 1,\ \delta = 8.75e^{-4} \tag{8.64}$$

3. Smoothed SMC with proportional and integral terms

$$u = g^{*-1}\left(\dot{y}_d - f^* - k\text{sat}(\frac{e}{\delta}) - k_p e - k_i \int edt\right)$$
$$k = 0.005,\ k_p = 4,\ k_i = 4,\ \delta = 8.75e^{-4} \tag{8.65}$$

Firstly, the smoothed SMC without proportional and integral terms is assessed. Figure 8.16 shows that the SMC controller without proportional and integral terms cannot cope with some flight points which means there is big uncertainty. The value k has to be increased if good performance throughout the whole flight profile is expected as described in section 8.2.2. Yet, a big value of k will give rise to big undesired chattering.

Secondly, let us evaluate the performance of the smoothed SMC with proportional term for these 4 typical flight points. It can be seen from figure 8.17 that the rise times are reduced due to the effect of proportional term and the damping is strengthened but still diverges. In other words, the proportional term is not sufficient to drive the error back to sliding surface.

Thirdly, figure 8.18 illustrates the assessment results of the smoothed SMC control law with proportional and integral terms. As you can see from this picture, all the responses move towards to the demand value and maintain at a value with a small steady state error. However, big overshoots occur at climb flight condition due to the introduction of an integral term.

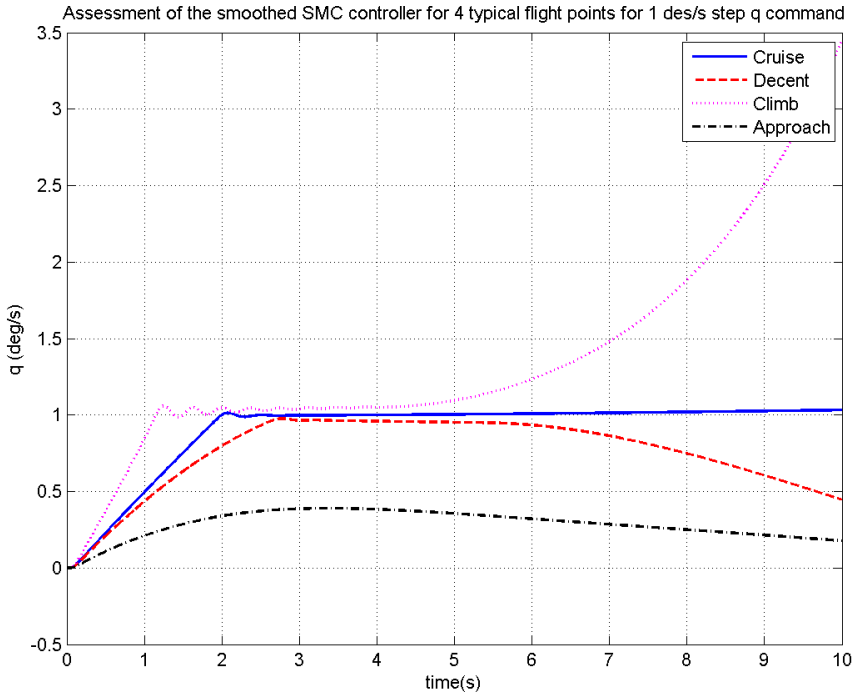

Figure 8.16: Assessment of the smoothed SMC controller for 4 typical flight points for 1 des/s step q command.

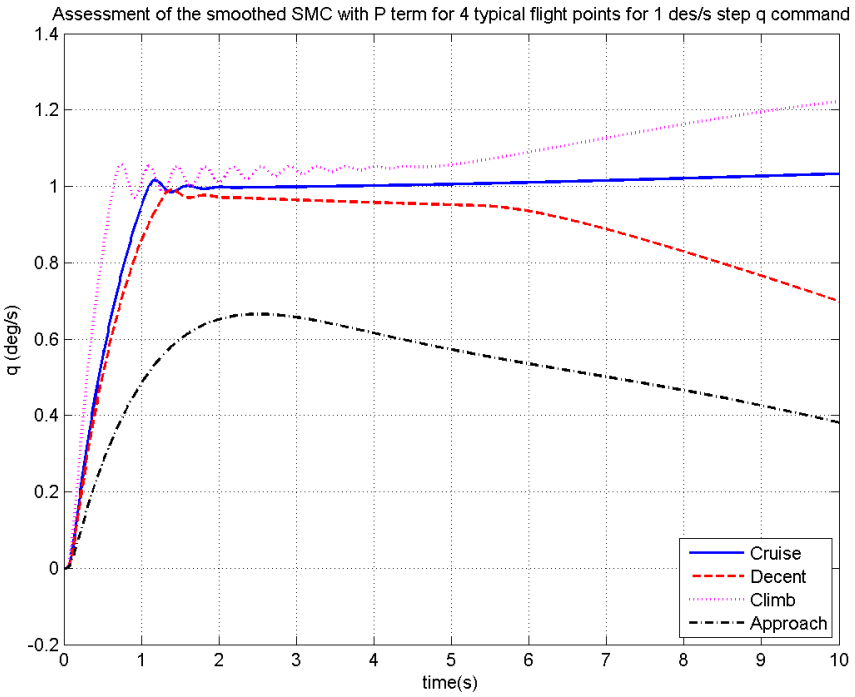

Figure 8.17: Assessment of the smoothed SMC with P term for 4 typical flight points for 1 des/s step q command.

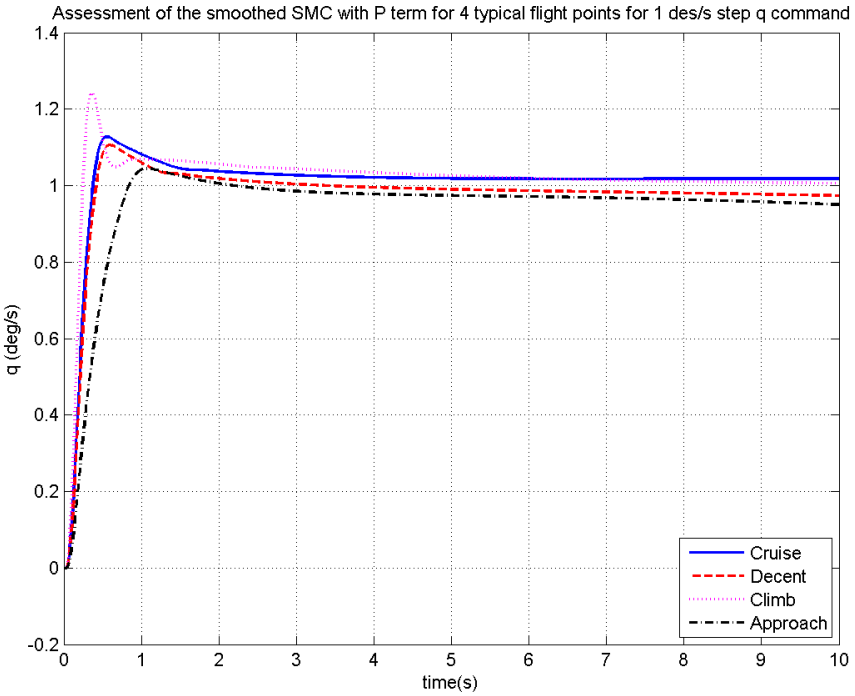

Figure 8.18: Assessment of the smoothed SMC with PI term for 4 typical flight points for 1 des/s step q command.

As discussed above, the SMC and proportional SMC are able to handle the uncertainties to some extent. If increase control gain k, the robustness performance is improved but this introduces adverse chattering. In contrast, the PI SMC control law is capable of coping with big uncertainty but causes overshoot simultaneously. Therefore, a way need to be found to solve this problem. In this thesis, the adaptive SMC is considered which tries to reduce the boundary of uncertainty in turn reduce the value of k. Let us remind a conclusion drawn in the last section: the magnitude of chattering and the amount of control activities are proportional to the value of SMC controller gain k. Besides, the value of controller gain k should be at least greater than the value of Q to guarantee the stability of SMC controller, in other words k is determined by the value of Q which stands for the boundary of uncertainty. Thus, the reduction of uncertainty means it is easier to be overcome and the gain k can be decreased as well, consequently the performance could be improved.

One way of adaptive SMC is to observe uncertainty directly which is adopted in reference [40] and [41]. An alternative way is online estimating the unknown parameter to calculate the uncertainty boundary. Next chapter tries to develop an adaptive control law for both NDI controller and SMC controller, and evaluates the performances of both controllers.

8.3 Summary

Sliding mode control is a nonlinear robust control theory. In this chapter, the sliding mode control law for Boeing 747 aircraft model is developed. A SMC control law is designed at cruise condition and then smoothed by replacing the sign function with saturation function. It is found that the convergence speed is proportional to the gain k of sign function whereas the magnitude of chattering is inversely proportional to the k.

The SMC control law could also has some variations by analogy with desired dynamics of the NDI control law. A proportional term and integral term are added into the SMC control law in section 8.2.4. From the evaluation results, the convergence speed to the sliding surface of the P SMC controller is accelerated without raising sign function gain k. The robust performance is improved significantly by adding integral term that provides the adverse effect, namely overshoot.

At last, these 3 types of SMC control law are evaluated for 4 typical flight conditions. The results are not perfect, thus the adaptive SMC control law is considered to solve the problem which is given in the next chapter.

Chapter 9

Adaptive SMC controller and Adaptive NDI controller design

9.1 Adaptive control introduction

Most controller design techniques are employed on condition that the plant model is well known. However, in some cases, the plant to be control is too complex and the dynamic model is not completely understood. In this case, system identification is introduced intuitively to make progressive understanding of plant at first and then the control law is applied based on the recursively updated plant model [25].

> We will see adaptive control, pragmatically, as a direct aggregation of a (non-adaptive) control methodology with some form of recursive system identification.[25]

In terms of the controller update way, adaptive control is categorized as direct adaptive control schemes, namely model reference adaptive controller, and indirect adaptive control schemes, namely so-called self tuning regulators. The direct method adapts the controller parameters directly aiming to make output achieve the reference model. The indirect method updates the controller parameters through a fixed transformation after recursively estimating system parameters. The non-adaptive control law in this two schemes can be the same, which means that the model reference adaptive controller is able to be seen as a special case of self tuning regulator with identity transformation between system parameters and controller parameters [25, p.9].

For the indirect adaptive schemes, the normal process is that we firstly parameterize plant model, secondly establish the error equation, then apply the adaptation algorithm to estimate system parameters, finally transform the estimated system parameters to controller parameters. The following figure indicates the typical structure of the self tuning controller.

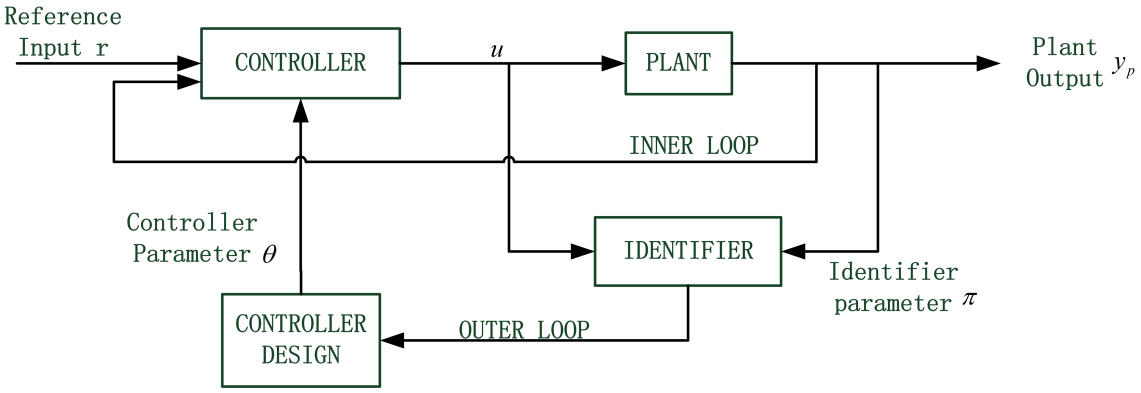

Figure 9.1: Self tuning controller structure

9.2 Identifier structure

9.2.1 Equation error identifier

The function of identifier is to produce a recursive estimate of the unknown parameter of the system. Following methods are described in Sastry S. and Bodson M. 's book [25]. A typical parameterization of a unknown plant transfer function is given as below equation

$$\frac{\hat{y_p}(s)}{\hat{r}(s)} = \frac{\alpha_n s^{n-1} + \cdots + \alpha_1}{s^n + \beta_n s^{n-1} + \cdots + \beta_1} \tag{9.1}$$

Equation (9.1) could be rewritten as

$$\hat{y_p}(s) = \frac{\alpha_n s^{n-1} + \cdots + \alpha_1}{\hat{\lambda}(s)}\hat{r}(s) + \frac{(\lambda_n - \beta_n)s^{n-1} + \cdots + (\lambda_1 - \beta_1)}{\hat{\lambda}(s)}\hat{y}_p(s) \tag{9.2}$$

where

$$\hat{\lambda}(s) = s^n + \lambda_n s^{n-1} + \cdots + \lambda_1$$

which is assumed to be Hurwitz but is otherwise arbitrary. If let

$$\begin{aligned} \hat{a}^*(s) &= \alpha_n s^{n-1} + \cdots + \alpha_1 = k_p \hat{n}_p(s) \\ \hat{b}^*(s) &= (\lambda_n - \beta_n)s^{n-1} + \cdots + (\lambda_1 - \beta_1) = \hat{\lambda}(s) - \hat{d}_p(s) \end{aligned} \tag{9.3}$$

The new parameterization of plant is obtained

$$\hat{y}_p(s) = \frac{\hat{a}^*(s)}{\hat{\lambda}(s)}\hat{r}(s) + \frac{\hat{b}^*(s)}{\hat{\lambda}(s)}\hat{y}_p(s) \tag{9.4}$$

A state space realization of the foregoing parameterization is found by choosing $\Lambda \in \mathbf{R}^{n\times n}$, $b_\lambda \in \mathbf{R}^n$ in controllable canonical form, such that

$$\Lambda = \begin{bmatrix} 0 & 1 & 0 & \cdot & \cdot & 0 \\ 0 & 0 & 1 & \cdot & \cdot & 0 \\ \cdot & \cdot & \cdot & \cdot & \cdot & \cdot \\ \cdot & \cdot & \cdot & \cdot & \cdot & 0 \\ 0 & 0 & \cdot & \cdot & \cdot & 1 \\ -\lambda_1 & \cdot & \cdot & \cdot & \cdot & -\lambda_n \end{bmatrix} \quad b_\lambda = \begin{bmatrix} 0 \\ \cdot \\ \cdot \\ \cdot \\ 0 \\ 1 \end{bmatrix}$$
$$(sI - \Lambda)^{-1} b_\lambda = \tfrac{1}{\hat{\lambda}(s)} \begin{bmatrix} 1 \\ s \\ \cdot \\ \cdot \\ \cdot \\ s^{n-1} \end{bmatrix} \tag{9.5}$$

In analogy with equation (9.3), define

$$\begin{aligned} a^{*^T} &:= (\alpha_1, \cdots, \alpha_n) \\ b^{*^T} &:= (\alpha_1 - \beta_1, \cdots, \alpha_n - \beta_n) \end{aligned} \tag{9.6}$$

Thus, we obtain the state space form of the plant, the vectors $w_p^{(1)}(t), w_p^{(2)}(t) \in \mathbf{R}^n$

$$\begin{aligned} \dot{w}_p^{(1)} &= \Lambda w_p^{(1)} + b_\lambda r \\ \dot{w}_p^{(2)} &= \Lambda w_p^{(2)} + b_\lambda y_p \end{aligned} \tag{9.7}$$

With initial conditions $w_p^{(1)}(0)$, $w_p^{(2)}(0)$. In Laplace transforms

$$\begin{aligned} w_p^{(1)}(s) &= (sI - \Lambda)^{-1} b_\lambda \hat{r}(s) + (sI - \Lambda)^{-1} w_p^{(1)}(0) \\ w_p^{(2)}(s) &= (sI - \Lambda)^{-1} b_\lambda \hat{y}_p(s) + (sI - \Lambda)^{-1} w_p^{(2)}(0) \end{aligned} \tag{9.8}$$

The description of the plant (9.4) becomes

$$\hat{y}_p(s) = a^{*^T} w_p^{(1)}(s) + b^{*^T} w_p^{(2)}(s) \tag{9.9}$$

and because the plant parameters a^*, b^* are constant, the same expression is valid in the time domain

$$y_p(t) = a^{*^T} w_p^{(1)}(t) + b^{*^T} w_p^{(2)}(t) := \theta^{*^T} w_p(t) \tag{9.10}$$

where

$$\begin{aligned} \theta^{*^T} &:= (a^{*^T}, b^{*^T}) \in \mathbf{R}^{2n} \\ w_p(t)^T &:= (w_p^{(1)^T}(t), w_p^{(2)^T}(t)) \in \mathbf{R}^{2n} \end{aligned} \tag{9.11}$$

Equations (9.6)-(9.11) define a realization of the new parameterization. The vector w_p is the generalized state of the plant and has dimension 2n. The set of unknown parameters θ^* relate linearly to the original parameters α_i, β_i by (9.6), and each corresponding to one of the equivalent parameterizations. So far, the plant has been parameterized as a state space form where the output depend linearly on the new parameters θ^*. We can construct an identifier with the same structure with the state space realization (9.7) and (9.10) showing as below.

$$\begin{aligned} \dot{w}^{(1)} &= \Lambda w^{(1)} + b_\lambda r \\ \dot{w}^{(2)} &= \Lambda w^{(2)} + b_\lambda y_p \end{aligned} \tag{9.12}$$

with the identifier signals

$$\begin{aligned} \theta^T &:= (a^T, b^T) \in \mathbf{R}^{2n} \\ w(t)^T &:= (w^{(1)^T}(t), w^{(2)^T}(t)) \in \mathbf{R}^{2n} \end{aligned} \tag{9.13}$$

The initial conditions in (9.12) is arbitrary, and the observer error $w(t) - w_p(t)$ fade exponentially to zero, even if the plant is unstable. In analogy with the expression of the plant output, the output of the identifier is defined to be

$$y_i(t) = \theta^T(t) w(t) \in \mathbf{R} \tag{9.14}$$

and defines the parameter error

$$\phi(t) := \theta(t) - \theta^* \in \mathbf{R^{2n}} \tag{9.15}$$

thus the identifier error is obtained

$$e(t) := y_i(t) - y_p(t) = \phi^T(t) w(t) \tag{9.16}$$

This type of error equation is called linear error equation with which the gradient identification algorithm and least square identification algorithm could be applied. Figure 9.2 shows this identifier structure.

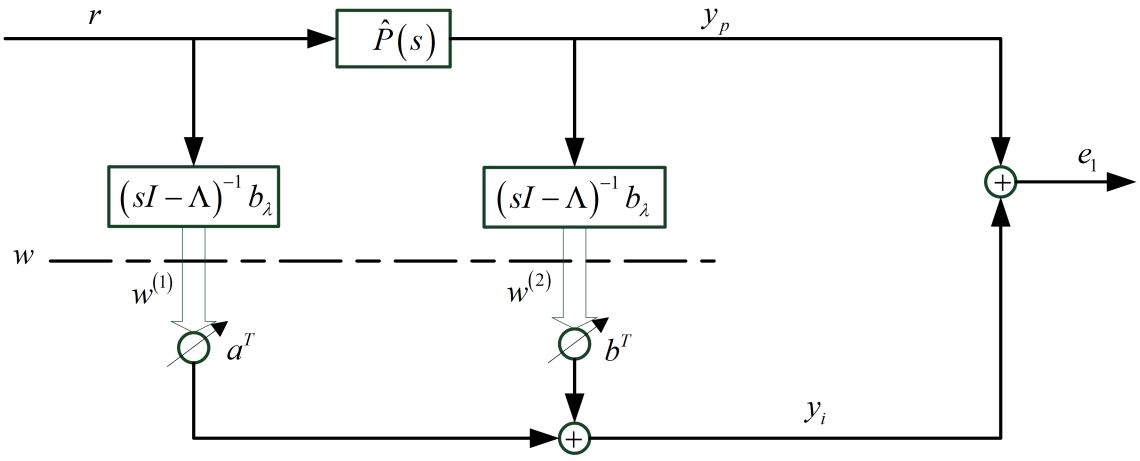

Figure 9.2: Linear error identifier

9.2.2 Model reference identifiers

The model reference identifier is based on another approach to parameterize the plant. Consider below representation of the plant, there exist unique $\hat{a}^*$, $\hat{b}^*$ such that the transfer function from $r \to y_p$ is the original transfer function $\hat{P}(s)$. The proof is given in reference [25, p.77-79]. In analogy with identifier structure of euqation error identifier in section 9.2.1, we define $\Lambda \in \mathbf{R}^{n-1\times n-1}$, $b_\lambda \in \mathbf{R}^{n-1}$ in controllable canonical form such that $det(SI - \Lambda) = \hat{(\lambda)}(s)$ and

$$(sI - \Lambda)^{-1} b_\lambda = \frac{1}{\hat{\lambda}(s)} \begin{bmatrix} 1 \\ s \\ . \\ . \\ . \\ s^{n-1} \end{bmatrix} \tag{9.17}$$

The model reference identifier structure is defined in [25, p.80-81] as

$$\begin{aligned} \dot{w}^{(1)} &= \Lambda w^{(1)} + b_\lambda r \\ \dot{w}^{(2)} &= \Lambda w^{(2)} + b_\lambda y_p \\ \theta^T &= [a_0, a^T, b_0, b^T] \\ w^T &= [r, w^{1^T}, y_p, w^{2^T}] \\ y_i &= \hat{M}(\theta^T w) \\ e_1 &= y_i - y_p \end{aligned} \tag{9.18}$$

$$e_1(t) = \hat{M}(\phi^T(t) w(t)) \tag{9.19}$$

It might be noticed that the $\hat{M}$ in equation (9.19) should be strictly proper and the relative degree of $\hat{M}$ should be no greater than the relative degree of the plant. Meanwhile, the $\hat{M}$ has to be stable and strictly positive real. Consequently, the model reference error equation is also called strictly positive real error equation. This type of error equation often uses gradient algorithms which will be introduced in the next section whereas preclude the application of least-squares algorithms. The model reference identifier may give rise to saving in computations contrast to the equation error scheme described in previous section [25]. Figure 9.3 shows the overall structure of the model reference identifier.

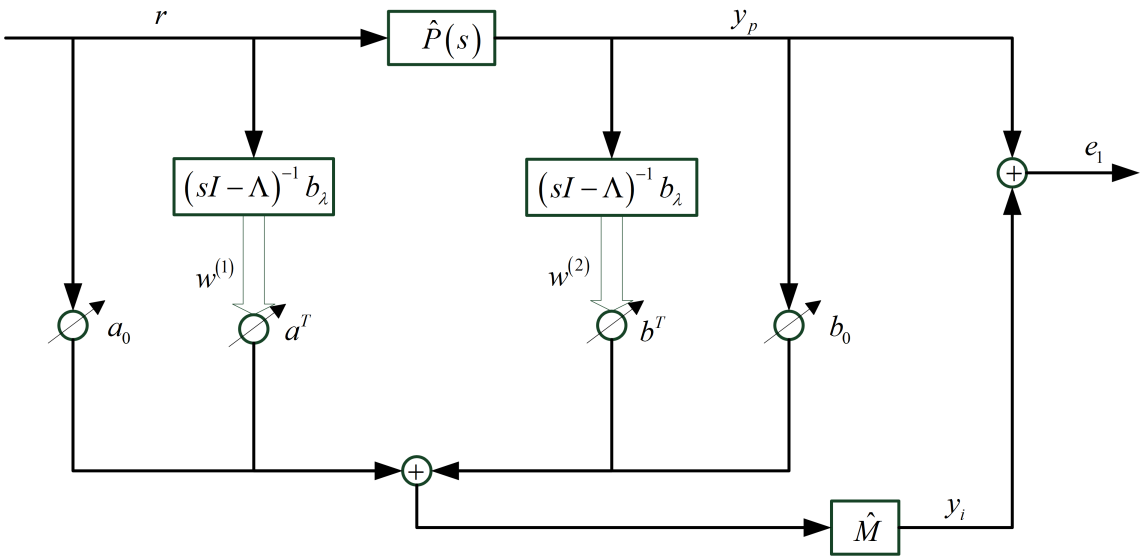

Figure 9.3: Model reference identifier structure

9.3 Identification algorithm

The identification algorithm is defined as an update law of the unknown parameters. Combined with the identification algorithms, the error equation are working as a dynamics system which ensures that the states, error signal e and parameter error ϕ, are stable or furthermore converges to zero.The most common algorithms are gradient algorithm and least-square algorithm which are described as follows respectively.

The update law

$$\dot{\theta} = -ge_1 w \qquad g > 0 \tag{9.20}$$

is defined as the standard gradient algorithm where g is a fixed strictly positive gain called adaptation gain. The gradient algorithms update law is considered as a steepest descent method since the right hand side of the equation is proportional to the gradient of the error square with respect to θ.

Another alternative algorithms commonly used is least-square algorithms whose normalized form is defined by

$$\begin{aligned} \dot{\theta} &= -g\frac{Pwe_1}{1+\gamma w^T P w} \qquad g, r > 0 \\ \frac{dP}{dt} &= -g\frac{Pww^T P}{1+\gamma w^T P w} \\ or \quad \frac{d(P)^{-1}}{dt} &= g\frac{ww^T}{1+\gamma w^T (P^{-1})^{-1} w} \end{aligned} \tag{9.21}$$

where g, γ are fixed parameters and $P(0) > 0$. This type of algorithms sometimes

is more complicated to implement, however have better convergence speed contrast to gradient algorithms [25].

9.4 Adaptive control combine with NDI controller

As mentioned in section 6.6 the NDI controller is very sensitive to the uncertainties which could be structured uncertainties, namely parametric uncertainties and unstructured uncertainties, namely unmodeled dynamics. The Boeing 747 model used in this project is a nonlinear parameter varying model resulting in the parametric uncertainties as all the aerodynamic derivatives are varying along the flight trajectory. In order to solve this problem, the adaptive control scheme is taken into account to endow NDI controller robustness property. Moreover, three variations of a model reference adaptive control design for a baseline NDI controller are given and evaluated in reference [42]. In this thesis, a direct adaptive control is implemented based on the baseline NDI controller which tunes the controller parameter directly by updating law.

In terms of the longitudinal mode, assuming ailerons and rudders inputs are zero, the system is simplified as a SISO system with elevator as input and pitch rate as output. For the direct adaptive control scheme, the NDI control law now become

$$\delta_e = \frac{1}{\hat{g}(x)}\left(v - \hat{f}_q(x)\right) \tag{9.22}$$

The original $g(x)$ and $f_q(x)$ in NDI control law (6.30) are replaced respectively by the estimated $\hat{g}(x)$ and $\hat{f}_q(x)$.

All the aerodynamic derivatives should be described as a set of linear function of Mach number and altitude. However, it is hard to attain adequately accurate linear functions of derivatives with respect to Mach number and altitude by interpolating the data points. Thereby, we have to confine the controller acting in a small regime where sits between two data point such that the interpolating is exactly the same with real plant.

For altitude greater than 35000ft, and Mach number is at between 0.6 to 0.8. We have following linear function of all the aerodynamic derivatives. Mach number is denoted as a.

$$\begin{aligned} M_u &= -0.00066a + 0.000721 \\ M_{\dot{w}} &= -0.000255a + 0.000088 \\ M_w &= -0.0004a - 0.00073 \\ M_q &= -0.55a + 0.101 \\ M_{\delta_e} &= -1.9a + 0.36 \end{aligned} \tag{9.23}$$

If substitute all the expressions into the differentiates equation of pitch rate in

equation (6.21), then following equation is obtained.

$$\begin{aligned}&\dot{q} = (-0.00066u - 0.000255\dot{w} - 0.0004w - 0.55q)\, a + \\ &(0.000721u + 0.000088\dot{w} - 0.00073w + 0.101q) - 1.9\delta_e a + 0.36\delta_e + \frac{(I_z - I_x)pr + I_{xz}\left(r^2 - p^2\right)}{I_y} \\ &= f_1(x)\, a + g_1(x)\, \delta_e a + R_1(x) + \beta\delta_e + I(p,r)\end{aligned} \tag{9.24}$$

Where

$$\begin{aligned} f_1(x) &= (-0.00066u - 0.000255\dot{w} - 0.0004w - 0.55q) \\ g_1(x) &= -1.9 \\ R_1(x) &= (0.000721u + 0.000088\dot{w} - 0.00073w + 0.101q) \\ \beta &= 0.36 \\ I(p,r) &= \frac{(I_z - I_x)\, pr + I_{xz}\,(r^2 - p^2)}{I_y} \end{aligned}$$

Substituting (9.22) into the differentiate equation of pitch rate (6.30), the (6.30) could be rewritten as

$$\begin{aligned} \dot{q} &= v + \left(f_q(x) - \hat{f}_q(x)\right) + \left(g_q(x) - \hat{g}_q(x)\right)\delta_e \\ &= v - \phi f_1(x) - \phi g_1(x)\,\delta_e \\ &= v + \phi\left(-f_1(x) - g_1(x)\,\delta_e\right) \end{aligned} \tag{9.25}$$

where

$$\begin{aligned} \theta &= a \\ \phi &= a - a^* \end{aligned}$$

a is the estimate of Mach number and a^* is the real Mach number. Choose the desired dynamic as

$$v = \dot{q}_c + \alpha\,(q_c - q) \quad \alpha > 0 \tag{9.26}$$

Substituting the above desired control law of v (9.26) into above equation (9.25), we obtain

$$e = \frac{1}{s+\alpha}\phi\left(-f_1(x) - g_1(x)\,\delta_e\right) \tag{9.27}$$

where $e = q - q_c$. Denoting $\left(-f_1(x) - g_1(x)\,\delta_e\right)$ as regressor w. Then

$$e = \frac{1}{s+\alpha}\phi w \tag{9.28}$$

Equation (9.28) is of the form strictly positive real error equation. Thereby, the gradient updating law could be applied with the SPR error equation according to theorem 2.6.3 in [25].

$$\dot{\phi} = \dot{a} = -gew \quad g > 0 \tag{9.29}$$

where g is the gain of update law determining convergence speed. Thus,

$$a(t) = a(0) + \int_0^t -ew$$

Once a is estimated all the aerodynamic derivatives could be calculated by (9.23). By substituting all the estimates of aerodynamic derivatives into the new adaptive NDI control law (9.22), the adaptive controller is completed. Setting $\alpha = 3$ the closed loop dynamics of the nominal condition is

$$\dot{e} + 3e = 0 \tag{9.30}$$

According to the theorem 7.3.1 in [25, p.310], output q is bounded and asymptotically converge to q_c. Furthermore, verify below persistency of excitation condition in [25, p.72-73].

If there exist $\alpha_1, \alpha_2, \delta > 0$ such that

$$\alpha_2 I \geq \int_{t_0}^{t_0+\delta} w\, w^T dt \geq \alpha_1 I \quad for\ all\ t_0 \geq 0$$

The PE condition is satisfied since regressor w is a bounded scalar value at any defined time t_0. Hence, the error ϕ exponentially converge to zero. The unknown Mach number estimation results and q response are indicated in figure 9.4.

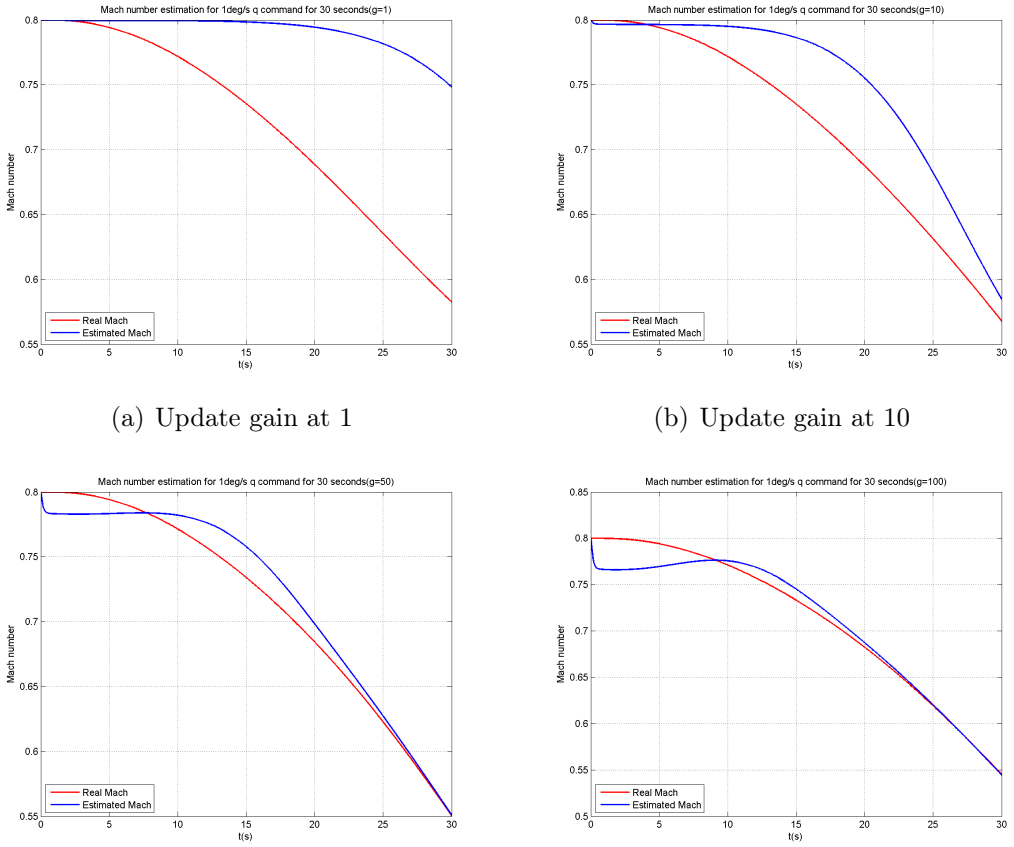

(a) Update gain at 1

(b) Update gain at 10

(c) Update gain at 50

(d) Update gain at 100

Figure 9.4: Mach number estimations of different value of update gain

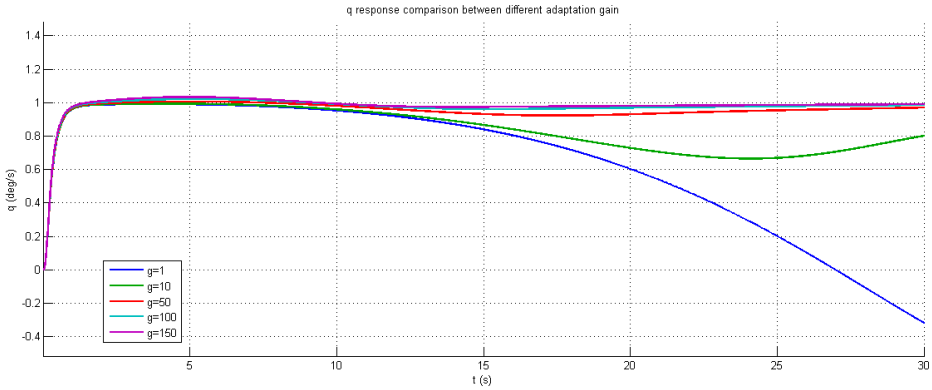

Figure 9.5: q response of adaptive NDI controller for 1 deg/s q command for 30 seconds

It can be seen that convergence time reduces as the update gain increases from figure 9.4. The q response of the controller with update gain at 1 goes still diverge after about first 8 seconds due to the slow convergence of estimation of Mach number. However, q response tries to go back to the steady state value after a few seconds if the gain value is higher, eventually the q response could almost maintain on demand value when the update gain reaches 100. Contrast to the results obtained in section 7.5, above results have been dramatically improved. Unfortunately, this adaptive NDI controller is only verified within a very limited flight regime due to the restriction of aircraft model. However, it provided a adaptive NDI controller framework which could significantly rise the NDI controller performance in presence of parameter uncertainty. This direct adaptive NDI controller might work well for all flight points on condition that the expressions of all aerodynamic derivatives are verified throughout overall flight envelope.

9.5 Observer based SMC controller design for Boeing 747

Sliding mode control is well known as a robust nonlinear control technique and have been applied to nonlinear system control successfully. Yet, pure sliding mode control has some shortcomings such as large control authority requirement and chattering as we have discussed in previous sections [43]. On-line parameter estimation schemes are considered to combine with SMC to overcome these problem in [44] and [45].

An alternative way to solve the problems is estimating the disturbance in turn reducing the chattering. The mismatch between the real plant model and the nominal model is considered as an equivalent disturbance acting on the nominal model. As discussed in section 8.2.5, the chattering could be reduced if the value of Q which stands for the boundary of uncertainty is decreased. After disturbance is estimated, the estimate of disturbance could be used to compensate the real disturbance, in

turn the requirement of SMC controller gain k could be dramatically reduced. Consequently, the SMC controller could maintain accurate control performance in the presence of parametric uncertainty provided that k is greater than the error between the estimate of disturbance and the real disturbance. In [46], a disturbance estimation scheme in addition to the sliding mode control is proposed in order to reduce the chattering. The H_∞ technique was applied for the design of the optimal disturbance observer in [47]. Liu [41] proposed a sliding mode disturbance observer for a specific nonlinear system control problem. Another type of disturbance observer was applied for nonlinear formation guidance law design in [40].

Here a disturbance observer with similar structure in [46] is developed in addition to the SMC controller. Let us consider the differential equation of the control variable q in (8.24) and assume the disturbance is a constant which stand for the difference between real flight condition and the nominal condition. Thus, following equations are obtained.

$$\begin{bmatrix} \dot{q} \\ \dot{d} \end{bmatrix} = \begin{bmatrix} M_q - \frac{M_{\dot{w}}(Z_q+U_e)}{Z_{\dot{w}}-1} & 1 \\ 0 & 0 \end{bmatrix} \begin{bmatrix} q \\ d \end{bmatrix} + \begin{bmatrix} M_{\delta_e} - \frac{M_{\dot{w}} Z_{\delta_e}}{Z_{\dot{w}}-1} \\ 0 \end{bmatrix} \delta_e + \begin{bmatrix} f^*(x_1) \\ 0 \end{bmatrix} \tag{9.31}$$

where

$$\begin{aligned} x_1 &= (u, w, \theta) \\ f^*(x_1) &= \left(M_u - \frac{M_{\dot{w}} Z_u}{Z_{\dot{w}} - 1}\right) u + \left(M_w - \frac{M_{\dot{w}} Z_w}{Z_{\dot{w}} - 1}\right) w + \left(\frac{M_{\dot{w}} g \sin\theta_e}{Z_{\dot{w}} - 1}\right) \theta \\ d &= \Delta f + \Delta g \delta_e \\ \Delta f &= f - f^* \\ \Delta g &= g - g^* \end{aligned}$$

and all the aerodynamic derivatives in above equation (9.31) are the values of nominal condition, namely controller design point and d denotes the disturbance. Following sliding mode disturbance observer is constructed.

$$\begin{bmatrix} \dot{\hat{q}} \\ \dot{\hat{d}} \end{bmatrix} = \begin{bmatrix} M_q - \frac{M_{\dot{w}}(Z_q+U_e)}{Z_{\dot{w}}-1} & 1 \\ 0 & 0 \end{bmatrix} \begin{bmatrix} \hat{q} \\ \hat{d} \end{bmatrix} + \begin{bmatrix} M_{\delta_e} - \frac{M_{\dot{w}} Z_{\delta_e}}{Z_{\dot{w}}-1} \\ 0 \end{bmatrix} \delta_e + \begin{bmatrix} f^*(x_1) \\ 0 \end{bmatrix} + \begin{bmatrix} K_1 \\ K_2 \end{bmatrix} \tilde{q} \tag{9.32}$$

where $\hat{q}$ denotes the estimate of q and $\hat{d}$ denotes the estimate of disturbance and $\tilde{q}$ denotes $q - \hat{q}$. The equation (9.33) is gained from (9.31) subtracting (9.32).

$$\begin{bmatrix} \dot{\tilde{q}} \\ \dot{\tilde{d}} \end{bmatrix} = \begin{bmatrix} M_q - \frac{M_{\dot{w}}(Z_q+U_e)}{Z_{\dot{w}}-1} - K_1 & 1 \\ -K_2 & 0 \end{bmatrix} \begin{bmatrix} \tilde{q} \\ \tilde{d} \end{bmatrix} \tag{9.33}$$

Let us consider the stability of the above dynamic system. All the poles should be on the left hand side plane to guarantee the stability. Denoting $M_q - \frac{M_{\dot{w}}(Z_q+U_e)}{Z_{\dot{w}}-1} - K_1$ as a_{44}, the expression of poles are

$$p_{1,2} = \frac{1}{2}(a_{44} - K_1) \pm \frac{\sqrt{(a_{44} - K_1)^2 - 4K_2}}{2} \tag{9.34}$$

The fact that the real parts of the two poles are negative is hold as long as

$$\begin{aligned} K_1 &> a_{44} \\ (a_{44} - K_1)^2 - 4K_2 &< 0 \end{aligned} \tag{9.35}$$

Above conditions guarantee that the estimate of disturbance and q converge to zero in finite time, provided that disturbance is assumed to be a constant. Thus, the positions of these two poles are

$$p_{1,2} = \frac{1}{2}(a_{44} - K_1) \pm \frac{\sqrt{4K_2 - (a_{44} - K_1)^2}}{2} i \tag{9.36}$$

on condition that (9.35) holds. Consequently, the damping ratio and frequency of dynamic system (9.33) are

$$\begin{aligned} \omega_n &= 2\sqrt{k_2} \\ \zeta &= \frac{k_1 - a_{44}}{4\sqrt{k_2}} \end{aligned} \tag{9.37}$$

Here the observer gain K_1 and K_2 are selected as 5 and 25 respectively. Then providing that $a_{44} = -0.5$ at design point (Mach 0.85 and Altitude 36000ft), we have

$$\begin{aligned} \omega_n &= 10 \\ \zeta &= 0.55 \end{aligned} \tag{9.38}$$

Next, the observer based sliding mode control law is designed. The basic concept is that the estimate of disturbance is added in to the control law to compensate the real disturbance resulting in the disturbance boundary reduction. Consider following sliding mode control law

$$u = g^{*-1}\left(\dot{q}_d - f^* - k\mathrm{sgn}(e) - \hat{d}\right) \tag{9.39}$$

By substituting above control law (9.39) into (8.34), below equation is obtained.

$$\begin{aligned} \dot{q} &= f + gg^{*-1}\left(\dot{q}_d - f^* - k\mathrm{sgn}(e) - \hat{d}\right) \\ &= \Delta f + \dot{q}_d + \Delta g g^{*-1}(\dot{q}_d - f^*) - \Delta g g^{*-1} k\mathrm{sgn}(e) - k\mathrm{sgn}(e) - gg^{*-1}\hat{d} \\ \Rightarrow \dot{e} &= \Delta f + \Delta g g^{*-1}(\dot{q}_d - f^*) - \Delta g g^{*-1} k\mathrm{sgn}(e) - \Delta g g^{*-1}\hat{d} - k\mathrm{sgn}(e) - \hat{d} \\ \Rightarrow \dot{e} &= d - \hat{d} - k\mathrm{sgn}(e) \end{aligned} \tag{9.40}$$

where

$$\begin{aligned} d &= \Delta f + \Delta g u \\ &= \Delta f + \Delta g g^{*-1}(\dot{q}_d - f^*) - \Delta g g^{*-1} k\mathrm{sgn}(e) - \Delta g g^{*-1}\hat{d} \end{aligned} \tag{9.41}$$

Verify the reachability condition

$$\begin{aligned} & e \cdot \dot{e} < 0 \\ & \Rightarrow e \cdot \left(d - \hat{d} - k\text{sgn}\left(e\right) \right) < 0 \\ & \Rightarrow k \left| e \right| > e \left(d - \hat{d} \right) \\ & \Rightarrow k > \left| d - \hat{d} \right| \end{aligned} \tag{9.42}$$

Let us compare the reachability condition of disturbance observer based SMC controller (9.42) with the reachability condition of the original SMC controller (8.41) which could be rewritten as

$$k > |d| \tag{9.43}$$

It is obvious that the original SMC controller requires k greater than the magnitude of disturbance boundary whereas the adaptive SMC controller requires k only greater than the magnitude of error between real disturbance and estimate of disturbance. Thereby, the value of k could be significantly reduced so that the chattering could be decreased dramatically. The overall structure of the disturbance observer based SMC controller is indicated as below figure 9.6.

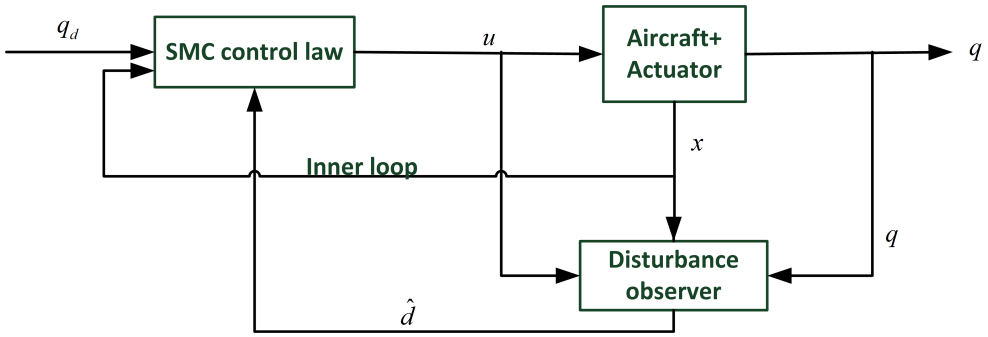

Figure 9.6: Disturbance observer based SMC controller overall structure.

According to the above disturbance observer based SMC controller design, select cruise flight point which is at Mach 0.85 and Altitude 36000ft as the design point namely the nominal condition. As the value of k can be reduced considerably, k is chosen as 0.005. The control action is also smoothed by the method described in section 8.2.3. This adaptive SMC controller is evaluated at 4 typical flight points as previous, moreover the estimations of the disturbance are also shown contrasting to real disturbance. The evaluations for more flight points could be found in Appendix C.

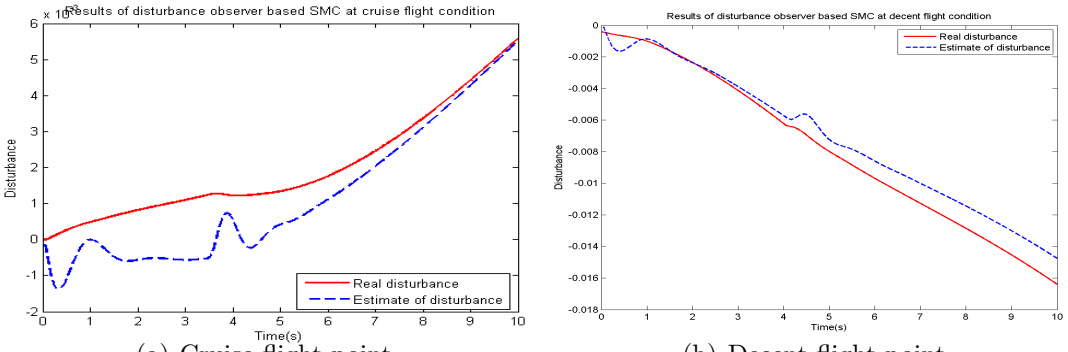

(a) Cruise flight point

(b) Decent flight point

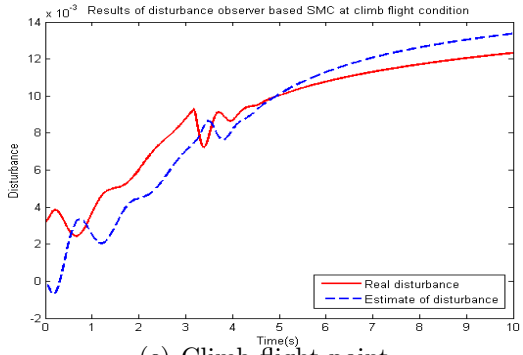

(c) Climb flight point

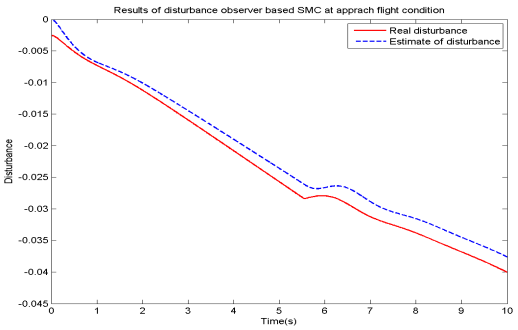

(d) Approaching flight point

Figure 9.7: The estimations of disturbance at 4 typical flight points contrasting to the real disturbance

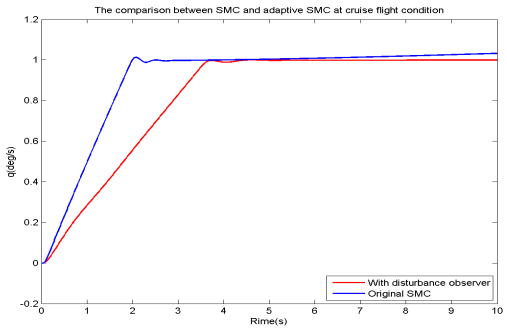

(a) Cruise flight point

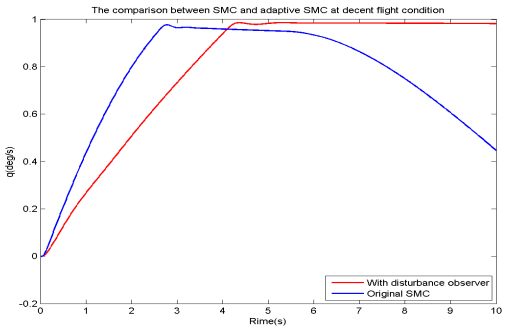

(b) Decent flight point

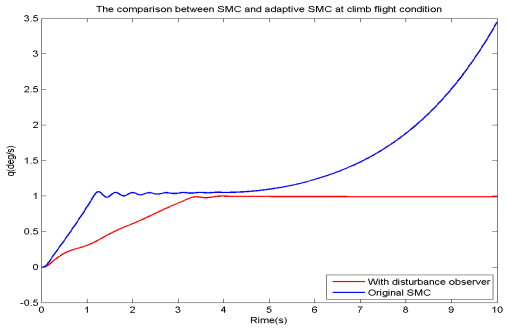

(c) Climb flight point

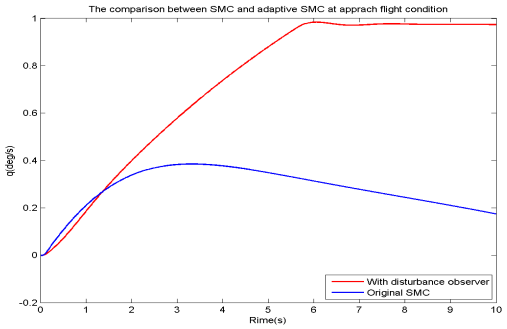

(d) Approaching flight point

Figure 9.8: q responses comparison between adaptive SMC and original SMC at 4 typical flight points for 1deg/s step q command

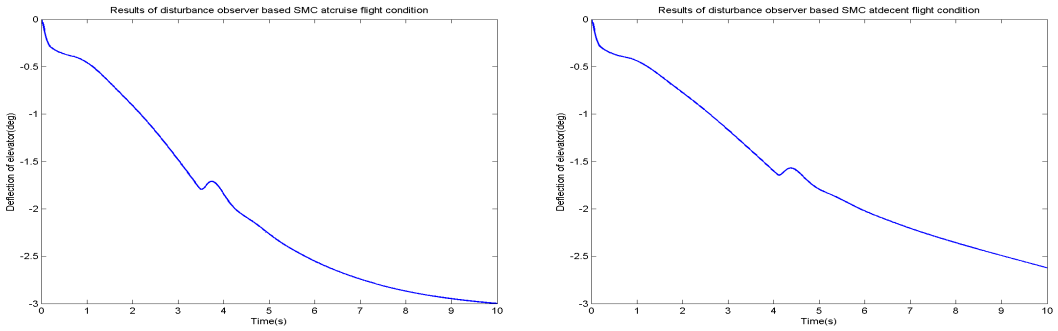

(a) Cruise flight point

(b) Decent flight point

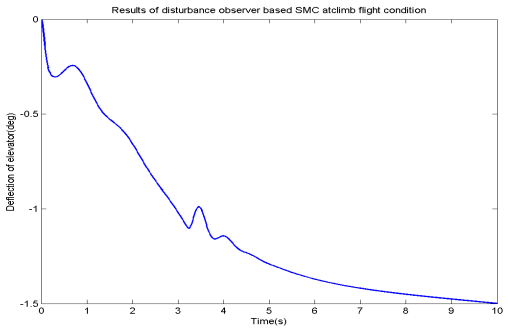

(c) Climb flight point

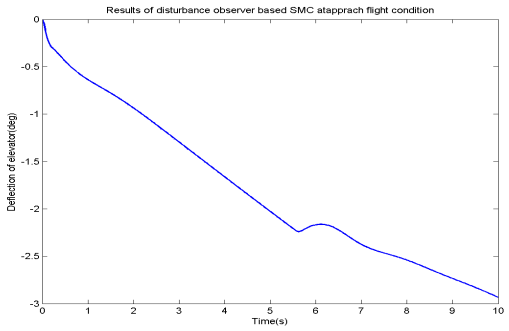

(d) Approaching flight point

Figure 9.9: The deflection of elevator at 4 typical flight points

It can be seen from figure 9.7 that there is a steady state error between the estimate of the disturbance and the real disturbance since the disturbance is assumed as a constant in observer but the real case is that disturbance is slowly varying. In addition, the steady state errors of 4 flight points are all less then 0.05 so that the value of control gain k is adequate enough to cope with the uncertainty at all these 4 points. Actually, it is verified that $k = 0.005$ could handle the uncertainty for the whole flight envelop based on the disturbance observer SMC controller. Beside, the control inputs, namely the deflections of elevator, could be inspected from figure 9.9. The control inputs are of small magnitude and smooth as well.

By comparison the q responses between adaptive SMC controller and original SMC controller from figure 9.8, it is found that the results of the adaptive SMC controller completely prevent chattering and possess good robustness property at different flight point whereas the original SMC controller cannot maintain at command value at non-nominal flight points. Moreover, the adaptive SMC control have considerably good control accuracy, providing the steady state errors stay within 2%. However, the only drawback is relatively low converge speed due to the small value of k. Intuitively, the proportional term is considered to be added into the control law liking we have discussed in section 8.2.4 to speed up the settle down process. If the proportional term is added, below adaptive SMC control law (9.44) is obtained.

$$u = g^{*-1}\left(\dot{q}_d - f^* - ksat\left(\frac{e}{\delta}\right) - k_p e - \hat{d}\right) \tag{9.44}$$

The k_p is selected as 1.5 for both proper convergence speed and overshoot. Following results are obtained from the adaptive SMC control law with proportional term.

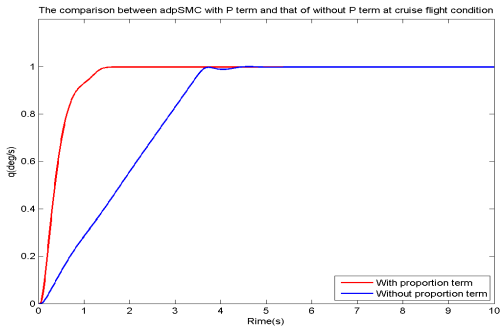

(a) Cruise flight point

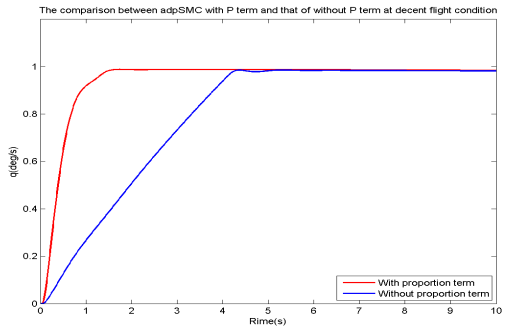

(b) Decent flight point

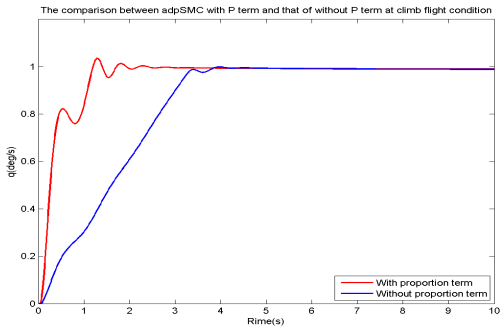

(c) Climb flight point

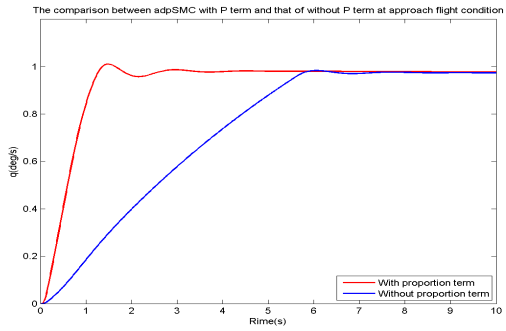

(d) Approaching flight point

Figure 9.10: The q responses comparisons between adpSMC with P term and that of without P term at 4 typical flight points

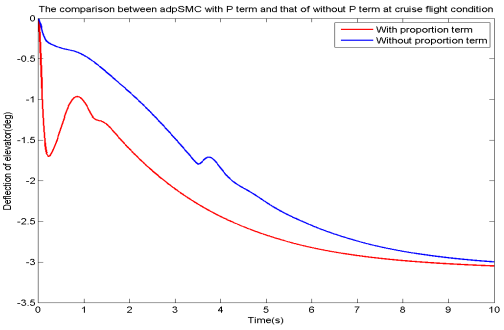

(a) Cruise flight point

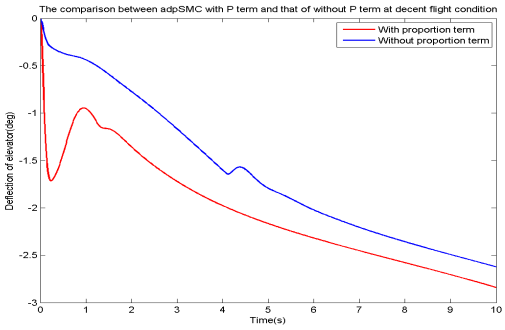

(b) Decent flight point

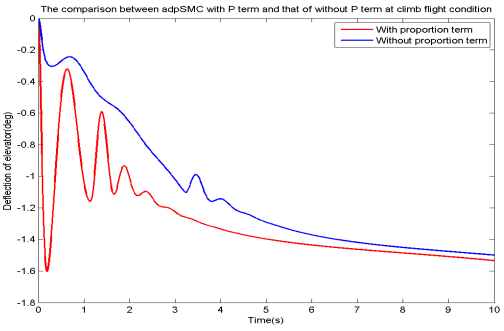

(c) Climb flight point

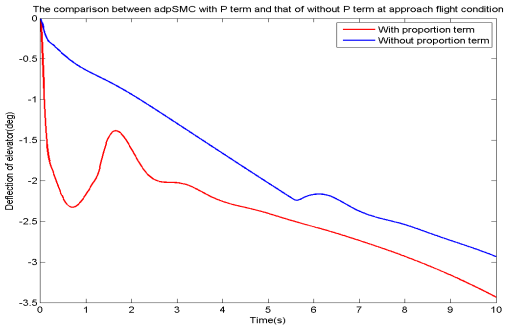

(d) Approaching flight point

Figure 9.11: The deflections of elevator comparisons between adpSMC with P term and that of without P term at 4 typical flight points

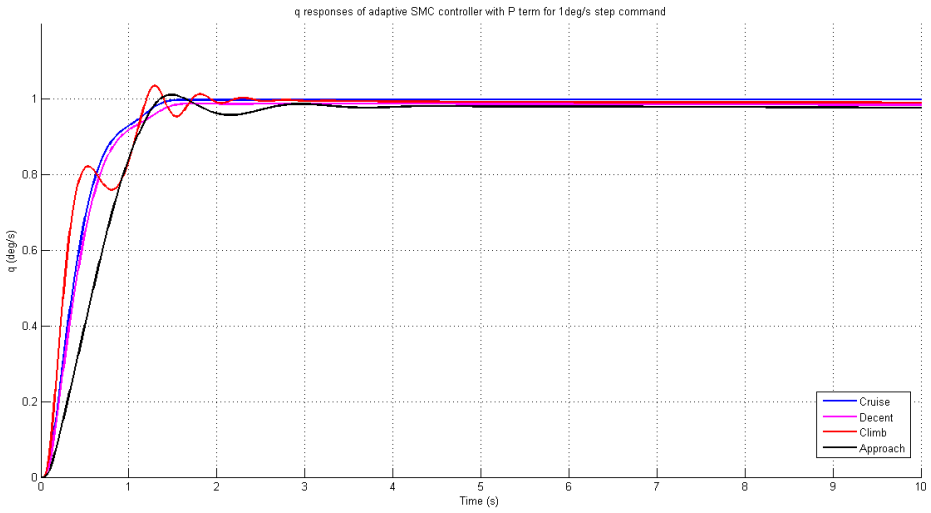

Figure 9.12: The comparison of q of adaptive SMC with kp at 1.5 between 4 flight points

Figure 9.10 indicates that the adaptive SMC controller with proportional term considerably accelerates the converge speed, at the same time remain the high control accuracy and robustness property. Figure 9.11 shows the comparisons between the deflection of adaptive SMC controller with proportional term with that of SMC controller without proportional term. The control inputs become slightly more intensive and maintain similar magnitude. Figure 9.12 illustrates all q responses of 4 typical flight points for 1 deg/s step q command. There are almost no overshoots and all the responses converge to command value quickly providing rise time at about 1 second and settle down at about 1.5 seconds. Moreover the steady state errors are confined within only 2% which is rather accurate throughout the whole flight profile. More flight points are assessed for the disturbance observer based SMC with P control law, shown in Appendix C. In summary, the adaptive SMC control law with proportional term improve the performance significantly and achieve highly robust performance simultaneously.

In addition, the integral term is not necessary to be added into the adaptive SMC control law since the uncertainty shrinks dramatically after the disturbance observer applied and more importantly integral term will introduce undesirable overshoot.

9.6 Controllers comparisons

9.6.1 Results comparison between NDI, SMC and adaptive SMC

So far the NDI controller, SMC controller and adaptive SMC controller are developed for Boeing 747 longitudinal mode control. Theoretically, adaptive SMC should perform best and the second best one should be SMC controller, finally the last one should be the NDI controller. Let us contrast results of the best design in each form at 4 typical flight points: the PI NDI controller, the smoothed PI SMC controller and the smoothed adaptive P SMC controller. Following figures are obtained referring to figure 7.10, figure 8.18 and figure 9.12. For easy reading, the control laws of these 3 types controllers are reminded here.

1. PI NDI control law:

$$u = g^{*-1}\left(\dot{q}_d - f^* - k_p e - k_i \int e dt\right) \quad k_p = 4,\ k_i = 4 \tag{9.45}$$

2. PI SMC control law:

$$\begin{aligned} u &= g^{*-1}\left(\dot{q}_d - f^* - k\mathrm{sat}(\frac{e}{\delta}) - k_p e - k_i \int e dt\right) \\ k &= 0.005,\ k_p = 4,\ k_i = 4,\ \delta = 8.75e^{-4} \end{aligned} \tag{9.46}$$

3. adaptive P SMC control law:

$$\begin{aligned} u &= g^{*-1}\left(\dot{q}_d - f^* - ksat\left(\frac{e}{\delta}\right) - k_p e - \hat{d}\right) \\ k &= 0.005,\ k_p = 1.5,\ \delta = 8.75e^{-4} \end{aligned} \tag{9.47}$$

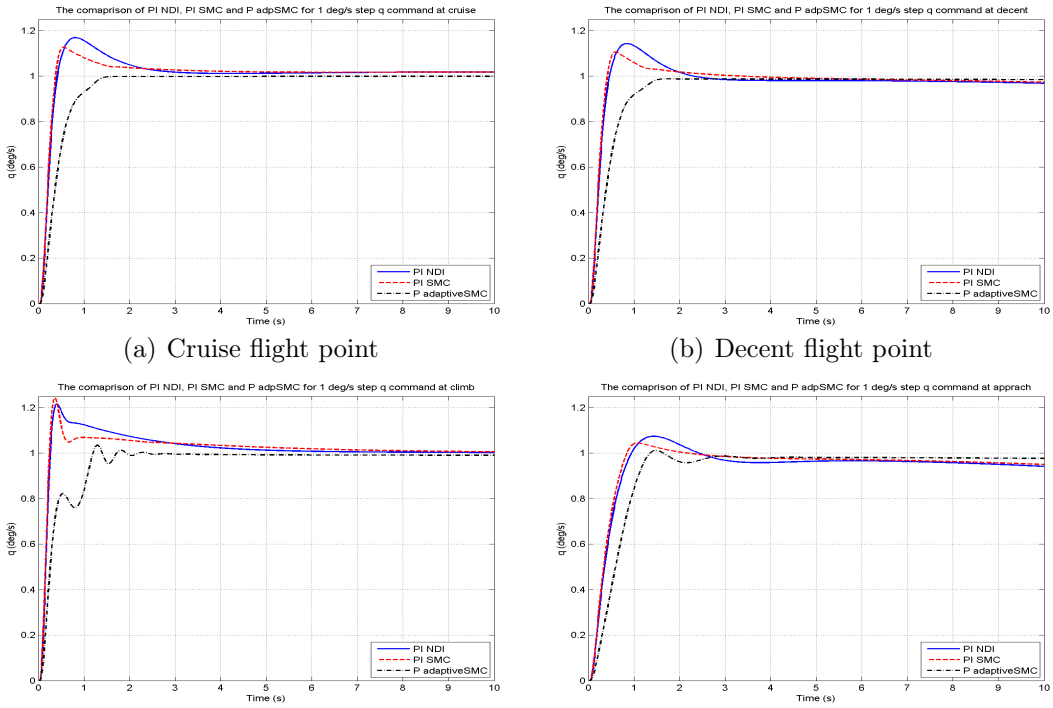

(a) Cruise flight point (b) Decent flight point

(c) Climb flight point (d) Approaching flight point

Figure 9.13: The comaprison of PI NDI, PI SMC and P adpSMC for 1 deg/s step q command at 4 typical flight points

As you can see from above figure 9.13, the PI SMC controller have less overshoots than PI NDI controller and rise up slightly quicker than PI NDI controller whereas the adaptive P SMC have almost no overshoots for 4 flight points. Despite the adaptive P SMC contoller has a little more rise times but possesses the shortest settle down time at about 1.5 seconds. With respect to steady state error, the adaptive P SMC decreases the steady state error significantly from 2% to 0 at cruise point, from 5% to 2% at approach point meanwhile the PI NDI and PI SMC have similar steady state error for 4 flight points. In conclusion, the PI SMC performs better than PI NDI and more importantly the adaptive SMC controller has the best transient performance, best control accuracy and best robustness performance.

9.6.2 Results comparison between NDI, adaptive NDI and adaptive SMC

In section 9.4, the adaptive NDI controller is developed by applying on-line parameter estimation. All the aerodynamics derivatives are expressed as linear function of Mach number in a confined region (Mach 0.6 0.8, Altitude above 35000ft), and then the Mach number is estimated by an adaptive scheme. Consequently, all the unknown aerodynamics derivatives are gained and updated along the flight condition, providing improved robust performance relative to the original NDI controller. However, the estimation have somewhat delay so that the performance is not per-

fect. Figure 9.14 illustrates the contrast between P NDI controller, adaptive P NDI controller and adaptive P SMC controller at flight point Mach at 0.8 and Altitude 40000ft. The control laws of these 3 types controller are also listed as below.

1. P NDI controller:
$$u = g^{*-1}\left(\dot{q}_d - f^* - k_p e\right) \quad k_p = 3 \tag{9.48}$$

2. Adaptive P NDI controller:
$$u = \hat{g}^{-1}\left(\dot{q}_d - \hat{f} - k_p e\right) \quad k_p = 3 \tag{9.49}$$

3. Adaptive P SMC controller:
$$u = g^{*-1}\left(\dot{q}_d - f^* - ksat\left(\frac{e}{\delta}\right) - k_p e - \hat{d}\right) \quad k = 0.005,\ k_p = 1.5,\ \delta = 8.75e^{-4} \tag{9.50}$$

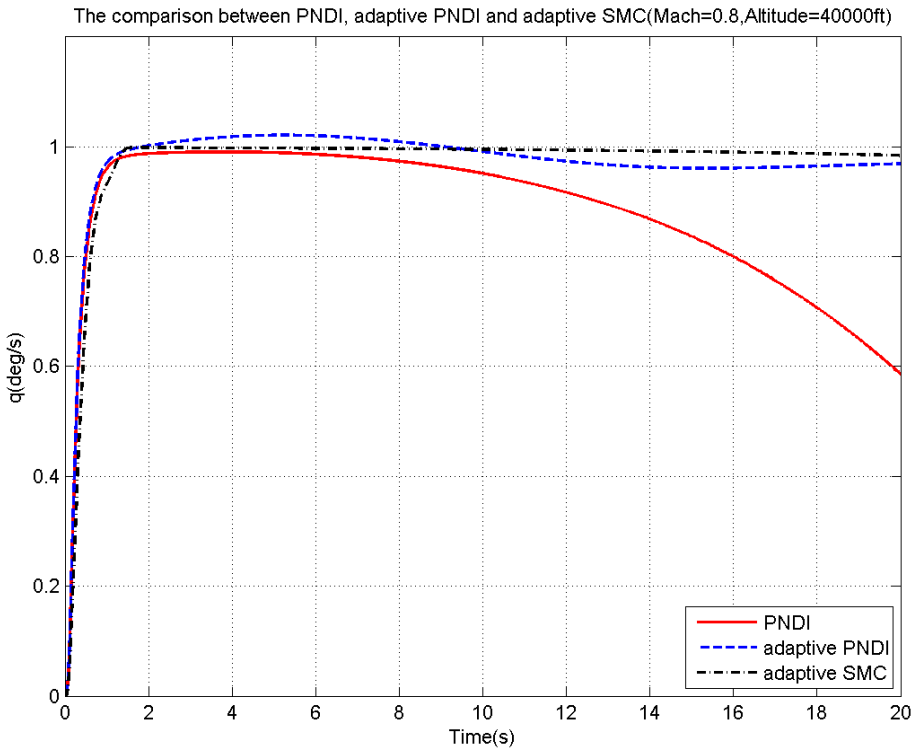

Figure 9.14: The comparison between PNDI, adaptive PNDI and adaptive SMC(Mach=0.8,Altitude=40000ft)

It is clear from the above figure that the original P NDI controller gradually diverges after 6 seconds due to the incomplete cancellation of dynamic inversion, whereas the adaptive P NDI controller and adaptive P SMC controller retain at the vicinity of the command value. Resulting from the inaccurate estimation the response of adaptive NDI controller move exceed the demand value and then converge to the command

value after a period of time due to the delay of estimation. The adaptive SMC controller has the best steady state performance, providing almost no steady state error. All 3 controllers have similar transient behavior. In summary, the disturbance based sliding mode control with proportional term controller performs best.

Chapter 10

Conclusion and future work

10.1 Conclusion

10.1.1 Aircraft model

- The Boeing 747 aircraft model is provided, which is a linear model by eliminating the hight order terms and coupled nonlinear terms such as the product of both longitudinal and lateral state variables. By reserving the product of state variables and the term containing inertia, the nonlinear coupling longitudinal motion equation and lateral motion equation are obtained as equations (6.21) and (6.22).

- The control surface actuators of Boeing 747 are modelled as second order transfer functions which are cascaded with motion rate limiting and deflection saturation, provided in reference [33].

10.1.2 NDI control

- After the NDI theory is presented in chapter 6, NDI controllers are developed for angular rate control for both longitudinal mode and later mode of Boeing 747 aircraft in chapter 7. NDI controller consists of 2 feedback loops: inner loop feedback linearization and the linear outer loop desired dynamic control law. Feedback linearization functions to cancel out the original aircraft dynamics resulting the aircraft model is replacing by a pure integral. The desired dynamics determines the close loop transfer function of the system.

- When doing feedback linearization, the control matrix must be invertible. $g(x)$ in (6.32) is not invertible for so-called differentially non-flat systems whose control variables are more than the control inputs. Hence, the number of system control variables is required to be less or equal to the number of control inputs, otherwise the system is under-actuated and not invertible. Even if

the control matrix $g(x)$ is invertible but the magnitude of $g(x)$ is very small, this may gives rise to control ineffectiveness, in other words, control surface becoming unbounded, in turn, causing actuator saturation. A technique called time-scale separation method is invented to resolve this problem. For Boeing 747 aircraft model, there are 3 inputs including elevator, rudder and aileron equalling to the number of outputs, namely 3 angular rates. Moreover, the control matrix $g(x)$ of Boeing 747 model is verified to be invertible.

- The NDI controller stability and performance could be dramatically deteriorated by the instability of internal dynamics. The relative degree of Boeing 747 longitudinal mode is 1 so that the order of internal dynamics is 3. Lateral mode have 2 inputs and the order of internal dynamics is $n - r = 3$. The stabilities of the internal dynamics of both longitudinal mode and lateral mode are checked to be stable by zero dynamic technique in section 7.4.

- The desired dynamic law is the key part of NDI control law which determines the close loop transfer function of the system. 4 types of desired dynamic law are carries out for Boeing 747 aircraft which include P, PI, ride quality and tracking desired dynamic laws. The evaluations of the pitch rate control illustrate that P, tracking and RQ desired dynamics all behave as expected for the first 5 seconds, but go diverge after that. Meanwhile, the output of PI control law retains in vicinity of command value but cannot meets the civil aircraft overshoot requirement ($<5\%$). Furthermore, PI desired control law shows the best robustness property after assessment for 4 typical flight points sitting in 4 different flight phases. Cruise point is selected as the design point by contrasting the results of other points as design point.

- High sensitivity to uncertainty is the principal disadvantage of the NDI controller. NDI controller could be deteriorated at the presence of uncertainty since the original dynamics cannot be completely compensated by feedback linearization. Some robust linear control techniques are recommended to design the outer loop linear control law.

10.1.3 SMC control

- In order to have robustness performance, the sliding mode control method is applied in chapter 8. The concept of SMC is that the system states are forced to reach and remain on a predefined surface which presents the desired dynamics within the states space. The principal advantages of SMC are: reducing system order and insensitive to matched uncertainty. The sliding surface of Boeing 747 SMC controller is designed as $s = e$ where e stands for the error between q command and q output. The reachability condition $e \cdot \dot{e} < 0$ has to be met for forcing the system trajectory to the sliding surface. Two conclusions might be drawn that: the magnitude of chattering is proportional to the value of sign function gain k; The settling time is inversely proportional to the value of the sign function gain k since the η in (8.19) increases as the control gain rises, consequently the settling time is reduced.

- Chattering is a big problem for SMC control causing highly intensive discontinuous control activity. A simple way to avoid chattering is replacing the sign function by saturation function in SMC control law but this will results in steady state error. Thus, the thickness of boundary layer δ should be carefully chosen since small values of δ may not solve the chattering problem whereas large values may increase the steady state error [38]. In the SMC controller for Boeing 747, δ is properly chosen at 5% of the command value.

- By analogy with various sorts of desired dynamics of the NDI controller, the P and PI control law could also be used in SMC control. The discussion of different types of SMC control law are proceeded in section 8.2.4. The results of assessments indicate that the proportional term is able to speed up the converge speed on condition that the gain k is greater than the magnitude of uncertainty, but is not adequate enough to cope with big uncertainty. However, the PI control law is capable of driving system trajectory back to sliding surface when facing large uncertainty. Therefore, PI SMC control law has the best robustness performance contrasting to the other two. The disadvantage of the PI control law is introducing undesired overshoot.

10.1.4 Adaptive control

- In section 9.5, a disturbance observer based SMC controller is developed. The disturbance is estimated on-line and used to compensate the real disturbance, in turn, the boundary of disturbance is reduced dramatically. Consequently the gain k can be reduced to decrease chattering. The disturbance observer based P SMC control shows great performance for all flight points: fast rising-up speed, little overshoot, short settling time and very small steady state error. A notable point is that an unrealistic assumption of constant disturbance is made so that steady state errors are presented in the disturbance estimation results.

- The development of adaptive NDI controller is presented in section 9.4. Mach number is estimated on-line and the NDI control is updated recursively. However, this adaptive scheme is confined to a specific region where altitude is greater than 35000ft, and Mach number is at between 0.6 to 0.8 due to the lack of aerodynamic derivative data.

10.2 Recommendations for future work

- As mentioned previously, the disturbance is assumed to be constant when constructing the disturbance observer. But the reality is that the disturbance is varying along the flight condition. Therefore, the disturbance observer need to be improved without assumption of the invariance of disturbance and then more accurate estimate is expected.

- There are various ways to design the sliding surface and the sliding surface of SMC controller for Boeing 747 is very simple, $s = e$. Thus, the sliding surface could be redesigned to improve the performance in future.
- In this thesis, the longitudinal mode is mainly concerned and the SMC control and adaptive control are not applied for lateral mode control. In future, nonlinear lateral mode control might be a research direction.
- Three angular rates are chosen as the control variables in this thesis which is called rate control attitude hold but the attitudes of aircraft are commonly the major control objectives. An attitude control loop out side the angular rate control loop can be designed to complete the controller design.

References

[1] R. Blockley, W. Shyy, and J. Wiley. *Encyclopedia of Aerospace Engineering.* 2010.

[2] American Militory. MIL-STD-1797A, 1995.

[3] M.V. Cook. Flying qualities and flight control lecture notes. Cranfield University, 2012.

[4] S.A. Snell and P.W. Stout. Robust longitudinal control design using dynamic inversion and quantitative feedback theory. *Journal of guidance, control, and dynamics*, 20(5), 1997.

[5] Jacob Reiner, G. Balas, and L. Garrard. Robust dynamic inversion for control of highly maneuvrable aircraft. *Journal of guidance, control and dynamics*, 18(1):18–24, 1995.

[6] Jams Aircraft Data Base. Boeing 747 Data.

[7] B747 Operating Manual Boeing 747-400 Aircraft Operations Manual. Technical report, Delta virtual Airline.

[8] W. Guo. *Gain scheduling for a passenger aircraft control system to satisfy handling qualities.* PhD thesis, 2010.

[9] M.V. Cook. *Flight dynamics principles.* 2007.

[10] TJJ Lombaerts and GHN Looye. Design and flight testing of manual nonlinear flight control laws. In *AIAA Guidance, Navigation, and Control Conference*, number August, pages 1–21, 2011.

[11] Ludwig E. Logemann Garza. *Design And Validation Of Autopilot Functions Using Nonlinear Dynamic Inversion.* PhD thesis, Cranfield University, 2004.

[12] B.L. Stevens and F.L. Lewis. Aircraft control and simulation. 2003.

[13] RK Heffley and WF Jewell. Aircraft handling qualities data. Technical report, NASA, 1972.

[14] B.A. White. Eigenstructure assignment: a survey. In *Proceedings of the Institution of Mechanical Engineers, Part I: Journal of Systems and Control Engineering*, 1995.

[15] A.N. Andry, E.Y. Shapiro, and J.C. Chung. Eigenstructure Assignment for Linear Systems. *IEEE Transactions on Aerospace and Electronic Systems*, AES-19(5):711–729, September 1983.

[16] Sigurd Skogestad and Ian Postlethwaite. *Multivariable Feedback Control analysis and design.* 1996.

[17] J.F. Magni, S. Bennani, and J. Terlow. Robust flight control(a design challenge). Technical report, Group for aeronautical research and technology in europe, 1997.

[18] L.Brogan William. *Modern control theory.* Prentice-Hall International, Inc., third edition, 1991.

[19] F. Wang. *Robust control of quasi-linear parameter-varying L2 point formation flying with uncertain parameters.* PhD thesis, 2012.

[20] Miroslav Krstic, Loannis Kanellakopoulos, and Petar Kokotovic. *Nonlinear and Adaptive Control Design.* John Wiley & Sons, Inc., 1995.

[21] JWC NRobison and U Nilsson. Design of a nonlinear autopilot for velocity and attitude control using block backstepping. In *AIAA Guidance, Navigation, and Control Conference and Exhibit*, 2005.

[22] L. Sonneveldt, Q.P. Chu, and J.A. Mulder. Constrained adaptive backstepping flight control: application to a nonlinear F-16/MATV model. In *AIAA Guidance, Navigation, and Control Conference and Exhibit*, 2006.

[23] D Ito and LBJS Center. Reentry vehicle flight controls design guidelines: dynamic inversion. Technical Report March, 2002.

[24] JJE Slotine and W. Li. *Applied nonlinear control.* 1991.

[25] S. Sastry and M. Bodson. *Adaptive control: stability, convergence, and robustness.* 1989.

[26] S. Antony Snell, Dale F. Enns, and William L. Garrard. Nonlinear Inversion Flight Control For A Supermaneuverable Aircraft. *Journal of guidance, control, and dynamics*, 15(4), 1992.

[27] J Georgie and J Valasek. Selection of longitudinal desired dynamics for dynamic inversion controlled re-entry vehicles. In *AIAA Guidance, Navigation, and Control Conference and Exhibit*, 2001.

[28] Özgï£¡R Atesoglu and M. Kemal Özgören. Control and Robustness Analysis for a High- α Maneuverable Thrust-Vectoring Fighter Aircraft. *Journal of Guidance, Control, and Dynamics*, 32(5):1483–1496, September 2009.

[29] SF Campbell and JT Kaneshige. A Nonlinear Dynamic Inversion Predictor-Based Model Reference Adaptive Controller for a Generic Transport Model. *American Control Conference*, 2010.

[30] Samir Bennani and Gertjan Looye. Flight control law design for a civil aircraft using robust dynamic inversion. 1998.

[31] G.J. Balas, W.L. Garrard, and Jakob Reiner. Robust dynamic inversion control laws for aircraft control. In *AIAA Guidance Navigation and Control Conference*, 1992.

[32] Hakan Fer and Dale F. Enns. An proach to select desired dynamic gains for dynamic inversion control laws. AIAA Guidance Navigation and Control Conference, 1997.

[33] M.M. Lone, Intelligent Systems Group, Computational Sciences, N M Rouyan, A K Cooke, and Control Group. A MATLAB / Simulink suite for the real-time flight simulation of large aircraft. Technical Report April, 2012.

[34] Taosong Hu. *Automatically Control Principle.*

[35] Christopher Edwards and Sarah K. Spurgeon. *Sliding mode control: theory and applications.* 1998.

[36] David Deering. *Sliding mode satellite formation control with application to xeus.* PhD thesis, 2001.

[37] Christian Tournes and Yuri Shtessel. Aircraft control using sliding mode control. San Diego, 1996. AIAA Guidance Navigation and Control Conference.

[38] S.M. Gadoue, D. Giaouris, and J.W. Finch. Genetic Algorithm Optimized PI and Fuzzy Sliding Mode Speed Control for DTC Drives. In *In Proceedings of the World Congress on Engineering*, number 0, 2007.

[39] Yong-Joon Choi and Min Cheol Lee. PID sliding mode control for steering of lateral moving strip in hot strip rolling. *International Journal of Control, Automation and Systems*, 7(3):399–407, May 2009.

[40] H.S. Shin, T.H. Kim, and MJ Hwang Tahk. Nonlinear formation guidance law with robust disturbance observer. *International Journal of The Aeronautical Sciences*, pages 1–6, 2009.

[41] Lei-Po Liu, Zhu-Mu Fu, and Xiao-Na Song. Sliding mode control with disturbance observer for a class of nonlinear systems. *International Journal of Automation and Computing*, 9(5):487–491, October 2012.

[42] Curt Hanson, M Johnson, and Jacob Schaefer. Handling qualities evaluations of low complexity model reference adaptive controllers for reduced pitch and roll damping scenarios. *AIAA Guidance Navigation and Control Conference*, (August):1–19, 2011.

[43] C. Ahn, Y. Kim, and H. Kim. Adaptive Sliding Mode Control for Non-affine Nonlinear Vehicle Systems. In *AIAA Guidance, Navigation, and Control Conference and Exhibit*, number August, pages 1–17, 2007.

[44] S.N. Singh. Nonlinear adaptive and sliding mode flight path control of F/A-18 model. *Aerospace and Electronic Systems*, 39(4), 2003.

[45] H Xu, MD Mirmirani, and PA Ioannou. Adaptive sliding mode control design for a hypersonic flight vehicle. *Journal of guidance, control, and dynamics*, 2004.

[46] Atsuo Kawamura, H Itoh, and K Sakamoto. Chattering reduction of disturbance observer based sliding mode control. *Industry Applications, IEEE Transactions*, 30(2):456–461, 1994.

[47] CC Wang and Masayoshi Tomizuka. Design of robustly stable disturbance observers based on closed loop consideration using H/sub/spl infin//optimization and its applications to motion control systems. In *American Control Conference*, pages 3764–3769, 2004.

Appendix A

The simulink models

Following figure A.1 and A.2 shows the aircraft model in Simulink including longitudinal mode and lateral mode.

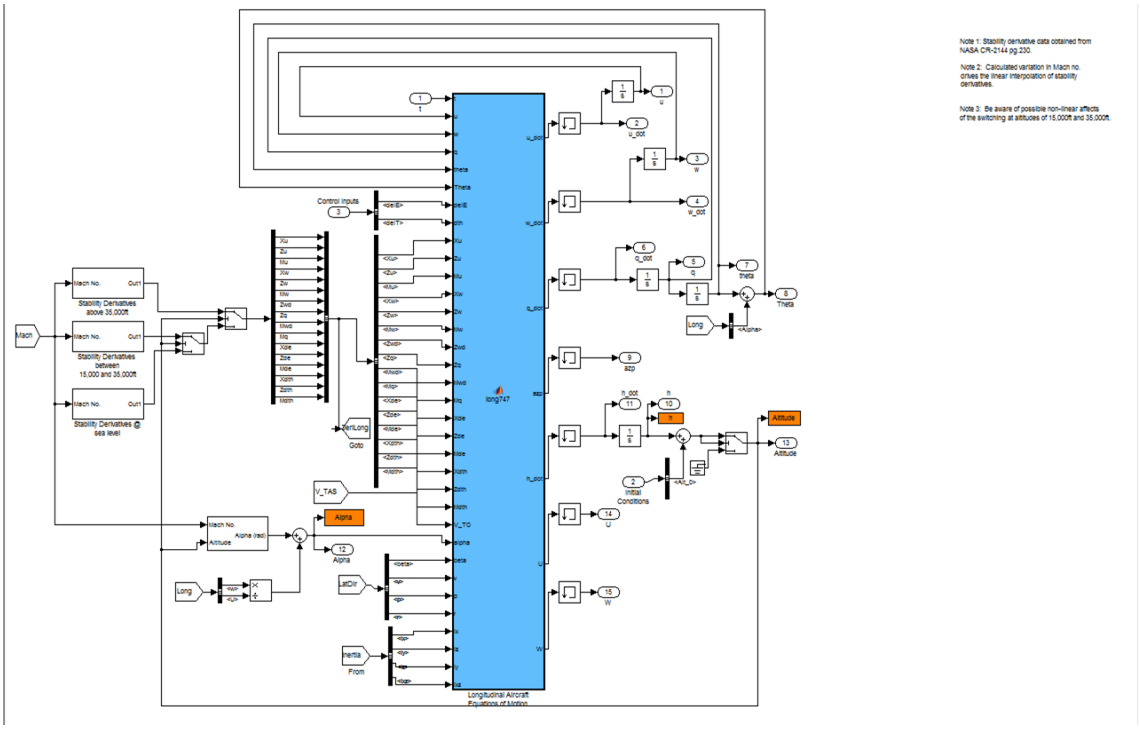

Figure A.1: Longitudinal Boeing 747 model

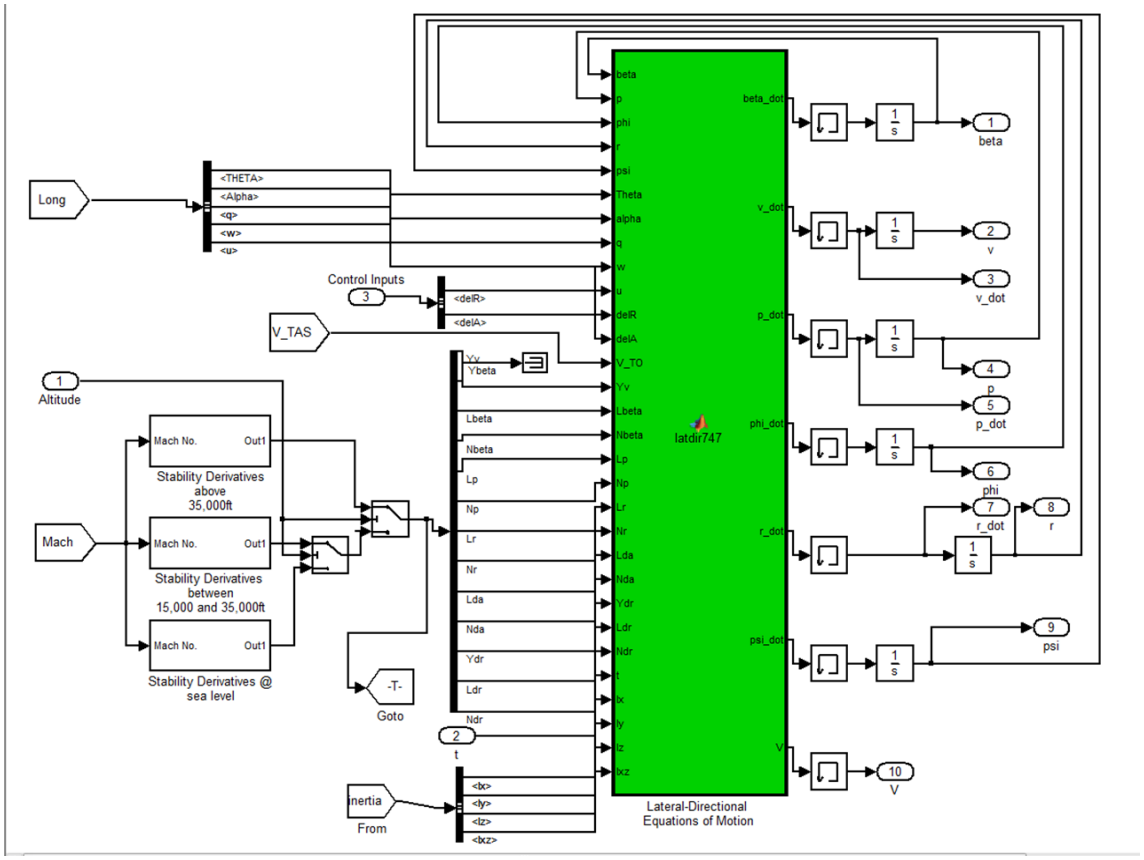

Figure A.2: lateral Boeing 747model

Appendix B

Some important Matlab code

The internal dynamics verification of longitudinal mode and lateral mode are shown below.

Listing B.1: Internal dynamics verification of lateral mode.

```
syms Ydr Lda Ldr Nda Ndr delR delA real;
syms Yv Lr Lp Lbeta Nbeta Nr Np real;
syms mu1 mu2 z1 z2 z3 real;
syms p r phi psi v real;
syms Theta W g U real;
%syms mu1_d mu2_d z1_d z2_d z3_d real;

%the lateral mode

v_dot = Ydr*delR + Yv*v + W*p - U*r +...
    g*(phi*cos(Theta) + psi*sin(Theta));
p_dot = Lda*delA + Ldr*delR + Lr*r + Lp*p + Lbeta*v/U;
phi_dot = p + r*tan(Theta);
r_dot = Nda*delA + Ndr*delR + Nbeta*v/U + Nr*r + Np*p;
psi_dot = r/cos(Theta);

%the solution of LgZ=0
%the new state space is:mu1=p,mu2=r,z1=phi,z2=psi,
%z3=v/Ydr*(Ndr/Nda-Ldr/Lda)+p/Lda-r/Nda;
%thus the normal form is presented as below
mu1_d=p_dot;
mu2_d=r_dot;
z1_d=phi_dot;
z2_d=psi_dot;
z3_d=v_dot/Ydr*(Ndr/Nda-Ldr/Lda)+p_dot/Lda-r_dot/Nda;
z3_d=expand(z3_d);
```

```
%the expression of original state with respect to new state.
%the original state xold=[v,p,r,phi,psi];
%the new states z=[p,r,phi,psi,v/Ydr*(Ndr/Nda-Ldr/Lda)+p/Lda-r/Nda]
%thus z=Rx, x=inv(R)*z
R=[0 1 0 0 0; 0 0 1 0 0; 0 0 0 1 0; 0 0 0 0 1;
    (Ndr/Nda-Ldr/Lda)/Ydr 1/Lda -1/Nda 0 0];
x=R\[mu1,mu2,z1,z2,z3]';


%obtain the expression of the zerodynamics.
z1_d=subs(z1_d,{v,p,r,phi,psi},{x(1),x(2),x(3),x(4),x(5)});
z2_d=subs(z2_d,{v,p,r,phi,psi},{x(1),x(2),x(3),x(4),x(5)});
z3_d=subs(z3_d,{v,p,r,phi,psi},{x(1),x(2),x(3),x(4),x(5)});

%set all the output equal to 0, namely p,r=0 and p_dot,r_dot=0;
z1_d=subs(z1_d, {mu1,mu2},{0, 0});
z2_d=subs(z2_d, {mu1,mu2},{0, 0});
z3_d=subs(z3_d, {mu1,mu2},{0, 0});


%obtain the A matrix of the zerodynamics
[z3d_z1,t1]=coeffs(z3_d,z1);
[z3d_z2,t2]=coeffs(z3_d,z2);
[z3d_z3,t3]=coeffs(z3_d,z3);
A=[0 0 0;
   0 0 0;
    z3d_z1(1), z3d_z2(1), z3d_z3(1)];

%calculate the eigenvalue of A at different flight conditions
Machdata=[0.7 0.75 0.8 0.85 0.9 0.95 0.95 0.95 0.95;
    0.5 0.55 0.6 0.65 0.7 0.75 0.8 0.8 0.8;
    0.198 0.25 0.3 0.35 0.4 0.45 0.5 0.6 0.65];%mach number
Altdata=[40000 20000 0];%altitude(ft)
simulation_times=0;
for m=[1:3]
    for n=[1:9]
      Mach=Machdata(m,n);
      Alt=Altdata(m);
      k=0;% count the unstable internal dynamics
      sim('obtain_derivatives_data_lat')
      simulation_times=simulation_times+1;
      poles=subs(A, {g,Theta,U,Ndr, Nda, Ydr, Ldr, Lda, Yv...
Lbeta,Nbeta},{32,0,Ua(1),Ndra(1),Ndaa(1) ,Ydra(1) ,Ldra(1),...
Ldaa(1) ,Yva(1) ,Lbetaa(1) ,Nbetaa(1)});
      poles=eig(poles);
      for i=[1:3]
```

```
            if poles(i)>0
                k=k+1;
            end
        end
    end
end
```

Listing B.2: Internal dynamics verification of longitudinal mode.

```
syms Xde Mde Zwd Zde delE Xu Xw Zu Zw Mu Mwd Mw Mq Zq real;
syms mu z1 z2 z3 real;
syms u w q theta real;
syms Theta W g U real;
syms z1d z2d z3d real;

%the longitudinal dynamic mode
u_dot = Xde*delE + Xu*u + Xw*w - W*q - g*cos(Theta)*theta;
w_dot = (Zde*delE +Zu*u + Zw*w + q*(Zq+U) -...
    g*sin(Theta)*theta)/(1 - Zwd);
q_dot = Mde*delE  + Mu*u  + Mw*w + Mq*q;%+Mwd*w_dot
theta_dot=q;

%the solution of LgZ=0
%mu=q, z1=theta, z2=u/Xde-q/Mde, z3=u/Xde-(1-Zwd)/Zde*w
%thus the normal form is presented as below
z1_d=q;
z2_d=u_dot/Xde-q_dot/Mde;
z3_d=u_dot/Xde-(1-Zwd)/Zde*w_dot;
z2_d=simplify(z2_d);
z3_d=simplify(z3_d);

%the expression of original state with respect to new state.
R=[0 0 1 0; 0 0 0 1; 1/Xde 0 -1/Mde 0; 1/Xde -(1-Zwd)/Zde 0 0];
x=R\[mu,z1,z2,z3]';
%mu=q, z1=theta, z2=u/Xde-q/Mde, z3=u/Xde-(1-Zwd)/Zde*w
%u=x(1), w=x(2), q=x(3), theta=x(4);

%obtain the expression of the zerodynamics.
z1_d=subs(z1_d,{u,w,q,theta},{x(1),x(2),x(3),x(4)});
z2_d=subs(z2_d,{u,w,q,theta},{x(1),x(2),x(3),x(4)});
z3_d=subs(z3_d,{u,w,q,theta},{x(1),x(2),x(3),x(4)});

%obtain the A matrix of the zerodynamics
[z2d_z1,t1]=coeffs(z2_d,z1);
[z2d_z2,t2]=coeffs(z2_d,z2);
[z2d_z3,t3]=coeffs(z2_d,z3);
[z3d_z1,t4]=coeffs(z3_d,z1);
```

```
[z3d_z2,t5]=coeffs(z3_d,z2);
[z3d_z3,t6]=coeffs(z3_d,z3);
A=[0  0  0;
    z2d_z1(1), z2d_z2(1), z2d_z3(1);
    z3d_z1(1), z3d_z2(1), z3d_z3(1)]

%calculate the eigenvalue of A at different flight conditions
Machdata=[0.7  0.8  0.9  0.9;
    0.5  0.65  0.8  0.8;
    0.198  0.249  0.45  0.65];%mach number
Altdata=[40000  20000  0];%altitude(ft)
k=0;
for m=[1:3]
    for n=[1:4]
      Mach=Machdata(m,n);
      Alt=Altdata(m);
      sim('obtain_derivatives_data_long')
      poles=subs(A, {g,Theta,Xde, Mde, Zwd, Zde, Xu, Xw, Zu, Zw,...
Mu, Mw, Mq, Zq},{32,0, Xdeb(1),Mdeb(1) ,Zwdb(1) ,Zdeb(1) ,Xub(1)...
Xwb(1) ,Zub(1) ,Zwb(1),Mub(1),Mwb(1),Mqb(1),Zqb(1)});
      poles=eig(poles);
      for i=[1:3]
          if poles(i)>0
              k=k+1;
          end
      end
    end
end
```

Appendix C

More assessments results

The assessment of disturbance observer based SMC controller with $\eta = 0.005$ for more flight points is indicated as below picture.

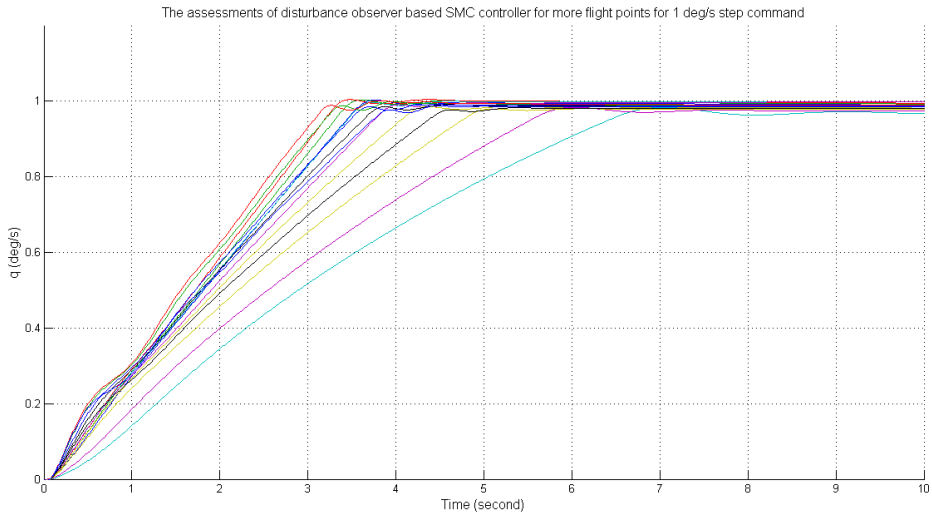

Figure C.1: The assessments of disturbance observer based SMC controller for more flight points for 1 deg/s step command

Below picture shows the assessment of disturbance observer based P SMC controller with $\eta = 0.005 and k_p = 1.5$ for more flight points.

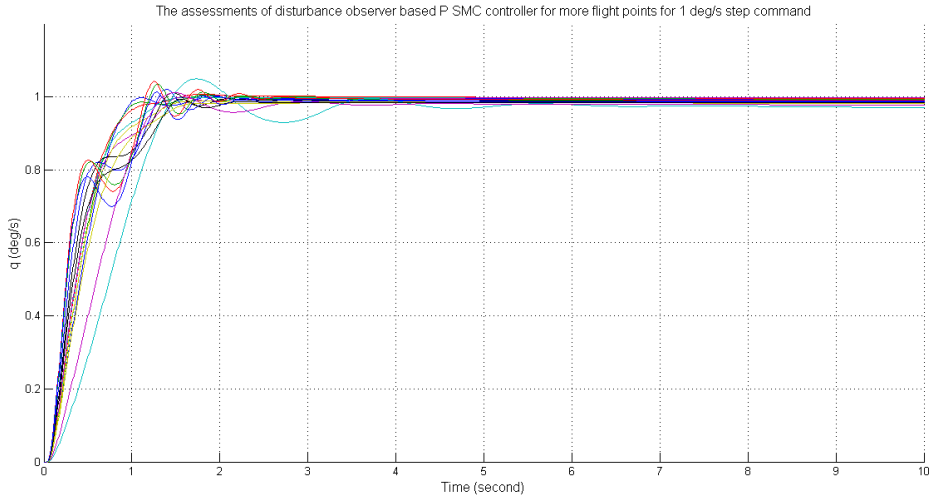

Figure C.2: The assessments of disturbance observer based P SMC controller for more flight points for 1 deg/s step command

Figure C.3 and figure C.4 show respectively the assessment of PI NDI controller ($k_p = 4$ and $k_i = 4$) and PI SMC ($k_p = 4, k_i = 4$ and $\eta = 0.005$) for more flight points.

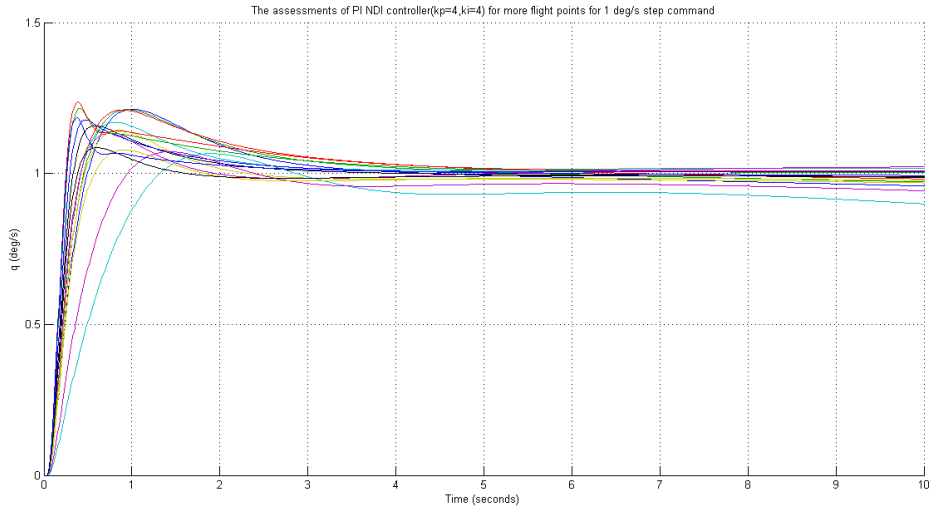

Figure C.3: The assessments of PI NDI controller(kp=4,ki=4) for more flight points for 1 deg/s step command.

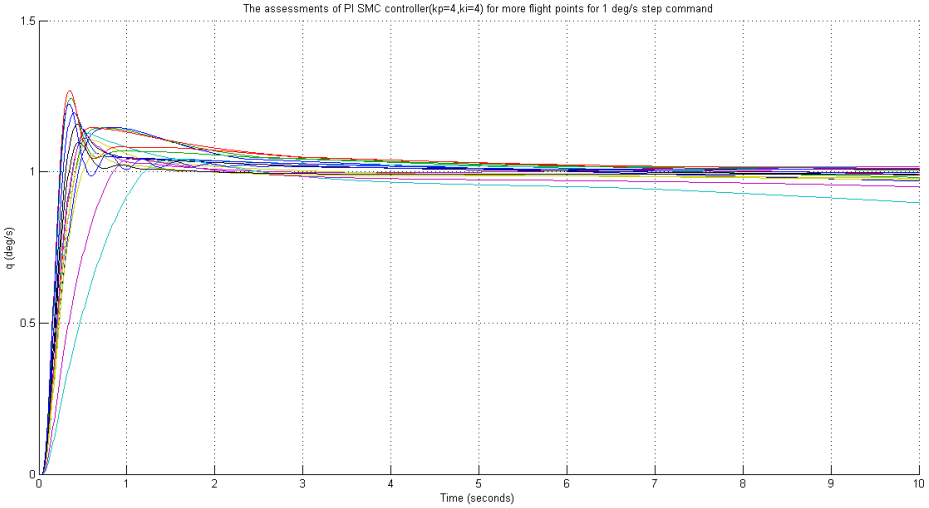

Figure C.4: The assessments of PI SMC controller(kp=4,ki=4 and $\eta = 0.005$) for more flight points for 1 deg/s step command.